Title
FINAL-STATE INTERACTIONS IN THE THREE-PION DECAY OF K MESONS

Author
Mathevs, Robert D.

Publication Date
1971

Submitted to Physical Review;
Also submitted as a PH. D. Thesis

UCRL-20247
Preprint

FINAL-STATE INTERACTIONS IN THE THREE-PION DECAY OF K MESONS

Robert D. Mathews

January 11, 1971

AEC Contract No. W-7405-eng-48

LAWRENCE RADIATION LABORATORY
UNIVERSITY of CALIFORNIA BERKELEY

DISCLAIMER

FINAL-STATE INTERACTIONS IN THE THREE-PION DECAY OF K MESONS

Contents

UCRL-20247

FINAL-STATE INTERACTIONS IN THE THREE-PION DECAY OF K MESONS*

Robert D. Mathews

Lawrence Radiation Laboratory
University of California
Berkeley, California 94720

January 11, 1971

ABSTRACT

We have made some steps towards solving numerically the equations of Khuri and Treiman for K and $\eta \to 3\pi$ and extending them to include P-wave interactions, the effects of a nonflat bare matrix element, and the effects of unequal masses for the charged and neutral pions. Our results show that it is rather difficult, with S waves alone, to get a steep enough slope for the matrix element on the Dalitz plot when the bare matrix element is a constant. The S-wave phase shifts required to fit the Dalitz plot data are usually quite unphysical (e.g., $a_0 - a_2 = -1.0$, an F_0 pole located just off the edge of the Dalitz plot, etc.). In our calculations the inclusion of P waves appears to have a large effect on the Dalitz plot. If we assume $I = 0$ phase shifts of either the up-down or the down-up variety, and if we assume $I = 1$ and $I = 2$ phase shifts that are consistent with the experimentally determined phase shifts, then the resulting solutions of the KT equations with a constant inhomogeneous term yield Dalitz-plot slopes which fit the data. The inclusion of P waves in the KT equations probably deserves more study, however, perhaps with different numerical approaches.

With the same assumption of a constant inhomogeneous term, the extension of the K-decay solutions to η decay follows trivially just from changing the mass of the decaying particle.

If the inhomogeneous term of the KT equations is given a linear term, $M_{bare} = 1 + \frac{1}{2} g(s_c - s_0)$, the effect is to tilt the solutions, but by an exaggerated amount. If the inhomogeneous term is changed to $M_{bare} = 1 + \frac{1}{2} gr \tanh[(s_c - s_0)/r]$, which gives a slope on the Dalitz plot but goes to a constant asymptotically, the effect is just to tilt the solutions in the region of the Dalitz plot by the amount $\frac{1}{2} g$.

When the masses of the charged and neutral pions are made unequal in the KT equations, the largest effects to be observed in the matrix element are cusps related to thresholds located in the physical region of the Dalitz plot and due to the presence of communicating subchannels. The calculated effects are in a direction agreeing with experiment, thus leading to the speculation that perhaps the unequal masses of the pions might be responsible in large part for the slight amount of $I = 2$ final state observed in the decay.

I. INTRODUCTION

The three-pion decay of the K meson has been studied since R. H. Dalitz first analyzed 13 τ events in 1953.[1] The decay modes observed are:

$$K^+ \to \pi^+\pi^+\pi^- \qquad \text{"}\tau^+ \text{ decay"}$$
$$\to \pi^+\pi^0\pi^0 \qquad \text{"}\tau'^+ \text{ decay";}$$

similarly for K^-;

$$K_L^0 \to \pi^+\pi^-\pi^0$$
$$\to \pi^0\pi^0\pi^0.$$

Because of the small amount of energy released in these decays, the experimental distribution of energy among the three pions is rather featureless except for gentle slopes to the Dalitz plots of these decays. Because of this small energy release, however, it is tempting to see if one cannot understand these slopes in terms of the low energy strong interactions amongst the three pions in the final state, rather than attribute it to some intrinsic slope in the matrix element of the bare weak interaction. A number of attempts in this direction have been made, but in more recent years explanations based on current algebra, relating the slope to the magnitude of the two-pion decay of K mesons, have become more popular (see review by Cabibbo[2]). The viewpoint we would like to adopt is a return to the original view that the slopes are caused only by dressing a bare, flat weak interaction with strong final-state interactions. Accordingly in this paper we assume various forms of the low energy $\pi\pi$ interaction and proceed to calculate slopes for the Dalitz plot.

This picture of having only final-state interactions has some virtues. First, if the picture is correct, one has the pleasing possibility of going the other way to infer some information about low energy $\pi\pi$ scattering from the observed slopes. There is not a particular wealth of unambiguous data for this important low energy $\pi\pi$ scattering, so it would be worth trying to sort out the interactions of a three-particle final state. Secondly, if the idea is correct and the assumption of a constant primordial matrix element applies to eta decay as well, it should be straightforward to include an explanation of the slope of the Dalitz plot for the electromagnetic decay of the η meson into three pions.

Our basic approach is that of Khuri and Treiman,[3] which was first proposed in 1960. The KT approach uses relativistic S-matrix theory and dispersion-relation techniques. Mathematically the approach requires the solving of a set of coupled, singular integral equations whose kernels are essentially $\pi\pi$ scattering amplitudes. In order to solve these equations Khuri and Treiman proceed to make a series of approximations which we will wish to re-examine in this paper and hopefully improve on.

Using just an S-wave scattering length approximation to low energy $\pi\pi$ scattering, Khuri and Treiman were able to fit the slopes of the various Dalitz plots with $a_0 - a_2 \approx -0.7$.[4] In a more phenomenological approach Brown and Singer[5] have proposed that the Dalitz plot spectra could be understood by assuming a low-energy broad-width $I = 0$ $\pi\pi$ resonance, the so called σ resonance. A fit to the data requires a mass, $m_\sigma \approx 390$-425 MeV, and a width,

$\Gamma_\sigma \approx 75$-100 MeV. It seems somewhat suspicious that the "resonance" has to be located just outside the edge of the Dalitz plot (≈ 360 MeV for K decay and ≈ 410 MeV for η decay), but the model provides a good mnemonic for the direction of the experimental Dalitz plot slopes, and indicates that large phase shifts are required in order to fit the data when using only $I = 0$ interactions. Barbour and Schult[6] and Schult and Barbour[7] used Faddeev equations with S- and P-wave nonlocal separable potentials to investigate final-state interactions in $K_{3\pi}$ decay. They find that using only S waves requires $a_2^2 - a_0^2 \approx 2$ in order to fit the data. By including P-wave and using small S-wave scattering lengths (≈ 0.2) they find that the P wave can become dominant and fits can be achieved with $a_2^2 < a_0^2$. These P-wave dominant solutions are sensitive to a cutoff used in the calculation, nevertheless it is interesting that they find that P waves could be important in the problem.

A recent attempt to use the KT equations has been made by Neveau and Scherk.[8] In their work they use the KT equations to find what corrections strong final state interactions might make on a bare weak interaction that has a linear slope equal to that predicted by current algebra. The $\pi\pi$ P-wave and $I = 2$ S-wave interactions are neglected and the $I = 0$ S wave is taken to have a resonance at about 700 MeV with a width of about 300 MeV. Two subtractions are made so that an arbitrary linear dependence can be introduced. An equation for the correction to this linear dependence is derived, and solved approximately by taking a major portion of the expected solution out in terms of

Omnes-type functions and using a one-iteration approximation for the remainder. They also consider the case of $\eta_{3\pi}$ decay and make arguments that perhaps the strong final-state interaction corrections can overcome the failure of simple current algebra to give a nonzero matrix element for the decay.

In this paper we should like to explore a technique for solving the KT equations more directly and numerically on a computer, to try to include P-wave $\pi\pi$ interactions in the KT prescription, and to investigate crudely the effects on the matrix element when one takes into consideration the mass difference between the charged and neutral pions.

II. BRIEF SKETCH AND REVIEW OF THE KHURI-TREIMAN EQUATIONS

A. Basic Idea of the KT Equations

The Khuri-Treiman approach uses the S-matrix ideas of analyticity, crossing, and unitarity. Rather than focusing attention on decay diagrams like Fig. 1a, one considers the general "scattering like" diagram shown in Fig. 1b. When analytically continued and considered on a Mandelstam plot this reaction amplitude will have s, t, and u physical regions like a normal reaction and will also have a Dalitz-plot physical region in the center because one of the particles is heavy enough to decay into the other three (Fig. 1c). One then assumes that this "scattering like" amplitude obeys a Mandelstam representation similar to that for a normal reaction.

For the discontinuity of the amplitude in a given channel, say s, the unitarity equation is used, that is

$$\frac{1}{2}\,\mathrm{Disc}_s\, A_{K\pi\to\pi\pi} = \sum_{\substack{\text{all open inter-}\\ \text{mediate states,}\\ \text{"int"}}} \frac{q_{int}(s)}{(s)^{\frac{1}{2}}}\, A^{*}_{K\pi\to int}\, A_{int\to\pi\pi}\,. \tag{1}$$

Next comes an important assumption. For the intermediate states we shall keep only $\pi\pi$. This means retaining in the unitarity equation only a diagram like Fig. 1d and ignoring intermediate states such as $K\pi$, 4π, etc. The foremost rationale for doing this is that it makes the problem simpler. But arguments can be put forward that the $K\pi$ and 4π thresholds are much higher than the $\pi\pi$ threshold and might therefore have less effect on the Dalitz-plot region. These thresholds

occur "beyond" the Dalitz plot, whereas the $\pi\pi$ threshold occurs right at the "beginning" of the Dalitz plot.

The sum over all the open intermediate states also implies integration over all angles of the intermediate state. Khuri and Treiman next make another important approximation which we hope to relax somewhat in Sec. III. They keep only S waves in the $\pi\pi$ amplitude. If this is done one can arrive at the following symmetric-looking set of equations, known as the KT equations:

$$A^{*}_{K\pi\to\pi\pi}(s,t,u) = A^{*}_{K\pi\to\pi\pi}(s_0,t_0,u_0) + \frac{s - s_0}{\pi}\int_{thr}^{\infty} ds'$$

$$\times \frac{\frac{1}{2}\,\mathrm{Disc}_s A_{K\pi\to\pi\pi}}{(s' - s + i\epsilon)(s' - s_0 + i\epsilon)} + \text{similar terms in } t \text{ and } u, \quad (2)$$

where $$\frac{1}{2}\,\mathrm{Disc}_s A_{K\pi\to\pi\pi} = \sum_{\substack{\text{charge}\\ \text{states}}} \frac{q}{(s)^{\frac{1}{2}}}\,\overline{A^{*}}_{K\pi\to\pi\pi}(s)\, A_{\pi\pi\to\pi\pi}(s)$$

and where $$\overline{A^{*}}_{K\pi\to\pi\pi}(s) \equiv \int_{-1}^{+1} \frac{dz}{2} A^{*}_{K\pi\to\pi\pi}(s,z).$$

(For this general discussion I shall gloss over questions of charge states and symmetries. They will be gone into later in more detail.) With the use of the $+i\epsilon$ prescription it can be seen that we have $A^{*}_{K\pi\to\pi\pi}$ both inside the integrals and outside and thus have an integral equation in three variables s, t, and u (actually only two because $s + t + u = \sum m_i^2$). The kernel of the integral equation is essentially the $\pi\pi$ scattering amplitude, $A_{\pi\pi\to\pi\pi}$. In practice one assumes the

$\pi\pi$ scattering amplitude to be known, and solves for the decay amplitude, $A^*_{K\pi\to\pi\pi}$. That it is a coupled integral equation can be seen by the fact that the intermediate-state pions may have different charge states from the final-state pions, so that there is a coupling between the amplitudes for the different charge modes of decay.

Notice that the KT equations cannot give the overall normalization of $A^*_{K\pi\to\pi\pi}$, since it appears linearly on both sides of (2). This means the KT equations can give only relative amplitudes compared with some chosen spot in the s, t, and u plane, such as the center of the Dalitz plot. In practice the subtraction constants are chosen to be real and of order 1 (for example the choice -2 and 1 for τ and τ' decays respectively satisfies $|\Delta I| = \frac{1}{2}$ requirements).

B. Critique of the Approximate Solution by Khuri and Treiman

Now comes the important question of how to solve this complicated set of coupled integral equations in two dimensions. Khuri and Treiman obtained an approximate solution by making one iteration of an iterative solution to the problem. The A^* inside the integral was replaced by the subtraction constant $A^*(s_0,t_0,u_0)$ so that with a given assumed form for the $\pi\pi$ scattering amplitude the integration could be done explicitly to obtain a closed expression for the amplitude. The $\pi\pi$ scattering amplitude chosen by Khuri and Treiman kept only S waves and used a scattering-length approximation. Specifically, they assumed

$$\frac{2q}{(s)^{\frac{1}{2}}} \cot \delta_I = \frac{1}{a_I}$$

and

$$\frac{q}{(s)^{\frac{1}{2}}} A_{\pi\pi \to \pi\pi} \equiv e^{i\delta} \sin\delta \approx \frac{2qa}{(s)^{\frac{1}{2}}},$$

where a_I is the scattering length for a pure I-spin state. Using these approximations and keeping up to linear terms in $s - s_0$ in the matrix element squared, Khuri and Treiman obtain an expression for the slope of the Dalitz plot which is proportional to $a_0 - a_2$. Fitting this to the observed slope then requires $a_0 - a_2 \approx -0.7$.

The KT paper was written in 1960, and since that time a theoretical prejudice has evolved that a_0 should be small and positive and that a_2 should be smaller and negative, in direct disagreement with the above result. As a guide to our thinking we can recall the values proposed by Weinberg[9] on the basis of soft pion theorems, namely $a_0 \approx +0.20$ and $a_2 \approx -0.06$.

Upon a second examination some of the above approximations made by Khuri and Treiman to solve their equations appear a bit shaky. For the purposes of this mathematical discussion let's consider a somewhat simpler equation in only one variable, namely the so-called "Omnes equation,"

$$A(s) = 1 + \frac{s - s_0}{\pi} \int_{thr}^{\infty} \frac{ds' \, F(s') \, A(s')}{(s' - s + i\epsilon)(s' - s_0 + i\epsilon)}, \quad (3)$$

where $F(s') \equiv e^{i\delta(s')} \sin\delta(s')$. Khuri and Treiman take

$$F(s') \approx \frac{2qa}{(s)^{\frac{1}{2}}}$$

and obtain, after one iteration,

$$A(s) = 1 + I(s) - I(s_0) ,$$

where

$$I(s) = -\frac{2qa}{(s)^{\frac{1}{2}}}\frac{1}{\pi}\log\left|\frac{1+\frac{2q}{(s)^{\frac{1}{2}}}}{1-\frac{2q}{(s)^{\frac{1}{2}}}}\right| - i\frac{2qa}{(s)^{\frac{1}{2}}}$$

$$\approx -\left(\frac{2q}{(s)^{\frac{1}{2}}}\right)^2 \cdot \frac{2a}{\pi} - i\frac{2q}{(s)^{\frac{1}{2}}}a \qquad (q \ll 1) .$$

This gives a reasonable behavior, that is, a matrix element decreasing with energy for positive a, and vice versa. However, if we use a non-relativistic effective-range approximation,

$$q \cot \delta = \frac{1}{a}$$

and

$$F(s') \approx qa,$$

we get

$$I(s) = -iqa.$$

Since here $I(s)$ is purely imaginary this leads to an $|A(s)|^2$ that is equal to one at the subtraction point, but is greater than one everywhere else in the physical region, thus exhibiting a bowl-shaped s dependence around the arbitrary subtraction point s_0. In fact, if one takes $F(s)/q(s)$ to be any real analytic function of s with at most a right-hand cut with a square-root branch point and no other singularities on the physical sheet, then $I(s)$ is purely imaginary.

Examples of such behavior are

$$F(s) = qa,$$

$$\frac{qa}{1 - iqa}, \quad a \text{ positive},$$

$$\frac{qa}{1 - bq^2 - iqa}, \quad a \text{ and } b \text{ positive},$$

or $$\frac{qa}{1 - bq^2 + cq^4 - iqa}, \quad a, b, \text{ and } c \text{ positive and } b^2 > 4c .$$

This seems like a fairly large class of kernels that leads to nonsensical results on first iteration.

It might be hoped that these problems could be cured by further iteration, that is, by using the output amplitude as a trial amplitude to be substituted back into the integral to generate another output amplitude, and so on. Since doing the integrals explicitly for repeated iteration soon becomes tedious, iteration was tried numerically on a computer. The effort was unsuccessful, however, most of the time. The solution most often "blew up," that is, for any $s \neq s_0$ it increased in magnitude with each succeeding iteration. For a few cases the numerical iteration was even started with the exact known solution for a trial solution, and yet the iterations still diverged. This could be due to numerical inaccuracies and propagation of error, but we suspect it may be due to violation of some unknown convergence criteria, which would lead to failure even if the integrals were done analytically.

Because of these problems a more direct method for solving (3) by matrix inversion was tried and found to be successful. The method involves choosing a set of N mesh points, replacing the integral by a sum, and deriving a set of N linear equations in N unknowns for the amplitude. Details for the numerical method can be found in Appendices A and B.

Next we come to a question of uniqueness. The exact solution for integral equation (3) is known, namely

$$A(s) = \frac{P(s)}{P(s_0)} \cdot \exp\left\{\frac{s - s_0}{\pi}\int_{thr}^{\infty} \frac{ds'\ \delta(s')}{(s' - s + i\epsilon)(s' - s_0 + i\epsilon)}\right\}, \tag{4}$$

where $P(s)$ is an arbitrary real polynomial in s. The highest order of polynomial that can be tolerated depends on the convergence of the integral in (3) and the number of subtractions. For example, if we use again the nonrelativistic effective range approximation

$$\delta = \tan^{-1}(qa),$$

the exact (but unnormalized) solution is

$$\frac{P(s)}{1 + iqa}, \quad a > 0\ ,$$

$$C(1 - iqa), \quad a < 0\ ,$$

where $P(s)$ is a first-order polynomial and C is a constant. This means, after normalization, that the solution is unique for $a < 0$, but not for $a > 0$. The reason for the nonuniqueness is due to the use

of "unphysical" phase shifts, i.e., phase shifts which do not go to zero as s goes to infinity as in nonrelativistic potential scattering. Now in the above example the solutions which seem physically reasonable are

$$\frac{C}{1 + iqa}, \quad a > 0,$$

$$C(1 - iqa), \quad a < 0.$$

That is, the matrix element squared should go down with energy for positive a and vice versa. The physically reasonable way to achieve uniqueness and extend the nonrelativistic potential scattering results then would be to select the solution with the lowest asymptotic behavior. Now, one might worry how this selection can be achieved in the numerical solution, but it is submitted that the manner for doing the numerical integration outlined in Appendix B introduces sufficient bias to select the lowest asymptotic behavior for our cases of interest. As a demonstration of accuracy, numerical solutions were obtained for (3) using nonrelativistic scattering lengths of $a = \pm 1.0$, and only 16 mesh points. Comparison of the amplitudes squared of the true and numerical solutions gives a discrepancy of 41% at the last mesh point, $s = 1000$, 3% at $s = 100$, and less than 1% for $s \leq 6.76$ (the Dalitz plot region for $K \to 3\pi$). For $s \leq 100$, then, there is virtually no difference between the solutions, and on the scales used in later figures there is no graphable difference between the solutions.

III. AN EXTENSION TO INCLUDE P-WAVE FINAL STATE INTERACTIONS; THE DERIVATION OF THE EQUATIONS USED FOR APPROXIMATE, NUMERICAL SOLUTION OF THE KT EQUATIONS

A. General Expression of the KT Equations

We now present a sequence of derivations and approximations leading up to the equations actually used for numerical calculation. To reduce the amount of algebra we may occasionally gloss over certain inessential complications for the particular topic under discussion. Also because of all the different charge cases possible we shall occasionally use just illustrative examples, in which the generalization to other charge cases is obvious.

Let us first write down a general expression for the $\pi\pi$ contribution to the discontinuity in a particular channel and then proceed to make simplifications. Let $A^*(K \to \pi_a\pi_b\pi_c) \equiv M_{\alpha\beta\gamma}(s_a, s_b, s_c)$, where α, β, and γ stand for the charge states of π_a, π_b, and π_c respectively, and where $s_a \equiv s_{bc}$, the invariant mass squared of $\pi_b\pi_c$, etc. Then

$$\frac{1}{2}\,\mathrm{Disc}_{s_a} M^*_{\alpha\beta\gamma}(s_a, s_b, s_c) = \sum_{\beta',\gamma'} \frac{q_{\beta'\gamma'}}{(s_a)^{\frac{1}{2}}}\,\theta[s_a - (m_{\beta'} + m_{\gamma'})^2]$$

$$\times \int \frac{d\Omega'_{bc}}{4\pi} M_{\alpha\beta'\gamma'}(s_a, s_{b'}, s_{c'})\, B_{\beta'\gamma',\beta\gamma}(s_a, \cos\theta_{bb'}), \qquad (5)$$

where $B_{\beta'\gamma',\beta\gamma}$ is the $\pi\pi$ matrix element for $\pi_b\pi_c \to \pi_{b'}\pi_{c'}$, and where the integration is over all possible angles of the intermediate state, $\pi_{b'}\pi_{c'}$ in the b'c' (or equivalently bc) center of mass.

Here also $q_{\beta'\gamma'}$ stands for the center-of-mass momentum, and $(m_{\beta'} + m_{\gamma'})^2$ the threshold for the b'c' intermediate state. Similar equations can be obtained for the s_b and s_c discontinuities. The normalization of B is such that if we projected onto a pure state of I spin and angular momentum the S matrix could be regained by

$$S_\ell = 1 + 2i \frac{(q^i q^f)^{\frac{1}{2}}}{(s)^{\frac{1}{2}}} B_\ell ,$$

where q^i and q^f are initial- and final-state momenta respectively. As mentioned before, the overall normalization of M is immaterial, since it appears on both the left- and right-hand sides of the above equations.

Equation (5) is deliberately written with general kinematics, in order to be useful when we consider what effects the difference in mass of the charged and neutral pions might have on the matrix elements. In what follows we shall consider the pions to be of equal mass. This means that all the thresholds are the same, that $q^i = q^f = q_{\beta'\gamma'} \equiv q$, that we can use I-spin amplitudes for the $\pi\pi$ interaction, etc.

B. Angular Integration Approximation

Since the KT integral equations involve the s_a, s_b, and s_c plane, some set of mesh points must be chosen for numerical calculation. Rather than try to cover the whole plane it was decided to economize on the number of mesh points and choose points along certain rays in the plane. In order to see the rationale behind the rays chosen we examine the angular integration in (5). One could use partial-wave projections

of the decay amplitude, but we can obtain almost equivalent results by using appropriate combinations of rays. Figure 2a shows the situation. The integration is in the bc (equivalently b'c') center of mass and is over all angles for the intermediate pion momentum $\underset{\sim}{p}_{b'}$. Now,

$$s_{c'} \equiv s_{ab'} = (p_{a\mu} + p_{b'\mu})^2 = m_a^2 + m_{b'}^2 + 2E_aE_{b'} - 2\underset{\sim}{p}_a \cdot \underset{\sim}{p}_{b'},$$

$$s_{b'} \equiv s_{ac'} = (p_{a\mu} + p_{c'\mu})^2 = m_a^2 + m_{c'}^2 + 2E_aE_{c'} - 2\underset{\sim}{p}_a \cdot \underset{\sim}{p}_{c'},$$

so that

$$s_{b'} - s_{c'} = 4\underset{\sim}{p}_a \cdot \underset{\sim}{p}_{b'}.$$

Notice that for fixed s_a, the angular integration, when viewed in the Mandelstam plane, will be over a variable that is "perpendicular" to s_a, namely $s_{b'} - s_{c'}$, with the center point of the integration at $s_{b'} - s_{c'} = 0$. Since we are including at most P waves in the $\pi\pi$ interaction, this integration will be sensitive at most to the linear variation of $M_{\alpha\beta\gamma}(s_a, s_{b'}, s_{c'})$ in $s_{b'} - s_{c'}$.

Along any given ray let

$$M_{\alpha\beta\gamma}(s_a, s_b, s_c) \equiv M_{\text{ray label}}(s),$$

where s, the only variable, goes from threshold to ∞ along the ray, and the ray label is any convenient mnemonic label. If for illustration we suppress the charge labels and choose to label the rays for M as shown in Fig. 2b, then in the vicinity of the s_a rays we make the following linear approximation to M, the decay amplitude,

$$M(s_a,s_{b'},s_{c'}) \approx \tfrac{1}{2}[M_{ab}(s_a) + M_{ac}(s_a)] + \tfrac{1}{2\Delta}[M_{ab}(s_a) - M_{ac}(s_a)] \times (s_{b'} - s_{c'}),$$

where 2Δ is the separation of the two rays, $M_{ab}(s_a)$ and $M_{ac}(s_a)$. On the Dalitz plot of course experiment indicates that $|M|^2$ is nearly linear, which is consistent with the above approximation. With only S and P waves the π-π scattering amplitude is

$$B_{\beta'\gamma',\beta\gamma}(s_a, \cos\theta_{bb'}) \approx C_0B_0(s_a) + C_2B_2(s_a) + C_1\cdot 3B_1(s_a)P_1(\cos\theta_{bb'}),$$

where $P_1(\cos\theta_{bb'}) = \dfrac{\underset{\sim}{p}_b\cdot\underset{\sim}{p}_{b'}}{|p_b|\cdot|p_{b'}|}$

and C_0, C_1, and C_2 stand for the appropriate I-spin Clebsch-Gordan coefficients. The angular integration in (5) can now be performed by using the rule that for any vectors $\underset{\sim}{a}$, $\underset{\sim}{b}$, and $\underset{\sim}{c}$

$$\int \frac{d\Omega_b}{4\pi} (\underset{\sim}{a}\cdot\underset{\sim}{b})(\underset{\sim}{b}\cdot\underset{\sim}{c}) = \tfrac{1}{3} b^2(\underset{\sim}{a}\cdot\underset{\sim}{c}) .$$

Thus

$$\tfrac{1}{2}\,\mathrm{Disc}_{s_a} M^*(s_a,s_b,s_c) = \frac{q}{(s_a)^{\frac{1}{2}}}\Big\{[C_0B_0(s_a) + C_2B_2(s_a)] \times \tfrac{1}{2}[M_{ab}(s_a) + M_{ac}(s_a)] + C_1B_1(s_a)\,\tfrac{1}{2\Delta}[M_{ab}(s_a) - M_{ac}(s_a)](s_b-s_c)\Big\}. \quad (6)$$

An important thing to observe is that the S-wave interaction multiplies the sum of M_{ab} and M_{ac} on the right-hand side of (6) and the P-wave interaction multiplies the difference. For an S-wave-only situation each set of parallel rays can be allowed to collapse to a single ray if desired by letting Δ go to zero. Another important thing to observe is that the final expression for the angular integration and discontinuity, (6), involves only relativistic invariants, so that it is natural to analytically continue this expression beyond the Dalitz plot, even though it was derived and motivated from the Dalitz plot physical situation.

As mentioned before, the choosing of rays yields an economy of mesh points and thus a reduction in the size of computer memory required. The added accuracy to be obtained by keeping explicit angular averaging was felt not to be worth the bother, at least at this stage of the exploration of the KT equations. This approximation is reversible if desired by substituting:

$$\frac{1}{2}[M_{ab}(s_a) + M_{ac}(s_a)] \rightarrow \bar{M}_0(s_a) \equiv \int \frac{d\Omega_{bc}}{4\pi} M(s_a, s_{b'}, s_{c'}),$$

$$\frac{1}{2\Delta}[M_{ab}(s_a) - M_{ac}(s_a)](s_b - s_c) \rightarrow \bar{M}_1(s_a, s_b, s_c)$$
$$\equiv \int \frac{d\Omega_{bc}}{4\pi} M(s_a, s_{b'}, s_{c'}) \cdot 3 \cdot P_1(\cos \theta_{bb'}).$$

C. Extension of the KT Equations to Include P-Wave Final-State Interactions

We should now like to examine how one can go from one-dimensional dispersion relations to a "three dimensional" KT dispersion relation. Holding s_c fixed we can write

$$M = \frac{1}{\pi}\int ds'_a \frac{M_a(s'_a,s_c)}{s'_a - s_a} + \frac{1}{\pi}\int ds'_b \frac{M_b(s'_b,s_c)}{s'_b - s_b} + G_c(s_a,s_b,s_c), \quad (7)$$

where G_c is an unknown function except that it has no cuts in the s_a or s_b variables. Similar equations can be written for holding s_a and s_b fixed. Let

$$M_a = F_{a+}(s_a)\,\frac{1}{2}[M_{ab}(s_a) + M_{ac}(s_a)] + F_{a-}(s_a)\,\frac{1}{2\Delta}[M_{ab}(s_a) - M_{ac}(s_a)](s_b - s_c), \quad (8)$$

where F_{a+} and F_{a-} are the appropriate S- and P-wave interactions, and similarly for M_b and M_c. If we have only S wave, i.e. $F_{a-} = F_{b-} = F_{c-} = 0$, then by comparing the symmetry of the single dispersion relations in s_a, s_b, and s_c we can deduce that

$$G_c(s_a,s_b,s_c) = \frac{1}{\pi}\int ds'_c \frac{M_c(s'_c)}{s'_c - s_c} + G_0(s_a,s_b,s_c),$$

where G_0 is an unknown function with no cuts in any of its variables. When we include P waves, however, the s'_a integral in (7) requires that we replace $s_b - s_c$ in (8) with $\sum m_i^2 - s'_a - 2s_c$. But then by comparing the three single-dispersion relations one cannot arrive at a

consistent choice for G_c. If, however, we use the trick $s'_a \to s'_a - s_a + s_a$, the $s'_a - s_a$ will cancel the denominator and we will have the constant

$$\int ds'_a \, F_{a-}(s'_a) \frac{1}{2\Delta}[M_{ab}(s'_a) - M_{ac}(s'_a)] ,$$

which we then can add to G_c. Notice that this constant depends on the P-wave interaction and on the solution of the problem, M_{ab} and M_{ac}, but it nevertheless does not depend on the external variables s_a, s_b, and s_c. With the inclusion of all such constants into their respective G's it is possible to deduce a consistent G_c. The equation for M then becomes

$$M = \frac{1}{\pi}\int \frac{ds'_a \, M_a(s'_a, s_b - s_c)}{s'_a - s_a} + \frac{1}{\pi}\int \frac{ds'_b \, M_b(s'_b, s_c - s_a)}{s'_b - s_b}$$

$$+ \frac{1}{\pi}\int \frac{ds'_c \, M_c(s'_c, s_a - s_b)}{s'_c - s_c} + G_0(s_a, s_b, s_c) , \qquad (9)$$

where G_0 as before has no cuts in any of its variables, and where M_a is a function of the two variables, s_a, and $s_b - s_c$, as given by (8), and is at most linearly dependent on $s_b - s_c$, and similarly for M_b and M_c. This is the extension of the Khuri-Treiman equations to include P-wave $\pi\pi$ interactions.

It is interesting to consider the physical interpretation of G_0. If all the $\pi\pi$ interactions were turned off, all that would be left would be G_0, so it is natural to regard it as something like the bare weak interaction. What is not clear, however, is whether G_0

contains any terms like the ones we had to add to G_c, in other words terms which may depend on the $\pi\pi$ interaction and the solution, M, of the integral equation. These terms, then, as well as the integrals in (9) might be related to the final-state enhancement of the decay. It is relevant here to observe that Amado and Noble[10] have looked at the general question of final-state enhancements for three-body weak decays, within the context of Faddeev equations for an exactly soluble S-wave separable-potential model. They find the final-state enhancement can vary over many orders of magnitude as some parameters of their model are changed. Their Dalitz plot distributions, however, can remain relatively unchanged as this overall enhancement varies. In our problem, since we are assuming the pure weak interaction contribution to be constant, we have assumed G_0 to be a constant and have performed one subtraction. Notice that terms like

$$(s_b - s_c)\cdot\frac{1}{s'_a - s_a}$$

go at most to a constant as one approaches ∞ along all rays but two in the s_a, s_b plane, so that making G_0 a first-degree polynomial or better would give it a stronger asymptotic behavior than the strong-interaction part and might require further subtractions.

D. Symmetries of the $|\Delta I| = \frac{1}{2}$ Rule

Experimentally the branching ratios to the various modes of decay plus the relative magnitudes of the Dalitz plot slopes indicate that in general the decays obey the $|\Delta I| = \frac{1}{2}$ rule with perhaps some small admixture of $|\Delta I| = \frac{3}{2}$ (i.e., the final state is $I = 1$ with

perhaps a small admixture of $I = 2$). In what follows we shall assume that the $|\Delta I| = \frac{1}{2}$ rule holds and that the final state is $I = 1$ only.

Following Khuri and Treiman we can as a matter of convenience pretend that the K meson has I spin = 1 and that I spin is conserved in the decay. Letting ρ, α, β, and γ be the charge indices of the K, π_a, π_b, and π_c mesons, we can write the invariant matrix element for the decay as

$$M_{\rho;\alpha\beta\gamma} = A\,\delta_{\rho\alpha}\,\delta_{\beta\gamma} + B\,\delta_{\rho\beta}\,\delta_{\gamma\alpha} + C\,\delta_{\rho\gamma}\,\delta_{\alpha\beta}, \qquad (10)$$

where A, B, and C are functions of s_a, s_b, and s_c. From the Bose statistics of the three pion system we have the symmetries

$$(s_b \longleftrightarrow s_c) \quad B \longleftrightarrow C, \quad A \longleftrightarrow A,$$

$$(s_a \longleftrightarrow s_c) \quad A \longleftrightarrow C, \quad B \longleftrightarrow B,$$

$$(s_a \longleftrightarrow s_b) \quad A \longleftrightarrow B, \quad C \longleftrightarrow C.$$

Applying (10) to some cases of interest we have, for example,

$$M_{++-}(s_a,s_b,s_c) = A + B,$$

$$M_{00+}(s_a,s_b,s_c) = -C,$$

$$M_{+-0}(s_a,s_b,s_c) = -C,$$

$$M_{000}(s_a,s_b,s_c) = A + B + C.$$

Expressing everything in terms of τ' decay, we then have the following relations between the amplitudes for the various charge modes of decay:

$$M_{++-} = -M_{+00} - M_{0+0},$$

$$M_{+-0} = M_{00+},$$

$$M_{000} = -M_{+00} - M_{0+0} - M_{00+}.$$

Thus if we wish to impose the symmetry of the $|\Delta I| = \frac{1}{2}$ rule, we can decouple the amplitudes for the different charge modes of decay in the KT equations and derive an equation for only a single amplitude, say the τ' amplitude. All other amplitudes can then be expressed in terms of that amplitude.

E. Equations for τ' Decay

Figure 3 shows the rays and ray labels chosen for τ' decay. For convenience one pair of parallel rays has been collapsed because there is no P wave in that channel. Because of the right-left charge symmetry of Fig. 3 there are only three independent rays, as is apparent in the ray labels chosen.

Putting together now all the things discussed in this section, and letting $\frac{q}{(s)^{\frac{1}{2}}} B \equiv F = e^{i\delta} \sin\delta$, we obtain the following equation for M_{00+}:

$$M_{00+}(s_a,s_b,s_c) = M_{00+}(s_0,s_0,s_0)$$

$$+ \frac{1}{\pi}\int ds' \left(\frac{1}{s' - s_a + i\epsilon} - \frac{1}{s' - s_0 + i\epsilon}\right) \cdot F_2(s')\, M_{1A}(s')$$

$$+ \frac{1}{\pi}\int ds' \frac{1}{s' - s_a + i\epsilon} \cdot F_1(s') \frac{1}{\Delta} M_{1D}(s')\, (s_b - s_c)$$

$$+ \frac{1}{\pi}\int ds' \left(\frac{1}{s' - s_b + i\epsilon} - \frac{1}{s' - s_0 + i\epsilon}\right) \cdot F_2(s')\, M_{1A}(s')$$

Equation (11) Continued next page

Equation (11) Continued

$$+ \frac{1}{\pi} \int ds' \frac{1}{s' - s_b + i\epsilon} \cdot F_1(s') \frac{1}{\Delta} M_{1D}(s')(s_a - s_c)$$

$$+ \frac{1}{\pi} \int ds' \left(\frac{1}{s' - s_c + i\epsilon} - \frac{1}{s' - s_0 + i\epsilon} \right)$$

$$\left\{ \left(\frac{2}{3} F_0(s') - \frac{2}{3} F_2(s') \right) M_{1A}(s') + F_0(s') M_2(s') \right\} , \qquad (11)$$

where

$$M_{1A}(s') \equiv \frac{1}{2}[M_{1U}(s') + M_{1L}(s')]$$

and

$$M_{1D}(s') \equiv \frac{1}{2}[M_{1U}(s') - M_{1L}(s')].$$

Here we have subtracted at the center of the Dalitz plot, $s_a = s_b = s_c = s_0 \equiv \frac{1}{3} \sum m_i^2$. The subtraction does not affect the F_1 terms because they are zero at that spot anyway.

To make a coupled set of integral equations out of (11) one merely evaluates the general matrix element on the left-hand side along the same rays as are being used on the right-hand side. Thus for $M_{1U}(s)$ we substitute into the right-hand side of (11) $s_a = s$, $s_b = \frac{3}{2} s_0 - \frac{1}{2} s + \frac{1}{2} \Delta$, and $s_c = \frac{3}{2} s_0 - \frac{1}{2} s - \frac{1}{2} \Delta$. Similarly for M_{1L}, $s_a = s$, $s_b = \frac{3}{2} s_0 - \frac{1}{2} s - \frac{1}{2} \Delta$, and $s_c = \frac{3}{2} s_0 - \frac{1}{2} s + \frac{1}{2} \Delta$; and for M_2, $s_a = \frac{3}{2} s_0 - \frac{1}{2} s$, $s_b = \frac{3}{2} s_0 - \frac{1}{2} s$, and $s_c = s$. Then for M_{1A} and M_{1D} one just adds and subtracts the appropriate equations for M_{1U} and M_{1L}.

IV. SPECIFIC CALCULATIONS

A. Preface to Specific Calculations

We shall next wish to investigate the solution of (11). Since the nature of the $\pi\pi$ interaction is not known exactly, the best that we can hope for is some sort of intuitive understanding by assuming a range of reasonable input $\pi\pi$ phase shifts and observing the range of output solutions. In order to try to separate the $I = 0$ and $I = 2$ S-wave, and P-wave effects, we shall consider F_0, F_2, and F_1 one at a time to be nonzero, and later combine them in concert.

A few comments about the numerical program for solving (11) might be of interest. Using 25 mesh points per ray requires the inversion of a 75-by-75 complex matrix. An accurate subroutine called LINIT[11] was used for this inversion. The total program required about 15-30 seconds and 76.000 words of storage locations on a CDC 6600 computer. The solution for M_2 was not sensitive to Δ, the amount of separation of the M_1 rays, so a value of $\Delta = 0.5$ was rather arbitrarily chosen and used.

In order to compare our solutions with data, we have taken as our "experimental data" the empirical form[12]

$$|M_2|^2 = 1 + g(s_c - s_0), \quad \text{where} \quad g \approx 0.4.$$

The value, $g \approx 0.4$, is the Dalitz plot slope predicted from an application of the $\Delta I = \frac{1}{2}$ rule to the τ decay data [$g(\tau') = -2g(\tau)$, where $g(\tau) \approx -0.2$], rather than the measured value, $g \approx 0.5$. The experimental data for τ decay are better known than for τ' decay, and the discrepancy between $g \approx 0.4$ and $g \approx 0.5$ indicates some

breaking of the $\Delta I = \frac{1}{2}$ rule, which we assumed in deriving (11). Considering the exploratory nature of the present work, this empirical form with $g \approx 0.4$ should be adequate for our purposes. Using $m_\pi = 1$ and $m_K = 3.6$, this leads on the Dalitz plot to

$$s_0 \equiv \frac{1}{3}\sum m_i^2 = 5.32,$$

$$s_{c\,min} \equiv 4m_\pi^2 = 4.0, \quad |M_2|^2_{min} = 0.47,$$

$$s_{c\,max} = (m_K - m_\pi)^2 = 6.76, \quad |M_2|^2_{max} = 1.57.$$

B. $F_0 \neq 0$

Since the $I = 2$, S-wave phase shift is known to be small, it is natural to begin with the $I = 0$, S-wave channel, which is expected to be more important, to see how close one can come to "fitting" the data using this channel alone. The $I = 0$, S-wave $\pi\pi$ phase shift is of course a subject of some controversy in the literature (for a short review of the current pion-pion phase-shift situation see Jackson[13]). There is agreement, however, that the phase shift should be positive and large ($>60°$) by 700 MeV.

We begin the analysis with just a nonrelativistic scattering length approximation

$$\delta_0 = \tan^{-1}(qa_0), \tag{12}$$

where a_0 is the scattering length. The numerical solution of (11) for M_2 for several choices of a_0 is shown in Fig. 4.[14] The results are somewhat disappointing because the slope of the Dalitz plot is in the wrong direction for positive a_0, and is small unless enormous

scattering lengths are used. The mathematical reason for this can be understood, however, if we return to consideration of the simple, one-dimensional Omnes equation and consult the exact solution, Eq. (4). Substituting

$$\delta = qa \tag{13}$$

into (4) yields a rather flat solution, $|A(s)| = 1.0$, for all s! In other words the solution to the Omnes equation is dependent not so much on the magnitude of the phase shift as it is in how the phase shift varies above or below (13). We can now see that (12) varies on the downward side (for positive a_0) of (13) and thus produces a declining solution for the Omnes equation and for Eq. (11). It is essentially for this reason that Khuri and Treiman get the result $a_0 - a_2 \approx -0.7$ and the possibility that a_0 is negative. We find that $a_0 \approx -1.0$ approximately fits the data, not only for (12) but also for the relativistic scattering length approximation (see Fig. 5),

$$\delta_0 = \tan^{-1}[qa_0/(1 + q^2)^{\frac{1}{2}}] \ . \tag{14}$$

If we wish to stay with the idea that δ_0 is positive, as is indicated by experiment, the way is clear. The phase shift must begin like (13) at low energies but then must rapidly rise above (13). Many forms for achieving this might come to mind. Historically the first form to be used was a pole, the so-called σ (or ϵ) resonance, proposed by Brown and Singer.[5] Using just a simple propagator approximation for the matrix element, they were able to fit the Dalitz plot data by assuming a low mass and moderate width for the resonance,

$m_\sigma \approx 390$-425 MeV and $\Gamma_\sigma \approx 75$-100 MeV, which puts it conveniently just off the edge of the Dalitz plot (360 MeV for K decay and 412 MeV for η decay). Recently there has been some suggestion that the pole could be at 750 MeV, "underneath" the ρ resonance. Using a simple Breit-Wigner form

$$\delta_0 = \tan^{-1}\left(\frac{m_\sigma \Gamma_\sigma(q)}{m_\sigma^2 - s}\right), \quad \text{where } \Gamma_\sigma(q) = \frac{q}{q_\sigma}\Gamma_\sigma, \tag{15}$$

we get the results shown in Fig. 6. Unfortunately, owing to numerical difficulties, we cannot get a good solution for a pole any closer to the Dalitz plot than 450 MeV (we shall discuss this point later). Nevertheless, if the 450- and 750-MeV cases are compared, the trend is clear that the Brown and Singer values in some sense represent an optimum. In order to get a steep incline it is necessary to bring the pole in as close as possible to the edge of the Dalitz plot, say 390-425 MeV. A choice for $\Gamma_\sigma > 100$ MeV will make the graph for $|M_2|^2$ not steep enough, and $\Gamma_\sigma < 75$ MeV will yield too much positive curvature for $|M_2|^2$ on the Dalitz plot.

Another phase-shift form that may be of interest to try is one corresponding to the so-called "up-down solution" of the literature.[13] This solution lies between 60° and 90° over the range 500-1000 MeV rather than rising rapidly through 90° to produce a resonance as for the "down-up solution." A form which rises faster than qa_0 initially (so as to produce a positive Dalitz plot slope), goes through 60° at an energy m_0, and then levels off at 90° is as follows:

$$\delta_0 = \tan^{-1}[qa_0 + (q/q_0)^3(\sqrt{3} - q_0a_0)] \qquad (16)$$

where a_0 is the scattering length, and $q_0 \equiv (m_0^2/4 - 1)^{\frac{1}{2}}$. For lack of a better expression let me refer to form (16) as a "hump." The results of using this form for various values of the parameters a_0 and m_0 is shown in Fig. 7. As can be seen, the steepest slope occurs for the lowest component of qa_0, namely $a_0 = 0$. Also the optimum value for m_0 occurs between 500 and 550 MeV. Values closer than this to the edge of the Dalitz plot produce too much negative curvature, and values further away produce slopes that are too small. Even for the optimum, however, the Dalitz plot slope is only about $\approx$60% of the required slope, so this phase-shift form by itself is inadequate to fit the data.[15]

An even more extreme case

$$\delta_0 = \frac{\pi}{2}\,\theta(E - 500\ \text{MeV})$$

was tried, but the results were not appreciably better; furthermore, this form leads to a logarithmic singularity on the real axis.

A few miscellaneous comments about the foregoing solutions might be of interest. First, for all the hump and scattering-length cases with positive asymptotic phase shift, the numerical $|M_2(s)|^2$ appears to go to zero as s goes to "infinity" (the last mesh point is $s = 1000$), which means that in Eq. (11) the inhomogeneous term, $M_{00+}(s_0,s_0,s_0) = 1.0$, is being cancelled off at "infinity" with a fair degree of accuracy. For example, using the nonrelativistic

scattering length approximation with $a_0 = +1.0$ produces an $|M_2|^2 = 3 \times 10^{-4}$ at $s = 1000$. In fact crude fits can be made to the asymptotic behaviors for the foregoing solutions with the general result that for an asymptotic phase, $\delta_0 = n\frac{\pi}{2}$, $|M_2|^2 \sim s^{-1.6n}$, whereas the amplitude squared for the Omnes equation would go like s^{-n}. For the F_0 poles the numerical problems are worse, but there still is a reasonable degree of cancellation of the inhomogeneous term ($|M_2|^2 = 9.0 \cdot 10^{-3} - 1.0 \cdot 10^{-3}$ at $s = 1000$). Secondly, the hump and scattering-length solutions were tested for cutoff sensitivity by introducing cutoffs past 1000 MeV. ($s \approx 53$). These cutoffs of course produce singularities in the solution at the cutoff point, but otherwise produce no graphable difference in the Dalitz plot region (i.e., less than 1% difference). Thirdly, an interesting numerical problem occurs in (11) and in the Omnes equation for phases outside the range, $-\frac{1}{2}\pi \leq \delta \leq \frac{1}{2}\pi$, as occurs, for example, for poles $(0 \leq \delta \leq \pi)$. The $F \equiv (e^{2i\delta} - 1)/2i$ has an ambiguity in that $\delta \pm n\pi$ gives the same F, so that a very reasonable phase shift such as $\delta = +135^\circ$ would be equivalent to another reasonable phase shift, $\delta = -45^\circ$. Normally the assumption of analyticity for F and M admits only one solution, but, for a numerical problem that does not stress analyticity for F and M, one can often get solutions that appear to correspond to changing the phase rapidly from δ to $\delta - \pi$ when δ becomes greater than $\frac{\pi}{2}$. For our calculations we get around this problem by factoring out of the unknown integrand the major expected violent behavior near poles, and treating that part more exactly. In this way the remaining unknown portion of the integrand is likely to be smoother (see Appendix

B for numerical integration techniques). With this improvement in integration we always managed to get the correct solution, provided that the pole is not too close to the Dalitz plot. The cause for the problem when the pole is near the Dalitz plot is still unclear. The major cause appears to be related to the fact that there is a cusp in M_{1A} at $s = 7.96$ [in (11), $\frac{3}{2} s_0 - \frac{1}{2} 7.96 = 4.0$]. The closer the pole approaches this cusp, from either above or below, the worse the solution becomes, going asymptotically to a large constant at $s = \infty$. It may be necessary to factor this cusp behavior out in some manner in the numerical integration of $F_0 M_{1A}$ in order to get a good solution. As long as $m_\sigma \geq 450$ MeV (550 MeV for η decay), however, no problem is encountered.

Lastly there is a threshold cusp problem, most noticeable for large negative s-wave scattering lengths. Numerous efforts were made to get rid of this cusp by improving the numerical accuracy of the calculation (e.g., increasing the number of mesh points near threshold, improving the weights for numerical integration by taking into better account the square root nature of the threshold branch point for F, etc.). All of these efforts consistently yielded the same solution, however. The cause for this cusp is still a mystery. The numerical solution of the Omnes equation using these same phase-shift forms produces no such curvature. Since experiment would appear to indicate that actual three-body final states in nature do not exhibit such cusps or positive curvature near the physical subenergy thresholds, it would

appear to be a fault of the model or numerical technique that they occur in our calculations. This cusp will not bother us so much in our more realistic examples, however.

C. $F_2 \neq 0$

Figures 8 and 9 show the effect of using nonrelativistic and relativistic scattering length approximations, respectively for F_2. The sharp break in M_2 that occurs at $s = 3\,s_0 - 8 = 7.96$ is due to the fact that s_a and s_b go below threshold at that point (see Fig. 3). In comparing the F_2 scattering-length results with F_0 one can make the remarkable observation that for $a_2 = -a_0$ one obtains very nearly the same graph for $s < 7.96$. This is in keeping with the KT result, $a_0 - a_2 \approx -0.7$, which depends only on the linear combination $(a_0 - a_2)$, and not on the individual magnitudes. Accordingly we find that $a_2 \approx +1.0$ will approximately fit the data.

As can be observed, the threshold cusp problem persists for F_2 as well as F_0. In fitting asymptotic behaviors we find that for $\delta_2 = n\,\frac{\pi}{2}$, $|M_2(s)|^2 \sim s^{-1.2n}$.

The experimental $I = 2$ phase shift is reasonably well known. The form used by most serious phase-shift analysts is the one by Baton et al.,[17]

$$\delta_2 = \tan^{-1}\left(\frac{qa_2}{1 + \frac{1}{2}\,a_2 r_2 q^2}\right) \qquad \text{where } a_2 \approx -0.052 \text{ and the effective range } r_2 \approx 1.9. \tag{17}$$

Analytically, however, (17) goes sharply to $-\pi$ at 1260 MeV ($s \approx 85$). To prevent this unreasonable behavior we artificially limit δ_2 to be -21° for 970 MeV ($s \approx 50$) and beyond, which is the last data point

of Baton et al. This form is our standard choice for a realistic $I = 2$ phase shift for use in later applications. We shall refer to this choice as the "Baton F_2," even though strictly speaking Baton et al. are responsible for only the first portion of it. A cutoff or any other similar procedure could just as easily have been used and would make little difference. Figure 10 shows the mild nature of the solution for M_2 for Baton's F_2 used alone.

D. F_0 and $F_2 \neq 0$

Since we previously found that exchanging $a_0 = \pm 1.0$ and $a_2 = 0.0$, for $a_0 = 0.0$ and $a_2 = \mp 1.0$, produced the same Dalitz plot curves, it might be interesting to test the KT hypothesis further, that is, that the slope depends only on the combination $a_0 - a_2$. In Figs. 11 and 12 are shown the results for various sets of nonrelativistic and relativistic scattering lengths respectively. In support of the KT hypothesis it can be seen that $a_0 \approx -0.5$ and $a_2 \approx +0.5$ will approximately fit the data, and that the sets $a_0 = +0.5$, $a_2 = +0.5$, and $a_0 = -0.5$, $a_2 = -0.5$, cancel out remarkably for $s < 7.96$ but behave quite differently beyond this point.

Figure 13 shows the results of combining the gentle Baton F_2 with two typical previous $I = 0$ cases. The solutions are changed very little for $s < 7.96$, but are slightly larger asymptotically. The combinations go nearly to zero asymptotically in spite of the fact that δ_2 by itself would produce a growing solution at infinity. The F_0 pole, $m_\sigma = 750$ MeV and $\Gamma_\sigma = 250$ MeV, was chosen for graphing because it showed the largest graphable difference when combined with δ_2.

E. F_0, F_1, and $F_2 \neq 0$

The first thing one might wish to try when analyzing the effects of the inclusion of P waves would be to try a P-wave case by itself. Upon setting $F_0 = 0$ and $F_2 = 0$ in (11), however, one discovers that the only solution is $M_{00+}(s_a,s_b,s_c) = M_{00+}(s_0,s_0,s_0) = 1.0$, regardless of F_1! The numerical solution of (11) reassuringly also yields 1.0. This result has an intuitive interpretation. If the "primordial weak amplitude," the inhomogeneous term in (11), is constant and so has no projection into any of the $I = 1$, P-wave, $\pi\pi$ channels, then there can be no P-wave rescattering unless there is some S-wave rescattering present which can give contributions to those channels. In other words there can be no P-wave rescattering amongst the pions unless there is also some S-wave rescattering amongst them. Mathematically the way that this shows up is that in the equation for M_{1D}, considered to be uncoupled for the moment, there is no inhomogeneous term. There are only effective inhomogeneous terms involving integrals over F_0 and F_2.

Accordingly, to begin an orderly investigation we shall first combine F_1 with F_0 and use nonrelativistic scattering lengths for both. For P waves this of course means

$$\delta_1 = \tan^{-1}(q^3 a_1), \tag{18}$$

where a_1 is the P-wave scattering length. Figure 14 shows the effect of adding increasing amounts of P wave to a case with $a_0 = 0.2$. Interestingly enough, the effect of adding small amounts of P wave is

to tilt the Dalitz plot slope in the desired direction. In the solution, what apparently happens is that a "line of zeros" appears in the s_a, s_b, s_c plane at $s_c = -\infty$ (that is, the solution is zero everywhere along a line of fixed s_c), and advances towards the Dalitz plot as the P wave is increased. This line of zeros can be seen approaching the Dalitz plot region if one looks at the solution for M_{1U} and M_{1L} (see Fig. 3), and after entering the Dalitz plot region the line can be seen in M_2 as well. This is what gives rise to the dramatic dips in Fig. 14. When the line of zeros approaches the subtraction point, $s_c = 5.32$, for $a_1 \approx 0.35$, the solution of course becomes quite violent. Since the experimentally observed Dalitz plot has positive slope, the line of zeros will have to have $s_c < 4$ in order to fit the data.

If a_0 is changed to +1.0 the picture looks much the same as Fig. 14, but rotated clockwise somewhat to account for the different starting point (the F_0-only solution). The line of zeros still crosses the subtraction point for $a_1 \approx 0.35$. If the Baton F_2 is added to the mix, the effect on the Dalitz plot is roughly the same as would be accomplished by reducing a_1 by about 25%.

A study of the effect of introducing cutoff into F_1 and F_0 was made to determine the sensitivity of the solution. It was found that introducing a cutoff into F_0 when F_1 is present makes a bigger change in the Dalitz plot slope than when F_1 is absent. Introducing the cutoff into F_1 with F_0 present makes a comparable change in slope, but in the opposite direction. Introducing a cutoff

into F_1 at $s = 51$ is comparable in effect to increasing a_1 by ≈ 0.1. The largest effect occurs for those cases in which the line of zeros is near the Dalitz plot and the subtraction point.

Figure 15 shows the effects of adding increasing amounts of scattering length P wave to an $I = 0$ hump case. The results are similar to those in Fig. 14 except that here, of course, the F_0-only solution already has a positive slope in the Dalitz plot. The best fit to the data occurs for an $a_1 \approx 0.15$.

The separation between the M_{1U} and M_{1L} rays in the Mandelstam plane corresponds to a smaller and smaller difference in $\cos\theta$, the cosine of the $\pi\pi$ scattering angle, as one goes out along the rays, if their separation, Δ, is a constant. Thus one might expect M_{1D} to become smaller and smaller at large s. This is in fact the case. If one makes Δ a growing, linear function of s, corresponding asymptotically to a constant difference in $\cos\theta$, M_{1D} does not fall off so rapidly, but then the integrals involving M_{1D} have a linear $\Delta(s')$ in the denominator so that there is no particular convergence problem. Importantly there is virtually no change in the solution for M_2 when Δ is "widened" in this manner.

To make use of more realistic δ_1's, we recognize the existence of good experimental data for δ_1 at the higher energies near the ρ pole, but note that the value of the scattering length is not so well determined. Accordingly we adopt a parametrization of δ_1 by Olsson[18] which will allow us to vary the scattering length and not disturb the pole parameters too greatly. Explicitly we take

$$\delta_1 = \tan^{-1}\left(\frac{c_1 a_c q^3/(1+q^2)^{\frac{1}{2}}}{1 + (c_1 - 2)\left(\frac{q}{q_r}\right)^2 + (1 - c_1)\left(\frac{q}{q_r}\right)^4} \right), \quad (19)$$

where $a_c \equiv w_r^2 \Gamma_r / 8 q_r^5$,

where $w_r = 755$ MeV ≈ 5.51 ,

$\Gamma_r = 110$ MeV ≈ 0.80 ,

$q_r \approx 2.57$,

and where c_1 is a free parameter. The scattering length is given by

$$a_1 = c_1 a_c \approx c_1 \times 0.0273.$$

The "effective scattering length" of the low energy portion of (19) is not so easily changed by c_1, however, because with large c_1, the higher-order terms in the effective range expansion soon become important. The net effect is to reduce the phase shift so as not to disturb the resonance features too greatly. To emphasize the care that must be used in comparing theoretical scattering lenths (defined at threshold) with empirical scattering lengths found from fitting low energy data, we give the following example. A fit of (19) to the low energy experimental data of Baton et al.[17] requires a $c_1 \approx 10$ or 20, which would imply $a_1 \approx 0.27$ or 0.54, but if one fits a scattering length to the lowest energy data point, at $q = 1.6$, one obtains a value of only $a_1 \approx 0.06$.

Figure 16 shows the effect of combining this F_1 pole with the $a_0 = 0.2$, $m_0 = 500$ MeV, F_0 hump, for several choices of c_1. As can be seen, the addition of the P wave dramatically steepens the

Dalitz plot slope in the proper direction. By comparing with Fig. 15 we can see that the ρ pole with $c_1 = 10$ is comparable in effect to a P-wave scattering length, $a_1 = 0.15$. Figure 17 shows the effect of combining the preceeding F_0 and F_1 with the limited Baton F_2. The effect of this addition is not large in the Dalitz plot. Mostly it lessens the slope of the $c_1 = 10$ and $c_1 = 20$ cases so that they come close to fitting the experimental data. If the above calculations are repeated with the $a_0 = 0.0$, $m_0 = 500$ MeV, F_0 hump, the $c_1 = 10$ and $c_1 = 20$ cases exhibit steeper slopes than the data, mainly because the initial slope of the F_0-only solution is greater.

Figure 18 shows the effect of combining the F_1 pole with the $m_\sigma = 750$ MeV, $\Gamma_\sigma = 250$ MeV, F_0 pole, for several choices of c_1. Again the addition of the P wave dramatically steepens the Dalitz plot slope in the proper direction. With the addition of F_2, in Fig. 19, the steepest slopes are dampened somewhat so that the $c_1 = 10$ and 20 cases come close to fitting the data again. If in the above the $m_\sigma = 450$ MeV pole is used, the resulting Dalitz plot slopes are too steep because of the steeper initial slope.

There is an ambiguity in the $I = 0$ phase shifts, of course, but it is interesting that if one takes the two most popular choices, corresponding to the up-down and down-up solutions, and adds reasonable amounts of P-wave and $I = 2$ interactions, one can come this close to fitting the experimental data.

Some comments are perhaps in order at this point. The first is that the addition of P wave to the problem appears to have a surprisingly large effect. This is consistent with the observation by

Schult and Barbour,[7] who found in their calculations that P waves could have large effects. Nevertheless the fact that it is large means that this portion of the calculation is likely to invite the most controversy. If one were to search for possible numerical weak points in the calculation, there are two that come to mind. First is the possibility that since the equation for M_{1D} has no inhomogeneous term, it may in some way be more unstable numerically. Secondly with regard to the F_1 pole, all the previously mentioned problems in obtaining a good numerical solution when a pole is present apply to the F_1 pole as well as the F_0 pole. In fact, although the same numerical techniques were used on the F_1 pole as for the F_0 pole (see Appendix B), the F_1 pole showed greater sensitivity to the exact nature of the techniques than did the F_0 pole. The numerical techniques for handling the poles were developed on the Omnes equation, for which there is an exact answer for comparison. Although it is reasonable to expect the same techniques to work for the coupled equations with F_0 and F_1 poles, they of course can never be compared with an exact answer. Since the equations involving the F_0 pole are more similar to the Omnes equation than the equations involving the F_1 pole, perhaps there can be greater confidence for the techniques to work for the F_0 pole than the F_1 pole.

F. η Decay

By just changing the mass of the K meson in the above calculations to that of the η meson ($m_K \approx 3.6$ and $m_\eta \approx 4.0$) we should be able to calculate the decay spectrum of the η meson. This simple procedure assumes that the "bare" decay matrix element for η

decay is a constant as before, in spite of a different decay mechanism. This is probably contrary to current algebra which gives zero for the decay rate if the matrix element is flat.[19] It should be observed here that Neveau and Scherk[8] have made an attempt to impose the constraints of current algebra at the two soft-pion points and generate corrections to the linear (and hence zero) matrix element via final-state interactions in twice-subtracted KT equations.

By virtue of the assumed I-spin symmetry of the final state, Eq. (10), the M_2 of τ' decay will correspond to the S_{+-} spectrum of $\eta \to \pi^+\pi^-\pi^0$. Figures 20-23 show the extension to η decay of some selected cases of interest from K decay. Again the "experimental points" shown are just the result of substituting into the empirical formula, $|M_2|^2 = 1 + 0.4\ (s_c - s_0)$, and shown here for rough comparison only (see Cnops et al.[20]). The general features of the calculations tend to confirm and accentuate our previous conclusions. It is just as impossible as before to fit the Dalitz plot with $I = 0$ cases alone unless one assumes a pole on the edge of the Dalitz plot. The F_0 pole closest to the Dalitz plot for which we can obtain a reliable numerical solution is $m_\sigma = 550$ MeV. This pole unfortunately has too large a mass to fit the data, but, as before, it indicates that a pole closer to the edge of the Dalitz plot would do better. The best $I = 0$ hump case does particularly poorly when extended to η decay. The best fits from before involving P wave, however, continue to fit as nicely for η decay, in accordance with the final-state interaction philosophy.

G. Nonflat Inhomogeneous Term

It is of interest to determine the changes that occur if the bare matrix element has some energy dependence, instead of being constant as in the foregoing discussion. There may be contributions to the inhomogeneous term which depend on the $\pi\pi$ final-state interactions, but we ignore this possibility for the moment and speak as if the inhomogeneous term were a Born term or bare weak interaction term. We chose a linear term of the form

$$M_{00+}(s_a,s_b,s_c)_{bare} = 1 + \frac{1}{2} g(s_c - s_0). \qquad (20)$$

For K decay, current algebra[2] predicts such a matrix element in the physical region with $g \approx 0.4$, which of course will fit the data.

Figure 24 shows the effect of using just a simple scattering length, $a_0 = 0.2$, with a bare term of varying amounts of g. The most striking observation is that the final-state interaction exaggerates the slope of the bare matrix element, $\frac{1}{2} g$, by roughly a factor of 4. The amount of exaggeration is a function of the $\pi\pi$ interaction. For example, for $a_0 = 0$ the factor is of course unity, for $a_0 = 1.0$ the factor is roughly 10, and for the hump case, $a_0 = 0.2$, $m_0 = 500$ MeV, it is also 10. There is apparently no problem of nonconvergence of integrals for these cases because if one measures the asymptotic behavior of F_0 cases for which $\delta_0 \sim \frac{\pi}{2}$ asymptotically, one obtains $|M_{1A}|$ and $|M_2| \sim s^{\alpha}$, with $\alpha \approx +0.6$. For comparison $\alpha \approx -0.8$ when $g = 0$. For F_2 cases in which $\delta_2 \sim \frac{\pi}{2}$ asymptotically, $\alpha \approx +0.6$ as compared with $\alpha \approx -0.6$ when $g = 0$. This suggests that negative scattering lengths will yield

divergent integrals, which indeed is found to be true. We were unable to measure the asymptotic behavior accurately for an F_0 pole case because of zeros near the "asymptotic region," but the α appears to be approaching something less than one and these cases presumably converge also.

Some scattering length cases for F_1 were tried by themselves, since (20) has a nonzero projection into the P-wave channels. The solutions appeared to converge, but showed an even stronger exaggeration of g, for example a factor of -38 for $a_1 = 0.1$. The combination $a_1 = 0.1$ and a small $g = -0.01$ can produce a solution that goes through the data points.

The slope of the bare matrix element (20) by itself causes a line of zeros in the Mandelstam plane. Because of the exaggeration of that slope by the $\pi\pi$ interaction, the zero rapidly enters the Dalitz plot, with increasing g, and approaches the subtraction point, s_0. If one wishes to test the response of previous cases of interest to the introduction of a bare interaction slope, one must do so gently, e.g., $|g| \leq 0.10$, otherwise the solutions rapidly lose their identity and any correspondence with reality. Figure 25 shows such a "gentle" perturbation of a hump case. This violent modification is in contrast to the results on K decay of Neveau and Scherk.[8] The explanation for the difference lies in the fact that they have two soft-pion subtraction points. Their amplitude is therefore less susceptible to the influences of the final-state interactions.

The sensitivity of solutions to g is due to the asymptotic behavior of (20). If instead we use a bare interaction term of the form

$$M_{00+}(s_a,s_b,s_c)_{bare} = 1 + \frac{1}{2} gr \tanh[(s_c - s_0)/r] \qquad (21)$$

this sensitivity disappears. Little or no exaggeration of the slope occurs, and all cases which previously converged for a flat matrix element, converge for (21). The only difference is that the solution in the region of the Dalitz plot is "tipped" an extra amount, given by $\frac{1}{2}$ g. An interesting aside observation is that solutions which would ordinarily have gone to zero asymptotically now go to approximately $\frac{1}{2}$ gr instead. Figures 26 and 27 show the effect of using (21) on some cases of interest, with r chosen to be 2.5 (the results are not sensitive to this particular choice of r).

V. EXTENSION OF THE KT EQUATIONS TO ALLOW UNEQUAL MASSES FOR THE CHARGED AND NEUTRAL PIONS

A. Derivation of the Equations Used for Approximate Numerical Solution of the KT Equations

It was felt that the KT equations might be an appropriate vehicle for studying the effects to be expected from the fact that the charged and neutral pions have slightly different masses. Accordingly a study was undertaken to try to incorporate the slight pion mass difference into the KT equations. The starting point is Eq. (5). There we can see immediately the most important changes to be made. First, the θ function means that the various discontinuities can "turn on" at different values of s, depending upon the masses of the pions in the intermediate state. Therefore we will have to begin the various integrals involved in the KT equations at the different thresholds. Secondly, there is a $q_{\beta\gamma}(s)$ factor, which originally came from phase space, and which also depends on the masses of the intermediate pions. This factor goes to zero, of course, at the intermediate-state threshold, and is rather insensitive to small variations in the threshold at large s. Thirdly, it can be seen that the $\pi\pi$ interaction will have to be expressed in the form of an invariant matrix element, for the various initial and final charge states. This invariant matrix element, of course, does not go to zero at any threshold, but goes smoothly to the appropriate scattering length, i.e., the q from phase space has the threshold kinematics and the B has the dynamics.

It was decided to make a calculation of only one test case, namely the τ and τ' system. Both τ and τ' are required because the intermediate-state pions can have different charge from the external pions, and thus the amplitudes for the τ and τ' decays will become coupled through the KT integral equations. Previously, with the equal-mass problem, we could reduce the complexity of the problem with the imposition of the $|\Delta I| = \frac{1}{2}$ rule and force the final state to be $I = 1$ only. But here the electromagnetic splitting of the pion masses is specifically an I-spin breaking effect so that exact $|\Delta I| = \frac{1}{2}$ will no longer hold. For the next step we make use of experimental evidence[12] that indicates that the τ and τ' decay final states are mostly $I = 1$, with some small admixture of $I = 2$, and no evidence for $I = 3$. A simple analysis of the various I-spin states of three pions[21] reveals that $I = 3$ will lead to a ratio of the τ and τ' amplitudes evaluated at the center of the Dalitz plot of $1/2$, as contrasted with $-2/1$ for $I = 1$. The $I = 2$ does not contribute at the center of the Dalitz plot. The evidence for the $I = 2$ admixture is that the ratio of the center-point τ and τ' amplitudes is just as it should be for the $|\Delta I| = \frac{1}{2}$ rule, but that the ratio of the Dalitz plot slopes is -2.60 ± 0.12, or about five standard deviations greater than the -2 ratio allowed by the $|\Delta I| = \frac{1}{2}$ rule. The way chosen to mimic this situation for the KT equations was to take -2 as the inhomogeneous term for the τ equation and $+1$ for the τ'. This will discriminate against the $I = 3$ final state and yet allow the ratio of the Dalitz plot slopes to vary from the strict $|\Delta I| = \frac{1}{2}$ rule value.

In order to keep the problem simple, no P-wave final-state interactions were assumed, so that the No. 1 rays could be collapsed to one (see Fig. 3). The ray labeling chosen is $\tau 1$, $\tau 2$, $\tau' 1$, and $\tau' 2$, similar to before, with the label, 2, referring to the odd pion spectra. There is a total of four rays of 25 mesh points each, which requires the solution of a 100-by-100 complex matrix. Using the numerical matrix inversion subroutine called LINIT,[11] the program to solve the KT equations required approximately 40 seconds on a CDC 6600 and 103,000 words of central memory core.

Defining the integral operators

$$L_a \equiv \int^{\infty} ds' \left(\frac{1}{s' - s + i\epsilon} - \frac{1}{s' - s_0 + i\epsilon} \right),$$

$$L_b \equiv \int^{\infty} ds' \left(\frac{1}{s' - (\frac{3}{2} s_0 - \frac{1}{2} s) + i\epsilon} - \frac{1}{s' - s_0 + i\epsilon} \right),$$

the set of coupled integral equations for the unequal-mass case is

$$M_{\tau 1}(s) = -2 + (L_a + L_b)(2q_{+-} B_{+-,+-} M_{\tau 1} + q_{00} B_{00,+-} M_{\tau' 2}) + L_b(q_{+-} B_{++,++} M_{\tau 2})$$

$$M_{\tau 2}(s) = -2 + L_a(q_{+-} B_{++,++} M_{\tau 2}) + L_b(4q_{+-} B_{+-,+-} M_{\tau 1} + 2q_{00} B_{00,+-} M_{\tau' 2})$$

Equation (22) continued next page

Equation (22) continued

$$M_{\tau' 1}(s) = 1 + (L_a + L_b)(2q_{+0}\, B_{0+,0+}\, M_{\tau' 1}) + L_b(2q_{+-}\, B_{+-,00}\, M_{\tau 1} + q_{00}\, B_{00,00}\, M_{\tau' 2}) ,$$

$$M_{\tau' 2}(s) = 1 + L_a(2q_{+-}\, B_{+-,00}\, M_{\tau 1} + q_{00}\, B_{00,00}\, M_{\tau' 2}) + L_b(4q_{+0}\, B_{0+,0+}\, M_{\tau' 1}) , \qquad (22)$$

where the appropriate θ function is understood to go with each of the q's.

In choosing the parametrization for the $\pi\pi$ invariant matrix elements the goal was to make them correspond as closely as possible to the familiar I-spin amplitudes, because the main reason for breaking the symmetry at lower energies is presumably just due to the mass splitting. It is probably adequate just to approximate the matrix elements by scattering lengths near threshold, but in order to ensure that the parametrization is unitary and has the correct analyticity properties at the various thresholds, we resort to a K-matrix formalism for nested thresholds. The matrix elements are:

$$B_{+-,+-}(s) = \tfrac{1}{2}\,[K_{bb}(s) - iq_{00}(s)]/D(s),$$

$$B_{00,+-}(s) = B_{+-,00}(s) = (\tfrac{1}{2})^{\frac{1}{2}}\,[-K_{ab}(s)]/D(s),$$

$$B_{00,00}(s) = [K_{aa}(s) - iq_{+-}(s)]/D(s),$$

$$B_{++,++}(s) = 1/[f_2(s) - iq_{+-}(s)],$$

$$B_{+0,+0}(s) = \tfrac{1}{2}/[f_2(s) - iq_{+0}(s)],$$

where $$q_{\alpha\beta}^{\,2}(s) \equiv [s - (m_\alpha + m_\beta)^2][s - (m_\alpha - m_\beta)^2]/4s,$$

$$K_{aa}(s) \equiv \tfrac{1}{3}[2f_0(s) + f_2(s)],$$

$$K_{ab}(s) \equiv -\frac{\sqrt{2}}{3}\,[f_0(s) - f_2(s)],$$

$$K_{bb}(s) \equiv \tfrac{1}{3}\,[f_0(s) + 2f_2(s)],$$

$$D(s) \equiv [K_{aa}(s) - iq_{+-}(s)][K_{bb}(s) - iq_{00}(s)] - K_{ab}^{\,2}(s),$$

and where $f_I(s) \equiv q(s) \cot \delta_I(s)$ is the real, analytic, isospin-invariant, effective range function.

There is a slight ambiguity as to which points in the τ and τ' Dalitz plots the relative normalization of $-2/1$ should refer to, because of the slightly different Q values of the two decays. However, such problems are of second order in nature and different choices of points near the centers of the Dalitz plots will give nearly identical solutions.

B. Specific Calculations

Numerical solutions were obtained for the set of coupled integral Eqs. (22), for some simple $I = 0$ and $I = 2$ cases of interest, namely a hump for $I = 0$ and a Baton choice for $I = 2$. When 1.0, 1.0, and 3.6 are substituted for the masses of the π^0, $\pi^{\pm}$, and K^+ respectively, i.e., the equal-mass case, the solutions obtained are nearly identical with those obtained previously with Eq. (11). This is a good verification that the prescription for using the inhomogeneous terms, -2 and +1, with the increased number of amplitudes will still yield the $|\Delta I| = \frac{1}{2}$ results in the limit of no mass splitting.

When the experimentally observed ratios, 1.0, 1.034, and 3.659, are substituted for the masses of the π^0, $\pi^{\pm}$, and K^+ respectively, solutions like that shown in Fig. 28 are obtained. The most striking feature of the solution is the cusp for $M_{\tau'2}$ at the $\pi^+\pi^-$ threshold ($s \approx 4.27$). Since the physical threshold for $M_{\tau'2}$ is the $\pi^0\pi^0$ threshold ($s = 4.0$), the cusp occurs in the physical region of the Dalitz plot and would occur as a "line of cusps" at $s_c = 4.27$, across one edge of the plot. Physically the situation is as follows. The K^+ can decay into $\pi^+(\pi^+\pi^-)$, but then the $\pi^+\pi^-$ can inelastically scatter into a channel with a lower threshold, namely $\pi^0\pi^0$. The subenergy of the $\pi^+\pi^-$ has to be above the $\pi^+\pi^-$ threshold, however, or otherwise this process cannot occur. Mathematically the cusp arises from the first integral in the $M_{\tau'2}$ equation of Eqs. (22). On the Dalitz plot $M_{\tau 1} \approx -2$, and near threshold $B_{+-,00} \approx \frac{1}{3}(a_2 - a_0)$.

Since $a_2 - a_0$ is expected to be negative, this first integral will be positive for s just below the $\pi^+\pi^-$ threshold. The integral will decrease rapidly as s goes further below threshold, causing the sharp break to appear in the solution at $s = 4.27$. When $a_2 - a_0 = 0$, no cusp appears in the solution.

The solution shown in Fig. 28 has a cusp for $M_{\tau 2}$ as well as $M_{\tau' 2}$, although it is not discernible, and above the $\pi^+\pi^-$ threshold the Dalitz plot slope of $M_{\tau' 2}$ is -2 times that of $M_{\tau 2}$ just as for the $|\Delta I| = \frac{1}{2}$ rule. However, the $M_{\tau 2}$ cusp is included in its physical region whereas the $M_{\tau' 2}$ cusp is not, so that the "average" slope of the $M_{\tau' 2}$ Dalitz plot will be steepened, compared with $M_{\tau 2}$, in the proper sense to agree with experiment. In fact if one makes least-squares fits of straight lines to the two physical region slopes of the example of Fig. 28, one obtains a slope ratio of roughly -2.6.

It is interesting that the unequal-mass effect has the proper direction and can have a proper order of magnitude to agree with experiment, but unfortunately when one examines the data of Davison et al.[22] on τ' decay, there is no evidence for a cusp at $s = 4.27$. One can get rid of the cusp in our calculations by setting $a_2 - a_0 \approx 0$, but that simultaneously makes the slope ratio revert to -2, and would imply that the $I = 2$ final-state admixture is due to some other mechanism besides the unequal mass of the pions. A different possibility is that $a_2 - a_0 \neq 0$, but that the cusp shown in our calculations is too large due to some poor approximation we may have made. It is interesting to speculate that perhaps just using S waves for the $\pi\pi$

amplitude is inadequate, because it can then be readily seen that the KT integral equations imply double discontinuities for the decay amplitude that have sharp, sector type boundaries (e.g., s and $t \geq 4$, s and $u \geq 4$, and t and $u \geq 4$) instead of the expected curved boundaries.

VI. AREAS OF IMPROVEMENT

Consider in what areas this study could be improved. The inclusion of more partial waves is probably not warranted right away, partly because of energy considerations, but mostly because the whole question of how to extend the KT equations to include more partial waves needs to be examined and answered satisfactorily first. This extension should of course be some well-defined approximation to the Mandelstam representation. In this paper we have made a guess at an extension which it is hoped is not too bad for P waves. Another possibility for improvement is to include the "initial state interactions" of S-wave $K\pi \to K\pi$ scattering. This would lead to a coupling of all the K-meson three-pion decay modes, but an imposition of the $|\Delta I| = \frac{1}{2}$ rule could reduce the problem to tractable size again. It would also introduce the complex conjugate of the unknown decay amplitude into the integral equation, which would require special handling. However, if the belief is held that the η- and K-decay Dalitz-plot slopes arise from the same origin, then the $K\pi$ intermediate state would not be expected to have large contributions because it is present in one case and not in the other.

One can also look for better numerical ways of approaching the problem. One possibility is that instead of solving for the amplitude at 25 mesh points along a ray one could expand the amplitude in a finite number of terms of some orthonormal basis along the ray, and then solve for the expansion coefficients. The hope of this kind of procedure would be that only a small number of basis terms would be required for comparable accuracy. This would also make the calculation

accessible to smaller computers because of the smaller matrix to invert. If it turned out that 25 basis terms for each ray were required to achieve comparable accuracy, then there would be no advantage to this approach. In this connection one would have to worry about the non-analytic behavior of the ray amplitudes at $s = 7.96$ $(\frac{3}{2} s_0 - \frac{1}{2} s = 4.0)$, and how many terms would be required to reproduce this behavior, especially along the No. 1 rays where this nonanalytic behavior is more

. Another possible approach would be to expand $M_{00+}(s_a,s_b,s_c)$ in partial waves in the various $\pi\pi$ subchannels and then obtain a coupled set of integral equations for these partial-wave amplitudes rather than for ray amplitudes. At some point in the derivation an equation similar to (9) will be reached, and where in order to partial-wave analyze the left-hand side, it will be necessary to integrate over two of the three singular denominators. With only one singular denominator remaining it may then be possible to convert the equation into a Fredholm equation by standard techniques (see Muskhelishvili[23] and Pogorzelski.[24,25]

VII. CONCLUSIONS

We have made some steps towards solving numerically the equations of Khuri and Treiman for K and $\eta \to 3\pi$ and extending them to include P-wave interactions, the effects of a nonflat bare matrix element, and the effects of unequal masses for the charged and neutral pions. Our results show that it is rather difficult, with S waves alone, to get a steep enough slope for the matrix element on the Dalitz plot when the bare matrix element is a constant. The S-wave phase shifts required to fit the Dalitz plot data are usually quite unphysical (e.g., $a_0 - a_2 = -1.0$, an F_0 pole located just off the edge of the Dalitz plot, etc.). In our calculations the inclusion of P waves appears to have a large effect on the Dalitz plot. If we assume $I = 0$ phase shifts of either the up-down or the down-up variety, and if we assume $I = 1$ and $I = 2$ phase shifts which are consistent with the experimentally determined phase shifts, then the resulting solutions of the KT equations with a constant inhomogeneous term yield Dalitz plot slopes which fit the data. The inclusion of P waves in the KT equations probably deserves more study, however, perhaps with different numerical approaches.

With the same assumption of a constant inhomogeneous term, the extension of the K-decay solutions to η decay follows trivially just from changing the mass of the decaying particle.

If the inhomogeneous term of the KT equations is given a linear term, $M_{bare} = 1 + \frac{1}{2} g(s_c - s_0)$, the effect is to tilt the solutions, but by an exaggerated amount. If the inhomogeneous term is changed to

$M_{bare} = 1 + \frac{1}{2} gr \tanh[(s_c - s_0)/r]$, which gives a slope on the Dalitz plot but goes to a constant asymptotically, the effect is just to tilt the solutions in the region of the Dalitz plot by the amount $\frac{1}{2} g$.

When the masses of the charged and neutral pions are made unequal in the KT equations, the largest effects to be observed in the matrix element are cusps related to thresholds located in the physical region of the Dalitz plot and due to the presence of communicating subchannels. The calculated effects are in a direction agreeing with experiment, thus leading to the speculation that perhaps the unequal masses of the pions might be responsible in large part for the slight amount of $I = 2$ final state observed in the decay.

VIII. ACKNOWLEDGMENTS

I thank Professor J. D. Jackson for suggesting this study, for many pleasant discussions, and for the encouragement necessary for its completion. I also thank Professor S. Mandelstam for helpful discussions.

APPENDIX A. METHOD OF DIRECT NUMERICAL SOLUTION OF INHOMOGENEOUS INTEGRAL EQUATIONS BY MATRIX INVERSION

The method outlined below for direct numerical solution of inhomogeneous integral equations by matrix inversion is a standard numerical technique and is included here only for completeness.[26]

Let us consider the inhomogeneous integral equation,

$$\phi(s) = \phi_0(s) + \int_a^b K(s,s')\,\phi(s')\,ds',$$

where the inhomogeneous term, $\phi_0(s)$, and the kernel, $K(s,s')$, are known functions of s and s', and $\phi(s)$ is the unknown function to be found. Choose a set of N mesh points $\{s_i\}$, and devise a method of approximate numerical integration so that the integral can be replaced by a sum,

$$\int_a^b K(s,s')\,\phi(s')\,ds' \approx \sum_{j=1}^{N} w_{ij}\,\phi_j,$$

where the w_{ij} is now a known set of weights, and where the i refers to s_i and j to s'_j.[27] The integral equation can now be rewritten as a set of N equations in N unknowns, ϕ_j,

$$\phi_i = \phi_{0i} + \sum_j w_{ij}\,\phi_j$$

or

$$\sum_j (w_{ij} - \delta_{ij})\,\phi_j = -\phi_{0i}.$$

This set can now be solved by standard matrix techniques by considering ϕ_j and ϕ_{0i} to be N-dimensional column vectors, and $(w_{ij} - \delta_{ij})$ to be an N-by-N matrix, to be inverted.

A set of m coupled integral equations [such as Eq. (11), where $m = 3$] can be solved in a like manner by combining the individual ϕ vectors "end to end" to make one mN-dimensional vector, and similarly for the matrices.

APPENDIX B. METHOD FOR EVALUATING SINGULAR INTEGRALS NUMERICALLY

Our experience has been that success in the direct numerical solution of singular integral equations by the matrix-inversion method depends heavily on the quality of the numerical integration techniques used. Accordingly it is perhaps useful to write down explicitly the methods that we used in this paper.

We shall wish to integrate numerically, singular integrals of the form

$$\int_{s_t}^{\infty} ds' \, \frac{f(s')}{s' - s}$$

in a manner useful for solving singular integral equations. That is, we shall wish to replace the integral by a sum over a set of mesh points

$$\sum_{j=1}^{N} w_{ij} \, f(s'_j),$$

where the w_{ij} are known weights, which can be evaluated once and used later to integrate an arbitrary function $f(s'_j)$. The naive weight

$$w_{ij} = \frac{1}{s'_j - s_i} \cdot \Delta s'_j$$

will not work because of the ambiguity that arises when $s'_j = s_i$. Besides, the pole is such a violent thing that sampling it with just a few mesh points is not likely to give very accurate results. Also the pole "moves" as s_i is changed, so that trying to put extra points

in the vicinity of the pole would just increase the mesh-point density everywhere. The general philosophy of our method is to try to factor the integrand into a "violent but known" part [such as $1/(s' - s)$] and an "unknown but smooth" part. Then we can handle the smooth part in some crude, approximate manner, and handle the violent part as exactly as possible. The application of this philosophy will become more clear as we proceed.

First let's dispose of the aside problem of the infinite upper limit of integration. We can use the general linear transformation of the form

$$s = \frac{\alpha + \beta x}{\gamma + \delta x}$$

to reduce the range of integration to something finite. If we impose the requirement that the points s_t, s_m, and ∞ map into the points $= -1$, 0, and $+1$, the transformation becomes

$$s = \frac{s_m + (s_m - 2s_t)x}{1 - x} .$$

Here s_m is still arbitrary and can be chosen to suit the particular problem. For our case, $s_t \approx 4$, and we chose $s_m = 8$ as a compromise between emphasizing the Dalitz plot region and the resonance region (e.g., the center of the Dalitz plot, $s \approx 5.3$, corresponds to $x \approx -0.50$, and the ρ resonance occurs at $s \approx +0.74$). The results of course are not sensitive to the choice of s_m. The integral then transforms into

$$\int_{s_t}^{\infty} ds' \, \frac{f(s')}{s' - s} \rightarrow \int_{-1}^{+1} dx' \, \frac{1 - x}{1 - x'} \cdot \frac{f(x')}{x' - x} .$$

The factor $(1 - x)/(1 - x')$ can either be considered part of the violent but known portion of the integrand or combined with the $f(x')$ to become part of the unknown but smooth portion, depending on the expected asymptotic behavior of $f(s')$. For a subtracted integral [such as occurs in Eq. (11) for the $I = 0$ and $I = 2$ portions] the factor can disappear altogether,

$$\int_{-1}^{+1} dx' \frac{1 - x}{1 - x'} \frac{f(x')}{x' - x} - \int_{-1}^{+1} dx' \frac{1 - x_0}{1 - x'} \frac{f(x')}{x' - x_0}$$

$$= \int_{-1}^{+1} dx' \, f(x') \left\{ \frac{1}{x' - x} - \frac{1}{x' - x_0} \right\} .$$

In general, the weight for a subtracted integral is just the difference of the two appropriate weights for the unsubtracted integrals [either with or without the factor $(1 - x)/(1 - x')$ being priorly removed].

Now to evaluate an integral of the form

$$\int_a^b dx' \frac{f(x')}{x' - x}$$

we shall choose a set of mesh points, $\{x_j\}$, and use linear interpolation for $f(x')$ between successive f_j,

$$f(x') \approx \frac{x' - x_{j+1}}{x_j - x_{j+1}} f_j + \frac{x' - x_j}{x_{j+1} - x_j} f_{j+1} . \qquad \text{(B1)}$$

We do not choose either a or b as mesh points because in our original problem $f(a)$ is always zero [due to $q(s)$ factors] and

$f(b)$ is occasionally indeterminate. In the left-end region, between a and x_1, we shall approximate f by just linear interpolation from 0 to f_1. This can be done easily in (B1) by defining $x_0 \equiv a$ and $f_0 \equiv 0$. In the right-end region, between x_N and b, we shall approximate f by just continuing the linear interpolation used between x_{N-1} and x_N. If the first and last mesh points are near the end points then these are not bad approximations.

By using the linear interpolation for f, the following weights can be obtained:

$$\int_a^b dx' \, \frac{f(x')}{x' - x} \approx \sum_{j=1}^{N} w_j f_j,$$

where for $1 \le j \le N-2$

$$w_j = \frac{1}{x_j - x_{j+1}} \left[\{ g(x_{j+1}) - x_{j+1} \, h(x_{j+1}) \} - \{ g(x_j) - x_j \, h(x_j) \} \right]$$

$$- \frac{1}{x_j - x_{j-1}} \left[\{ g(x_{j-1}) - x_{j-1} \, h(x_{j-1}) \} - \{ g(x_j) - x_j \, h(x_j) \} \right],$$

w_{N-1} = same as above except that $g(x_N) \to g(b)$ and $h(x_N) \to h(b)$,

$$w_N = \frac{1}{x_N - x_{N-1}} \left[\{ g(b) - x_{N-1} \, h(b) \} - \{ g(x_{N-1}) - x_{N-1} \, h(x_{N-1}) \} \right], \tag{B2}$$

where g and h are defined as

$$g(t) = \int^t dx' \, \frac{1}{x' - x} = t + x \log(t - x)$$

and

$$h(t) = \int^{t} dx' \frac{1}{x' - x} = \log(t - x).$$

One can put an $x \pm i\epsilon$ prescription easily into the above weights by just using complex logarithms and a small ϵ. If a principal value integral is desired then the arguments of all logs must be the absolute value of the quantities shown. Also in the computer program for a principal value integral, there would have to be a separate test for indeterminate $0 \times \log(0)$ cases, a problem which doesn't occur in the $i\epsilon$ prescription. For $x = x_i - i\epsilon$, $\mathrm{Im}\, w_j = -i\pi\delta_{ij}$ as it should, and for an x between two mesh points [as occur in Eq. (11) denominators of the form $s' - (\frac{3}{2} s_0 - \frac{1}{2} s) + i\epsilon$, for example] the $-i\pi$ is distributed linearly between the weights of the two mesh points, the closer point receiving the larger weight.

Next we come to the problem cases which require special treatment, namely cases in which the $f(x')$ itself has singularities, for example a "square root pole" at $x' = +1$, or poles in the complex plane near the real axis.

If $f(x')$ has some known, violent structure or behavior, $u(x')$, then one can factor it out in the following manner: $f(x') = u(x')[f(x')/u(x')]$, where $u(x')$ can then be regarded as a "violent but known" factor to be collected with the $1/(x' - x)$ to be treated as exactly as possible, and $f(x')/u(x')$ is the new "unknown but smooth" function. In (B2) this can be accomplished by using

$$g(t) = \int^{t} dx' \frac{x'\, u(x')}{x' - x} \quad \text{and} \quad h(t) = \int^{t} dx' \frac{u(x')}{x' - x}$$

and dividing the resulting weight by $u(x_j)$.

Examples of where these problem cases arise are as follows. The $f(x')$ is of course some $F(x')\cdot M(x')$ where $F = (e^{2i\delta} - 1)/2i$ is the $\pi\pi$ interaction and $M(x')$ is the unknown solution to the integral equation. If we consider just the simple Omnes equation and let δ go to $-\frac{\pi}{2}$ asymptotically (e.g., a negative scattering length), then F is finite but $M \propto s^{\frac{1}{2}}$ asymptotically. Mathematically the subtracted integral converges of course, but whereas the true solution rises rapidly in the vicinity of $x' = +1$, the numerical solution exhibits large oscillations near this point. The use of $u(x') = 1/(1 - x')^{\frac{1}{2}}$ cures this problem nicely.

When F contains a pole near the real axis this pole should obviously be factored out into $u(x')$. However, from the physics of the situation we know that a pole in F will produce a pole in M at a complex conjugate point, so this pole should be factored out into $u(x')$ also.[28] The prescription for handling the F_0 pole cases is as follows:

For the $F_0 M_2$ integrands,

$$u(x') = \frac{(1 + x')^{1/2} (1 - x')^{3/2}}{(x' - x_p)(x' - x_p^*)},$$

and for the $F_0 M_{1A}$ integrands,

$$u(x') = \frac{(1 + x')^{\frac{1}{2}} (1 - x')^{\frac{1}{2}}}{x' - x_p},$$

where x_p is the pole of F_0. With the above $F_0 M_2$ integrand prescription used in the Omnes equation with our F_0 pole cases, the

integral is done exactly, that is, the remaining unknown but smooth portion is just a constant. The u for the $F_0 M_{1A}$ integrands just reflects the structure of F_0 and nothing of M. The prescription we used for the F_1 pole and the $F_1 \cdot M_{1D} \cdot (1 - x)/(1 - x')$ integrand is

$$u(x') = \frac{(1 + x')^{\frac{1}{2}} (1 - x')^{\frac{1}{2}}}{(x' - x_p)(x' - x_p^*)}$$

and where the $(1 - x)/(1 - x')$ is included with the unknown but smooth portion. The fact that we have used $(1 + x')^{\frac{1}{2}}$ in u instead of $(1 + x')^{3/2}$ makes little difference. The justification for the asymptotic form of u is that $F_1 \propto (1 - x')^{\frac{1}{2}}$ asymptotically and empirically $M_{1D} \propto (1 - x)$, even if u is changed somewhat. There is, however, some sensitivity of the overall solution to this asymptotic form of u for the F_1 pole.

FOOTNOTES AND REFERENCES

* This work was supported in part by the U.S. Atomic Energy Commission.

1. R. H. Dalitz, Phil. Mag. 44, 1068 (1953).

2. N. Cabibbo, Proceedings of the Thirteenth International Conference on High Energy Physics, Berkeley, California, August 31-September 7, 1966 (University of California Press, Berkeley, 1966), p. 35.

3. N. N. Khuri and S. B. Treiman, Phys. Rev. 119, 1115 (1960).

4. Throughout all this work we shall use pion mass units unless otherwise indicated.

5. L. M. Brown and P. Singer, Phys. Rev. 133, B812 (1964).

6. I. M. Barbour and R. L. Schult, Phys. Rev. 155, 1712 (1967).

7. R. L. Schult and I. M. Barbour, Phys. Rev. 164, 1791 (1967).

8. A. Neveau and J. Scherk, Ann. Phys. 57, 39 (1970).

9. S. Weinberg, Phys. Rev. Letters 17, 616 (1966).

10. R. D. Amado and J. V. Noble, Phys. Rev. Letters 21, 1846 (1968); idem Phys. Rev. 185, 1993 (1969).

11. W. M. McKeeman, Commun. Assoc. Computing Machinery 5, 553 (1962); with corrections ibid 7, 421 (1964); ibid. 8, 104 (1965).

12. T. S. Mast et al., Phys. Rev. 183 No. 5, 1200 (1969).

13. J. D. Jackson, Rev. Mod. Phys. 42, 12 (1970).

14. It will be noticed that there appears to be a small cusp or positive curvature at threshold that is noticeable for the large negative scattering lengths. More will be said about this anomaly later.

15. It is interesting, though, that form (15) with the optimal parameters corresponds closely to the best solution by Gore, Ref. 16 (his $\lambda = 0.02$), based on dispersion relations and crossing symmetry for $\pi\pi$ scattering.

16. B. F. Gore, An S-Wave $I = 0$ $\pi\pi$ Resonance, University of Maryland preprint, August 1970.

17. J. P. Baton et al., Nucl.Phys. B3, 349 (1967).

18. M. G. Olsson, Phys. Rev. 162, 1338 (1967).

19. D. G. Sutherland, Phys. Letters 23, 384 (1966).

20. A. Cnops et al., Phys. Letters 27B, 13 (1968).

21. G. Kallen, Elementary Particle Physics (Addison-Wesley Publishing Company, Inc., Reading, Mass., 1964), p. 428.

22. D. Davison et al., Phys. Rev. 180 No. 5, 1333 (1969).

23. N. I. Muskhelishvili, Singular Integral Equations (P. Noordhoff N. V., Groningen, Holland, 1953), Ch. 6.

24. W. Pogorzelski, Integral Equations (Pergamon Press, New York, 1966), Ch. 17.

25. The author thanks Dr. Robert Riddell for this suggestion.

26. The limits of applicability for this numerical method are not clear. However, since the technique allows one to reproduce the exact solutions of the Omnes equation, (5), to typically three significant figures for 25 mesh points, it was assumed to be applicable to the KT equations.

27. For the simplest integration technique one could think of, w_{ij} would just be $K(s_i,s'_j)\cdot\Delta s'_j$, where $\Delta s'_j$ is the distance between mesh points. However, if $K(s,s')$ or $\phi(s')$ is a rapidly varying function of s', as in our case, one must use the knowledge of that behavior to devise a more appropriate set of weights (see Appendix B).

28. An alternative idea one might entertain is to define $M(s) \equiv [M'(s)]/(s - s_p)$ and rewrite the integral equations to solve for $M'(s)$ instead of $M(s)$, but this approach leads to the same integrals for g and h and gives the same answers.

FIGURE CAPTIONS

Fig. 1. (a) Decay diagram for $K \to 3\pi$.

(b) General "scattering like" diagram for $K\pi \to \pi\pi$.

(c) Sketch of the physical regions of the general amplitude.

(d) Diagram showing intermediate states kept in the unitarity equation in each of the subchannels.

Fig. 2. (a) The momentum vectors of p_a, p_b, p_c, $p_{b'}$, and $p_{c'}$ as seen from the bc (equivalently b'c') center-of-mass system.

(b) An illustrative set of ray labels for a decay matrix element.

Fig. 3. The ray label choice for $M_{00+}(s_a,s_b,s_c)$. The "1U" and "1L" stand for "upper" and "lower" branches of ray number 1, and "1A" and "1D" for the "average" and "difference" of the amplitudes.

Fig. 4. $|M_2(s)|^2$ versus s for numerical solutions of Eq. (11) with a nonrelativistic scattering-length approximation for F_0, Eq. (12) with $a_0 = +1.0, +0.5, +0.2, -0.5$, and -1.0. $M_2(s)$ is defined (see Fig. 3) as the invariant matrix element for $K^+ \to \pi^0\pi^0\pi^+$ evaluated along the ray, $s_{00} = s$, and either $s_{0+} = \frac{3}{2} s_0 - \frac{1}{2} s$. The matrix element has been normalized to 1 at the center of the Dalitz plot, $s_0 = 5.32$. The extent of the Dalitz plot is indicated along the line $|M_2|^2 = 1.0$ and again along the bottom of the graph. The open boxes (□) roughly indicate the experimental data and lie along a

curve given by the empirical formula $|M_2|^2 = 1 + g(s - s_0)$, with $g = 0.4$.

Fig. 5. $|M_2(s)|^2$ versus s for the relativistic scattering length approximation for F_0, Eq. (14) with $a_0 = +1.0$, $+0.5$, $+0.2$, -0.5, and -1.0.

Fig. 6. $|M_2(s)|^2$ versus s for an $I = 0$, S-wave pole, Eq. (15) for the following sets of parameters $(m_\sigma, \Gamma_\sigma; s_\sigma)$: (450 MeV, 75 MeV; 10.8), (450 MeV, 100 MeV; 10.8), (750 MeV, 125 MeV; 30), and (750 MeV, 250 MeV; 30).

Fig. 7. $|M_2(s)|^2$ versus s for a "hump" in the $I = 0$, S-wave phase shift, Eq. (16). Shown in (a) is $m_0 = 500$ MeV ($s = 13.4$) and $a_0 = 0.0$, 0.1, 0.2, and 0.3. Shown in (b) is $a_0 = 0.0$ and $m_0 = 450$, 500, 550, and 700 MeV ($s = 10.8$, 13.4, 16.2, and 26.1).

Fig. 8. $|M_2(s)|^2$ versus s for the nonrelativistic scattering-length approximation for F_2, with $a_2 = +1.0$, $+0.5$, -0.06, -0.5, and -1.0.

Fig. 9. $|M_2(s)|^2$ versus s for the relativistic scattering-length approximation for F_2, with $a_2 = +1.0$, $+0.5$, -0.06, -0.5, and -1.0.

Fig. 10. $|M_2(s)|^2$ versus s for the experimentally determined $I = 2$ phase shift of Baton et al. (1967), Eq. (17) with $a_2 = -0.052$ and $r_2 = 1.9$. For $s > 50$, δ_2 is limited to be $-21°$.

Fig. 11. $|M_2(s)|^2$ versus s for nonrelativistic scattering-length approximations for F_0 and F_2 for the following scattering-

length sets (a_0,a_2): (-0.5, +0.5), (+0.5, +0.5), and (-0.5, -0.5).

Fig. 12. $|M_2(s)|^2$ versus s for relativistic scattering-length approximations for F_0 and F_2 for the following scattering-length sets (a_0,a_2): (-0.5, +0.5), (+0.5, +0.5), and (-0.5, -0.5).

Fig. 13. $|M_2(s)|^2$ versus s for two F_0 cases, with and without Baton's F_2. The two F_0 cases used are (1) a hump with $a_0 = 0.0$ and $m_0 = 500$ MeV, and (2) a pole with $m_\sigma = 750$ MeV and $\Gamma_\sigma = 250$ MeV.

Fig. 14. $|M_2(s)|^2$ versus s using nonrelativistic scattering-length approximations for F_0 and F_1. Here $a_0 = 0.2$, and $a_1 = 0.0$, 0.1, 0.2, 0.3, 0.4, and 1.0.

Fig. 15. $|M_2(s)|^2$ versus s using a nonrelativistic scattering-length approximation for F_1 and a hump for F_0. Here $a_0 = 0.2$, $m_0 = 500$ MeV, and $a_1 = 0.0$, 0.1, 0.15, and 0.2.

Fig. 16. $|M_2(s)|^2$ versus s using the ρ pole parametrization, (19), for F_1, and an $a_0 = 0.2$, $m_0 = 500$ MeV hump for F_0. The values of c_1 are 2, 5, 10, 20.

Fig. 17. $|M_2(s)|^2$ versus s using the same F_0 and F_1 as Fig. 16, and adding the Baton F_2.

Fig. 18. $|M_2(s)|^2$ versus s using the ρ pole parametrization, (19), for F_1, and an $m_\sigma = 750$ MeV, $\Gamma_\sigma = 250$ MeV pole for F_0. The values of c_1 are 2, 5, 10, and 20.

Fig. 19. $|M_2(s)|^2$ versus s using the same F_0 and F_1 as Fig. 18 and adding the Baton F_2.

Fig. 20. η decay $|M_2(s)|^2$ versus s for the F_0 hump case, $a_0 = 0.0$, $m_0 = 500$ MeV, and the F_0 pole case, $m_\sigma = 550$ MeV, $\Gamma_\sigma = 100$ MeV. Both cases are shown with and without the Baton F_2.

Fig. 21. η decay $|M_2(s)|^2$ versus s for the F_0 hump case, $a_0 = 0.2$, $m_0 = 500$ MeV, with and without the F_1 scattering length $a_1 = +0.15$.

Fig. 22. η decay $|M_2(s)|^2$ versus s for the F_0 hump case, $a_0 = 0.2$, $m_0 = 500$ MeV, the F_1 pole, (19), with $c_1 = 10$, and 20, and the Baton F_2.

Fig. 23. η decay $|M_2(s)|^2$ versus s for the F_0 pole, $m_\sigma = 750$ MeV, $\Gamma_\sigma = 250$ MeV, and the F_1 pole, (19), with $c_1 = 10$, and 20, and the Baton F_2.

Fig. 24. $|M_2(s)|^2$ versus s for a nonrelativistic scattering length, $a_0 = 0.2$, and using (20) for an inhomogeneous term in Eq. (11). Here $g = -0.2$, -0.1, 0.0, $+0.1$, and $+0.2$.

Fig. 25. $|M_2(s)|^2$ versus s for a hump case, $a_0 = 0.2$, $m_0 = 500$ MeV, and using (20) for an inhomogeneous term in Eq. (11). Here $g = -0.1$, 0.0, $+0.1$.

Fig. 26. $|M_2(s)|^2$ versus s for a nonrelativistic scattering length, $a_0 = 0.2$, and using (21) for an inhomogeneous term in Eq. (11). Here $g = -0.2$, 0.0, $+0.2$, $+0.4$.

Fig. 27. $|M_2(s)|^2$ versus s for a hump case $a_0 = 0.2$, $m_0 = 500$ MeV, and an F_1 scattering length, $a_1 = +0.15$, and using (21) for an inhomogeneous term. Here $g = -0.2, -0.0, +0.2, +0.4$.

Fig. 28. $|M_{\tau 2}(s)|^2$ and $|M_{\tau' 2}(s)|^2$ versus s for numerical solutions of (22). The masses for the π^0, $\pi^{\pm}$, and K^+ mesons are taken to be 1.0, 1.034, and 3.659 respectively. For $I = 0$ the case used was a hump with $a_0 = 0.2$ and $m_0 = 500$ MeV, and for $I = 2$ the Baton F_2 was used.

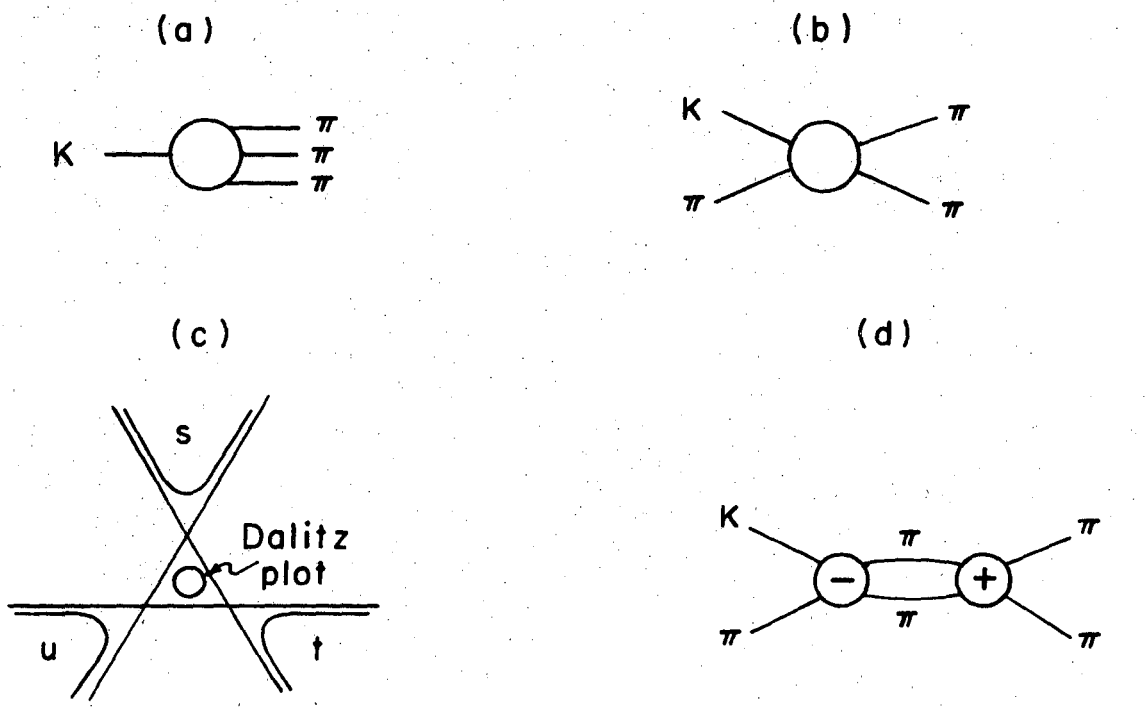

XBL711-2616

Fig. 1.

(a)

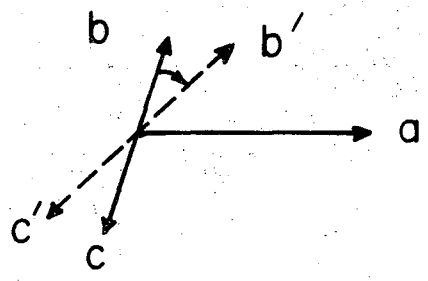

(b)

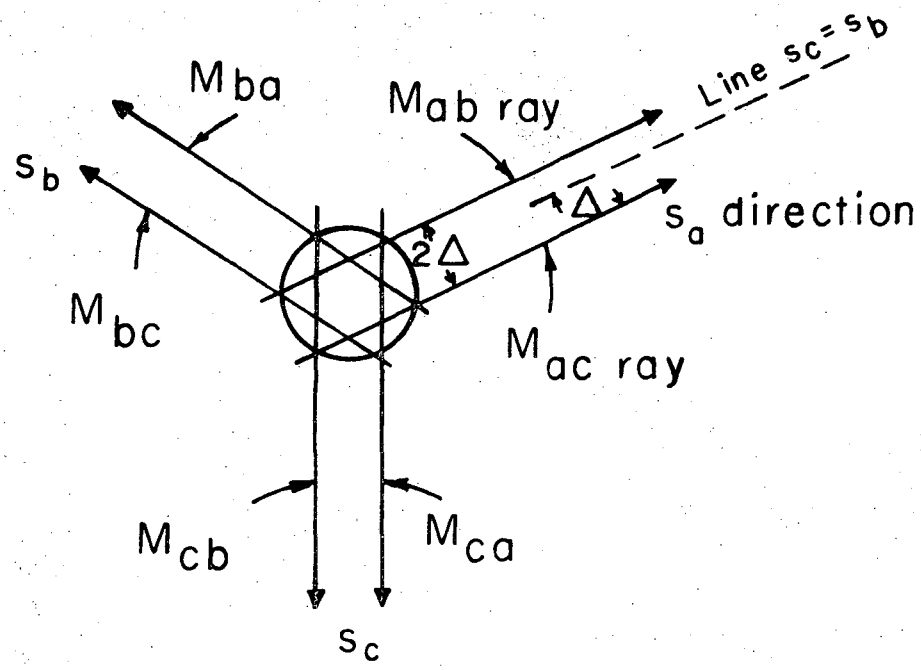

XBL711-2617

Fig. 2.

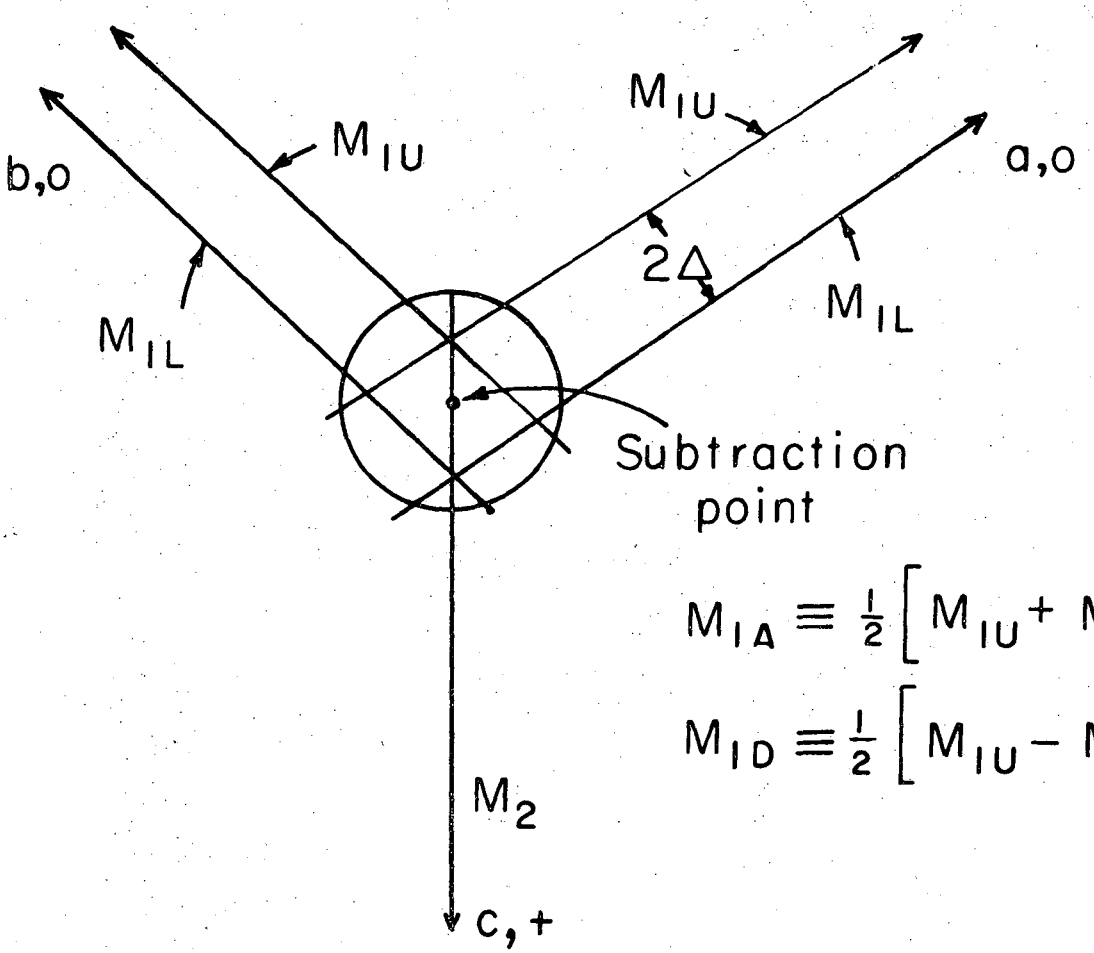

XBL711-2618

Fig. 3.

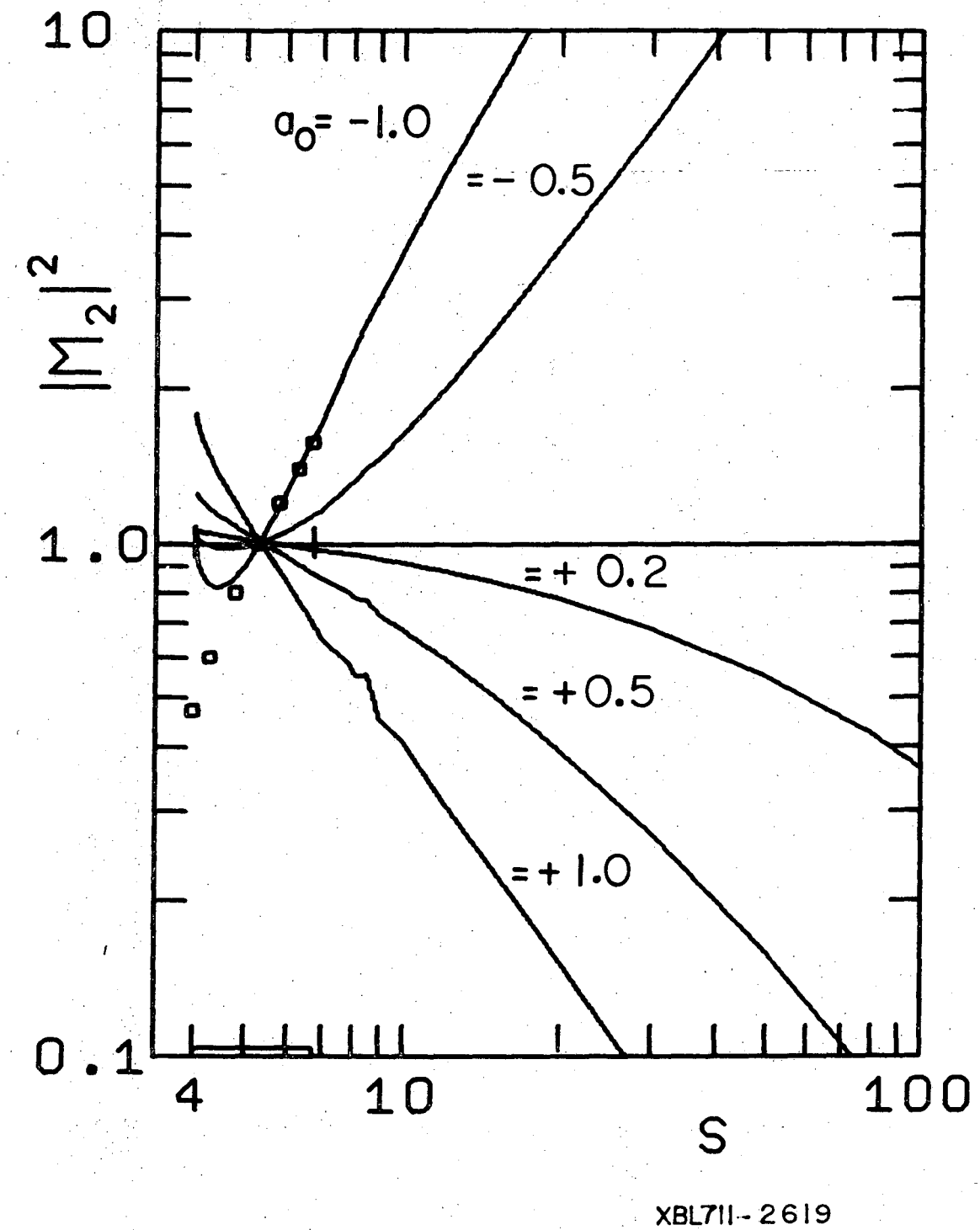

Fig. 4.

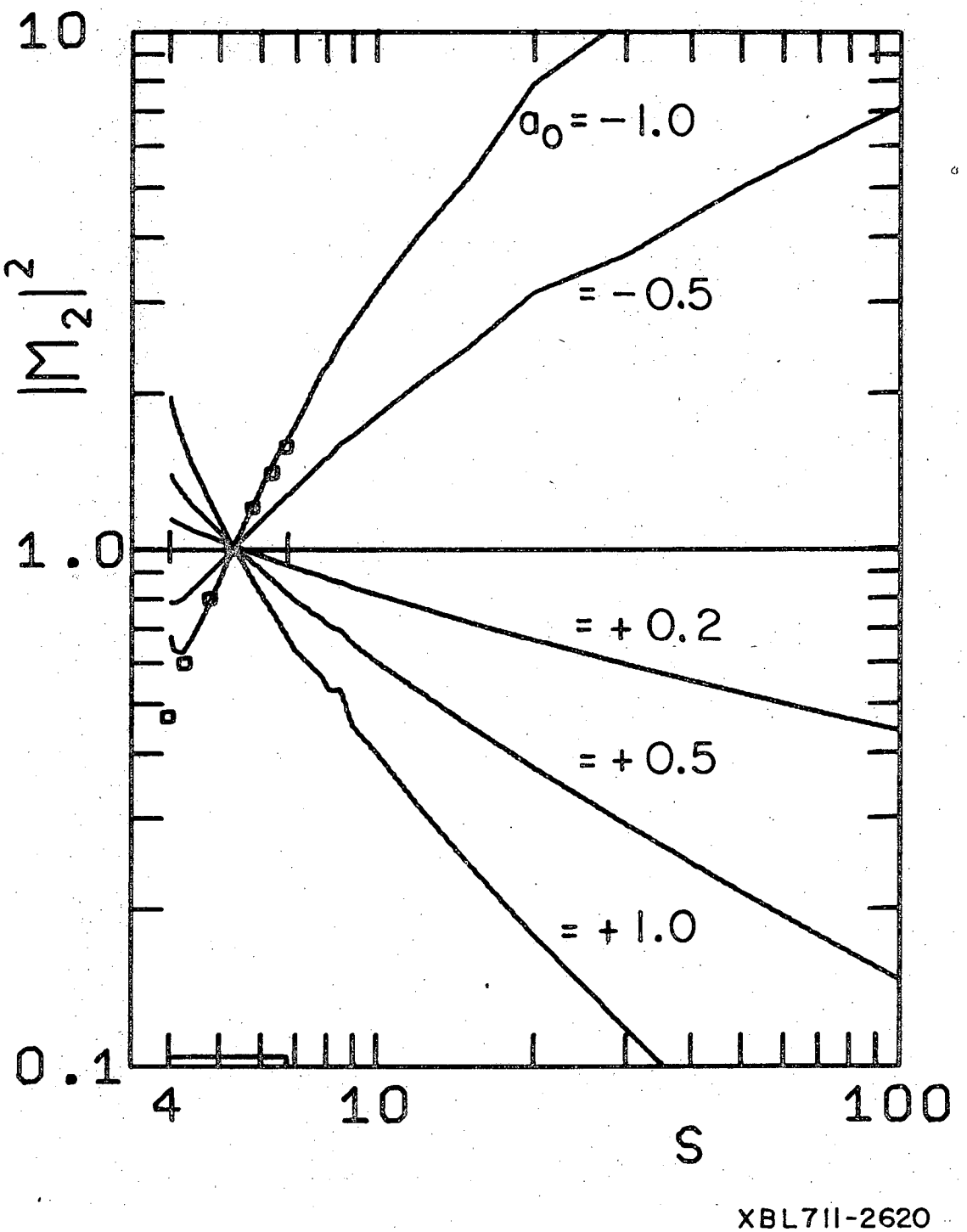

Fig. 5.

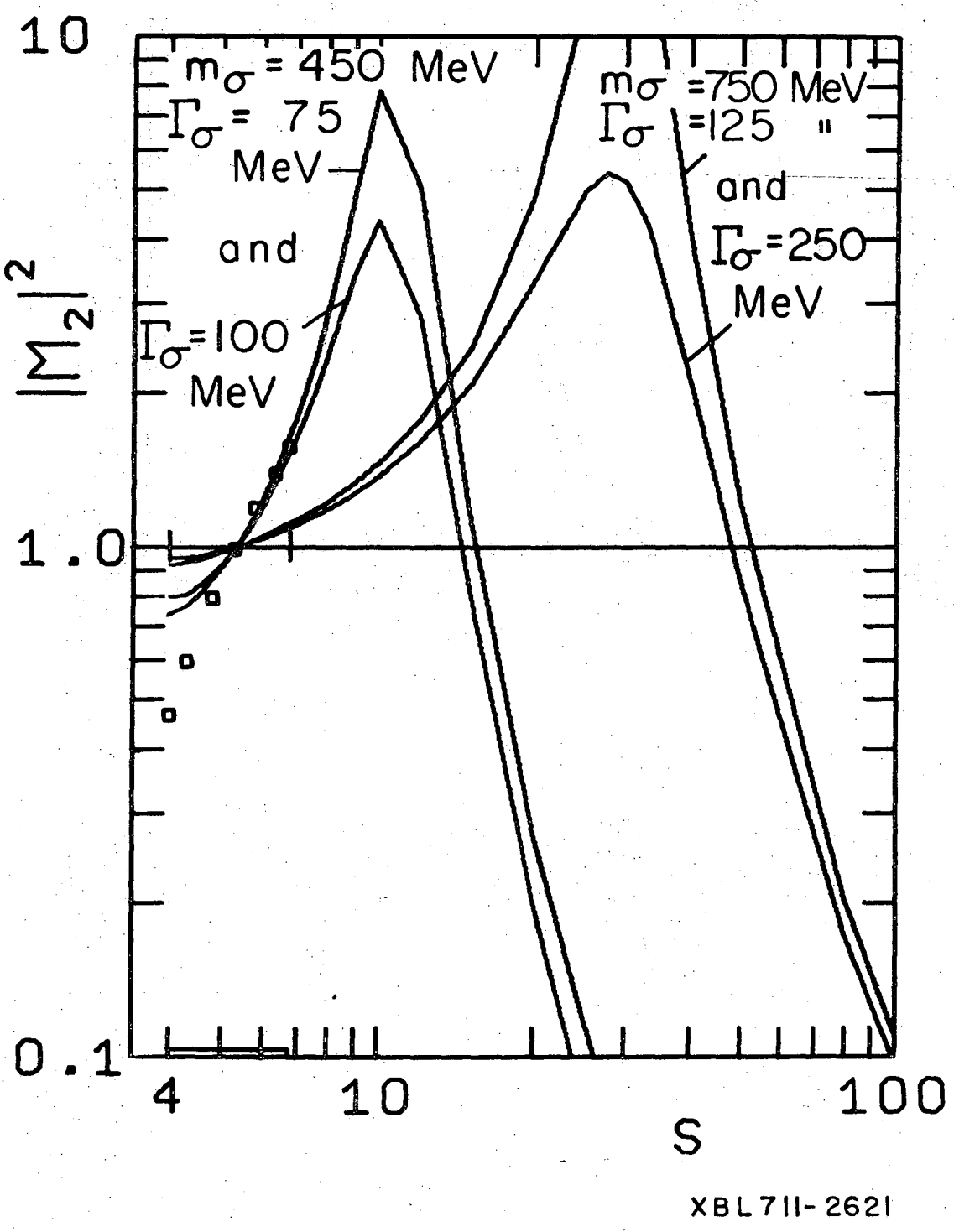
10
1.0
0.1
$|\Sigma_2|^2$
m_σ = 450 MeV
Γ_σ = 75 MeV
and
Γ_σ = 100 MeV
m_σ = 750 MeV
Γ_σ = 125 "
and
Γ_σ = 250 MeV
4
10
100
S
XBL711-2621

Fig. 6.

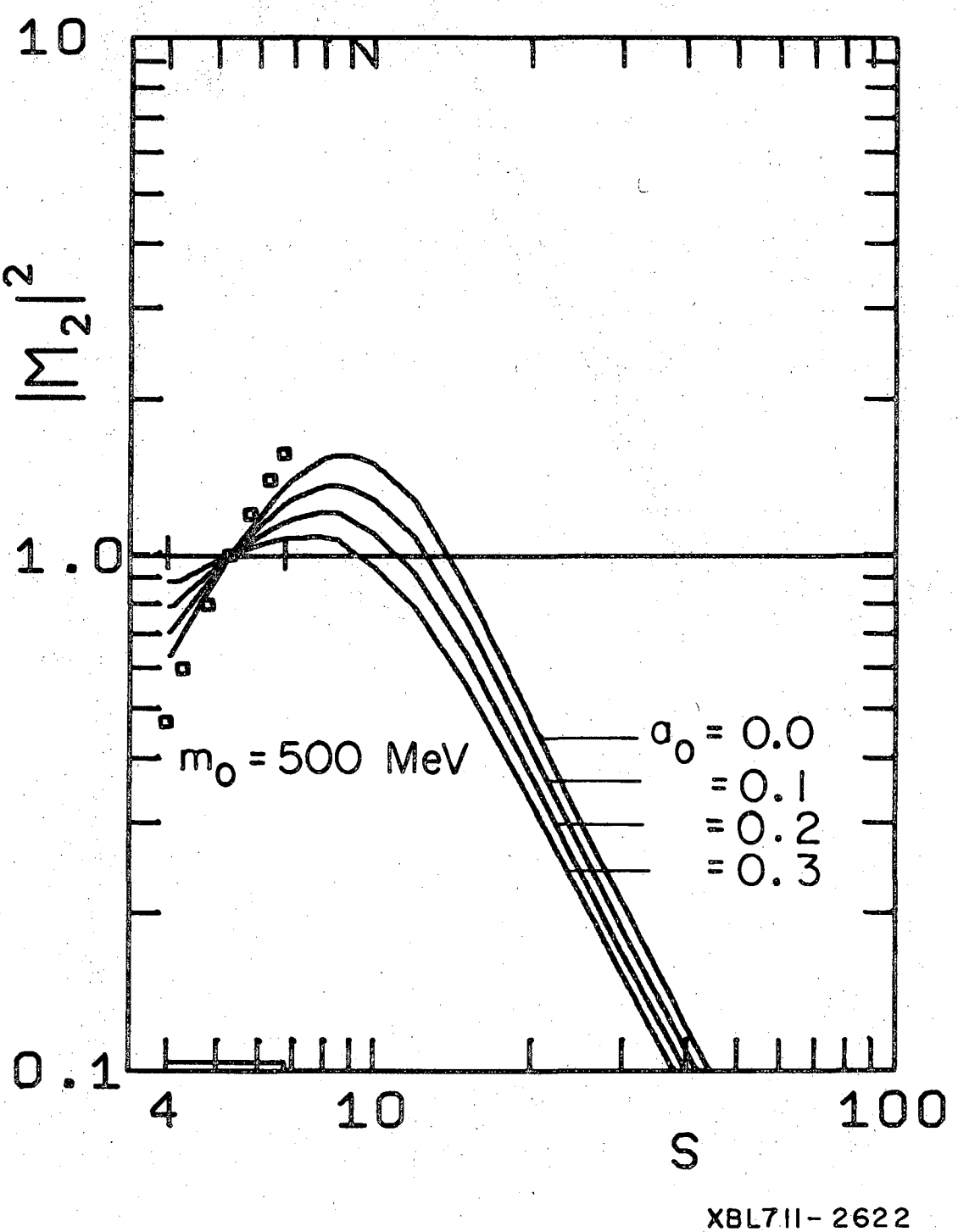

Fig. 7a.

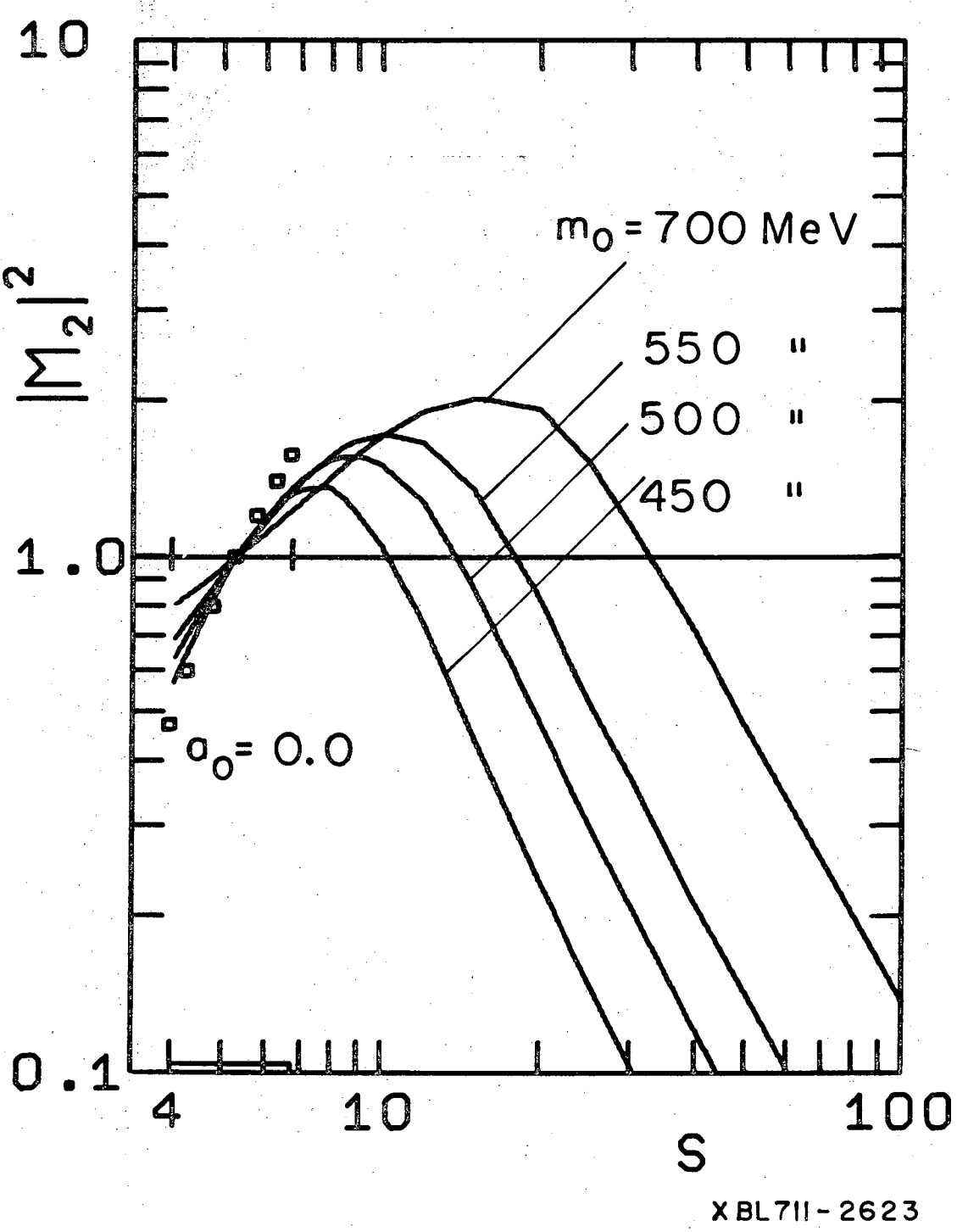

Fig. 7b.

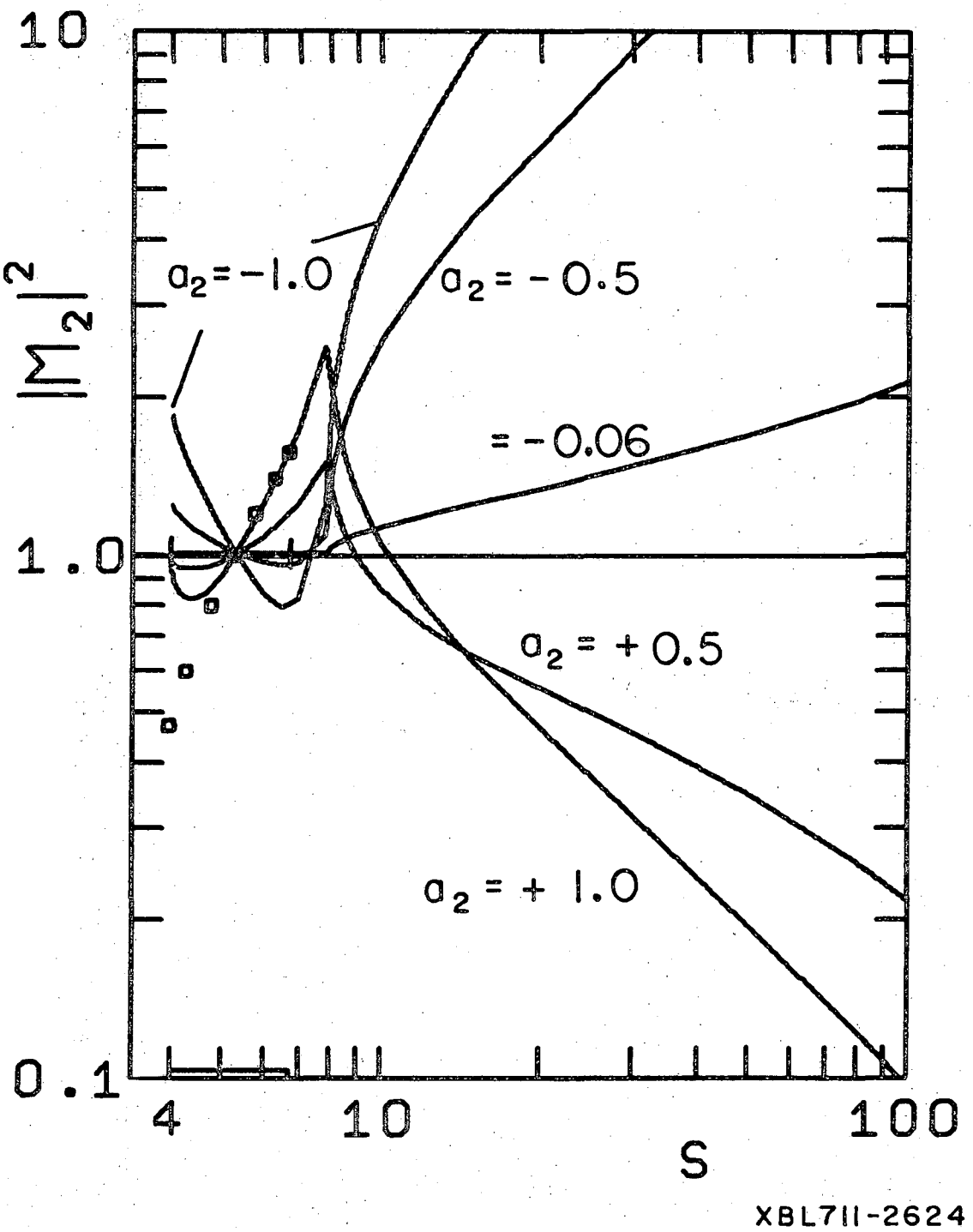

Fig. 8.

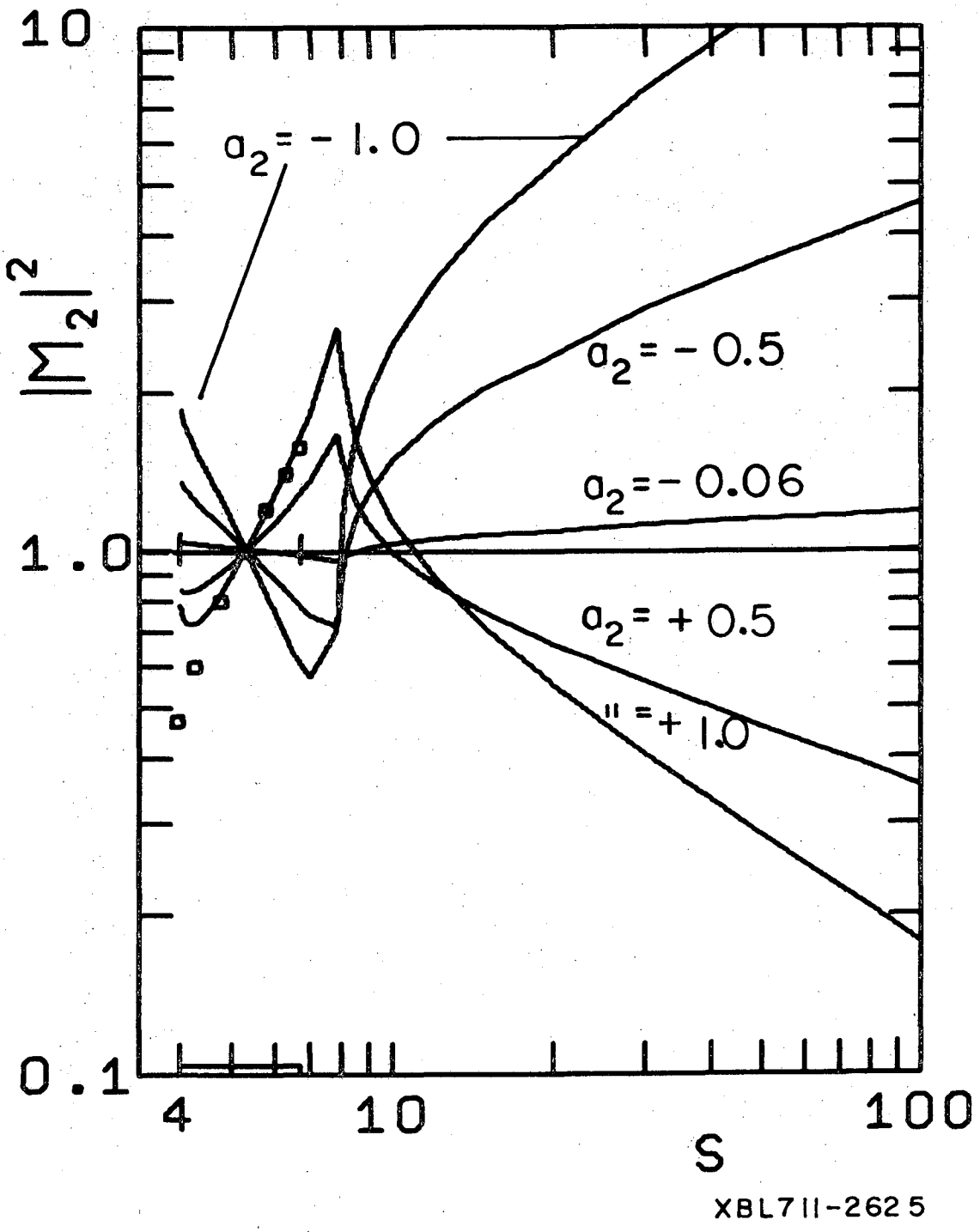

Fig. 9.

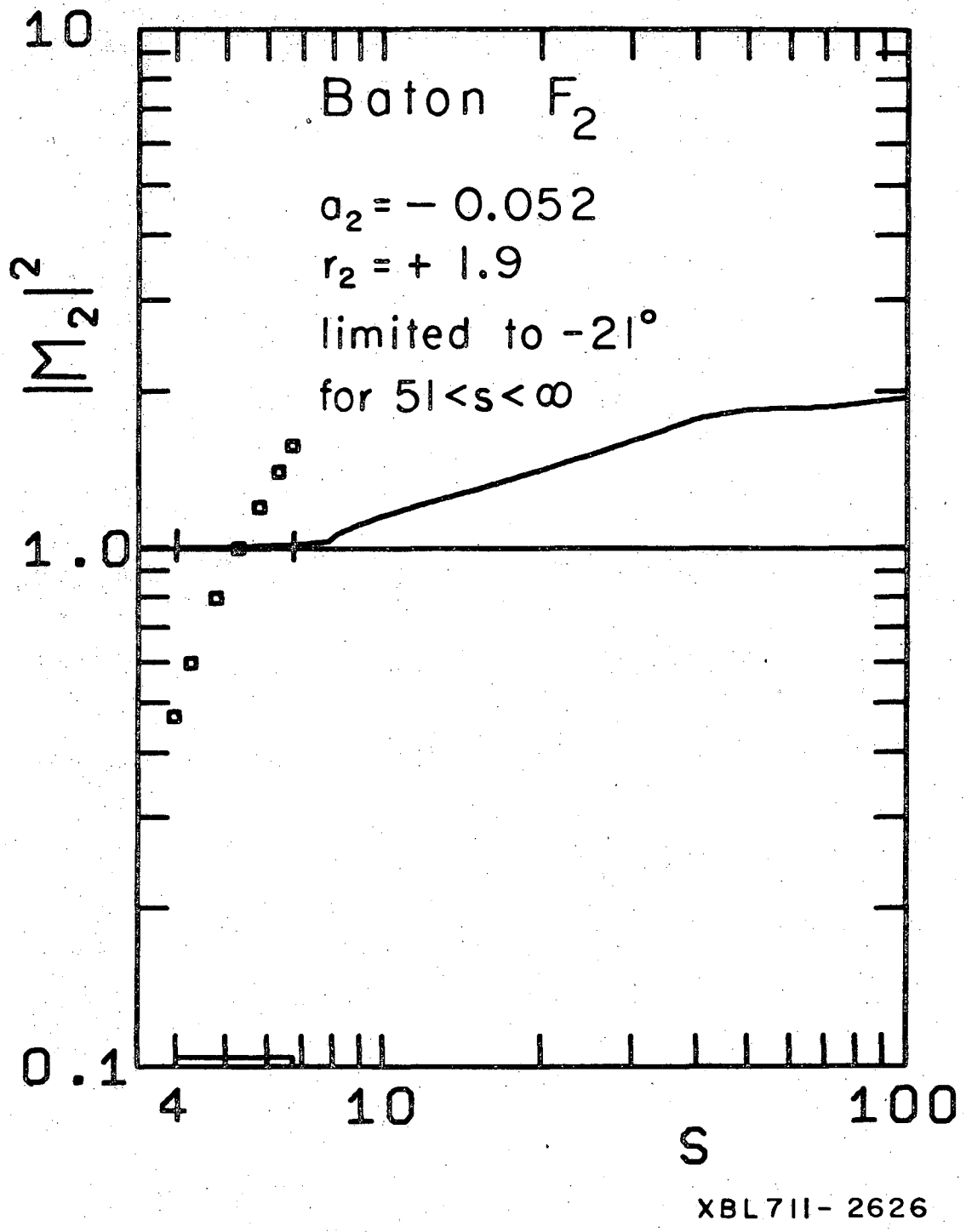
10
1.0
0.1
$|\Sigma_2|^2$
Baton F_2
$a_2 = -0.052$
$r_2 = +1.9$
limited to -21°
for $51 < s < \infty$
4
10
100
S
XBL711-2626

Fig. 10.

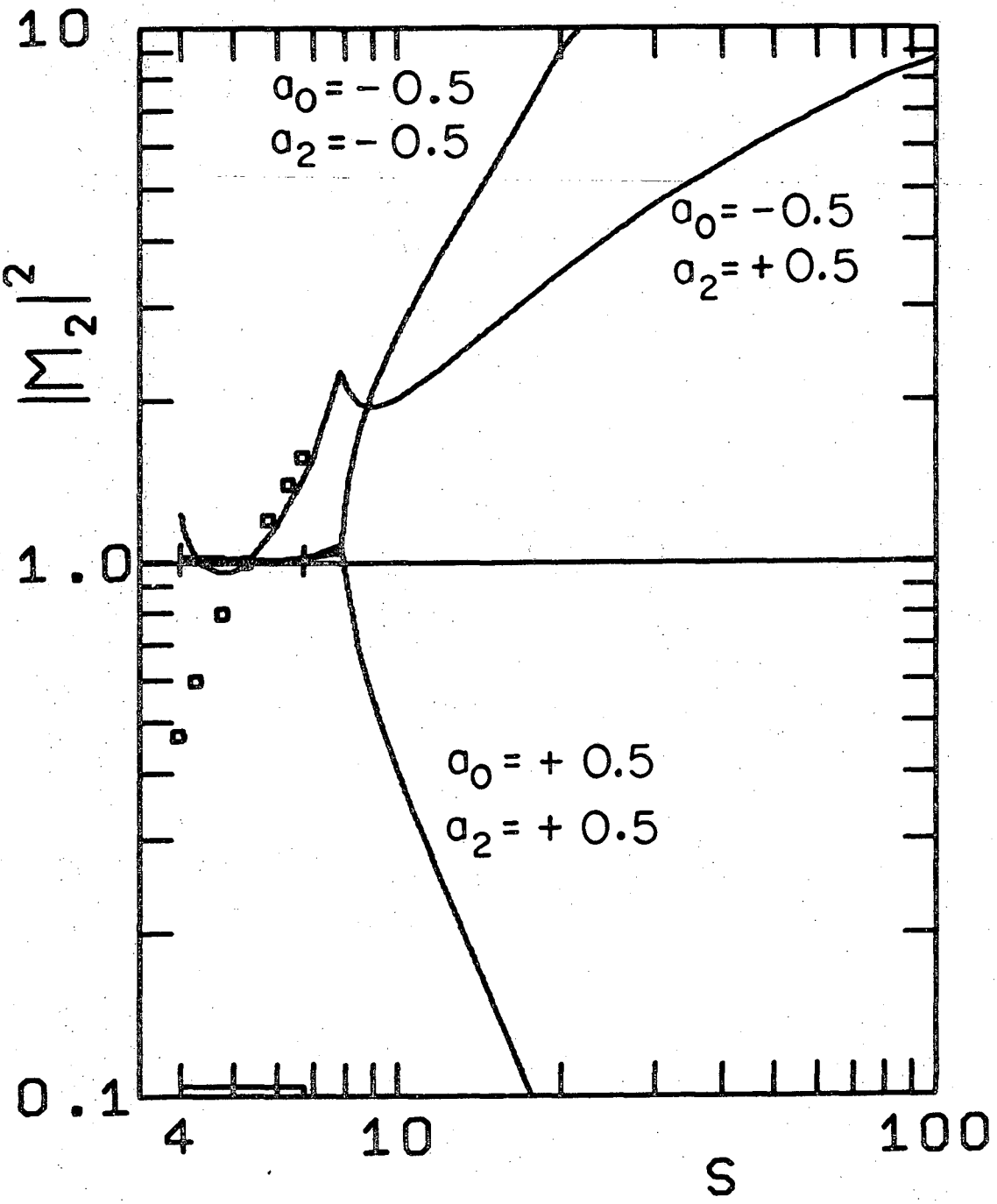
10
1.0
0.1
$|M_2|^2$
$a_0 = -0.5$
$a_2 = -0.5$
$a_0 = -0.5$
$a_2 = +0.5$
$a_0 = +0.5$
$a_2 = +0.5$
4
10
100
S
XBL711-2627

Fig. 11.

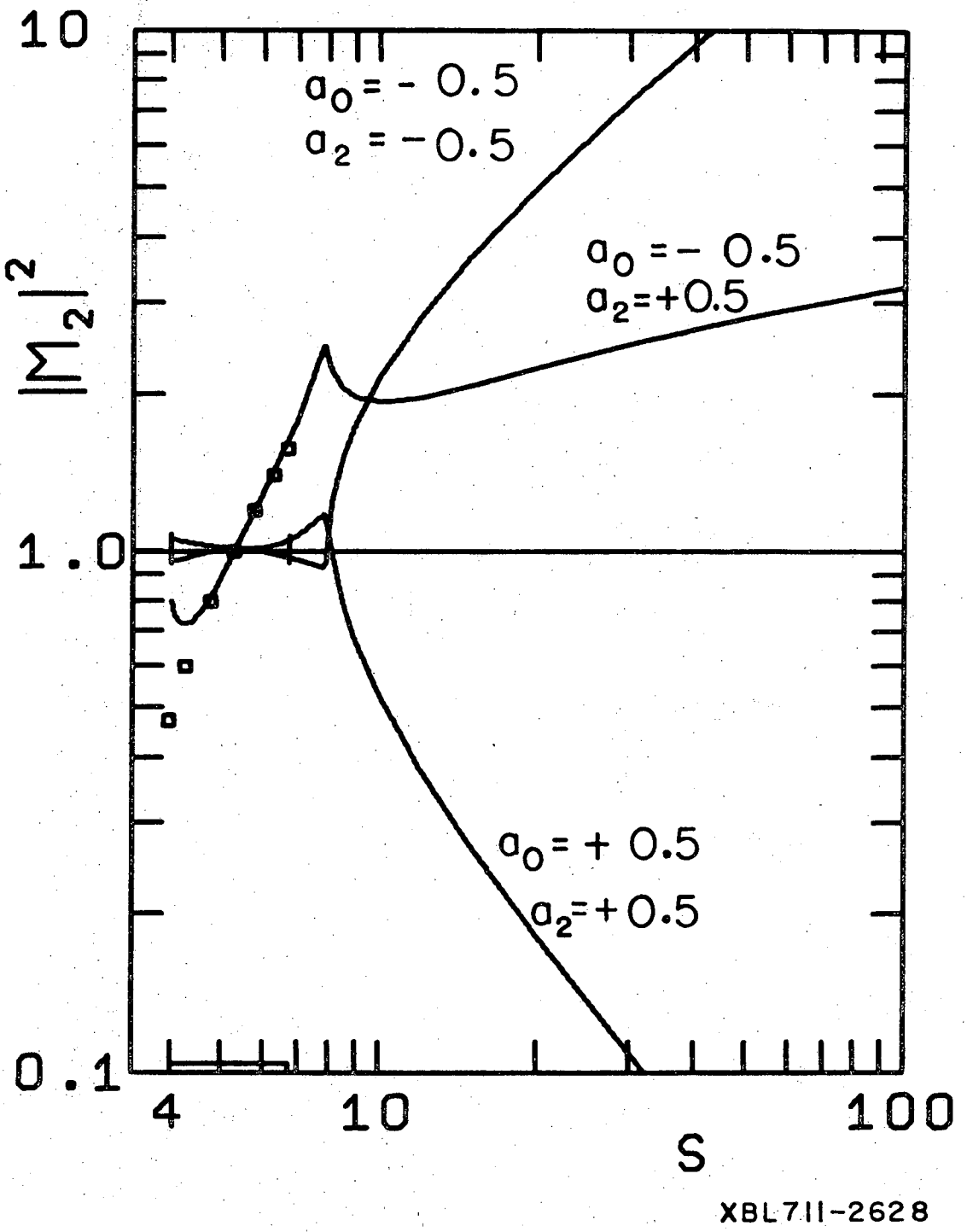
10
1.0
0.1
$|\Sigma_2|^2$
$a_0 = -0.5$
$a_2 = -0.5$
$a_0 = -0.5$
$a_2 = +0.5$
$a_0 = +0.5$
$a_2 = +0.5$
4
10
100
S
XBL711-2628

Fig. 12.

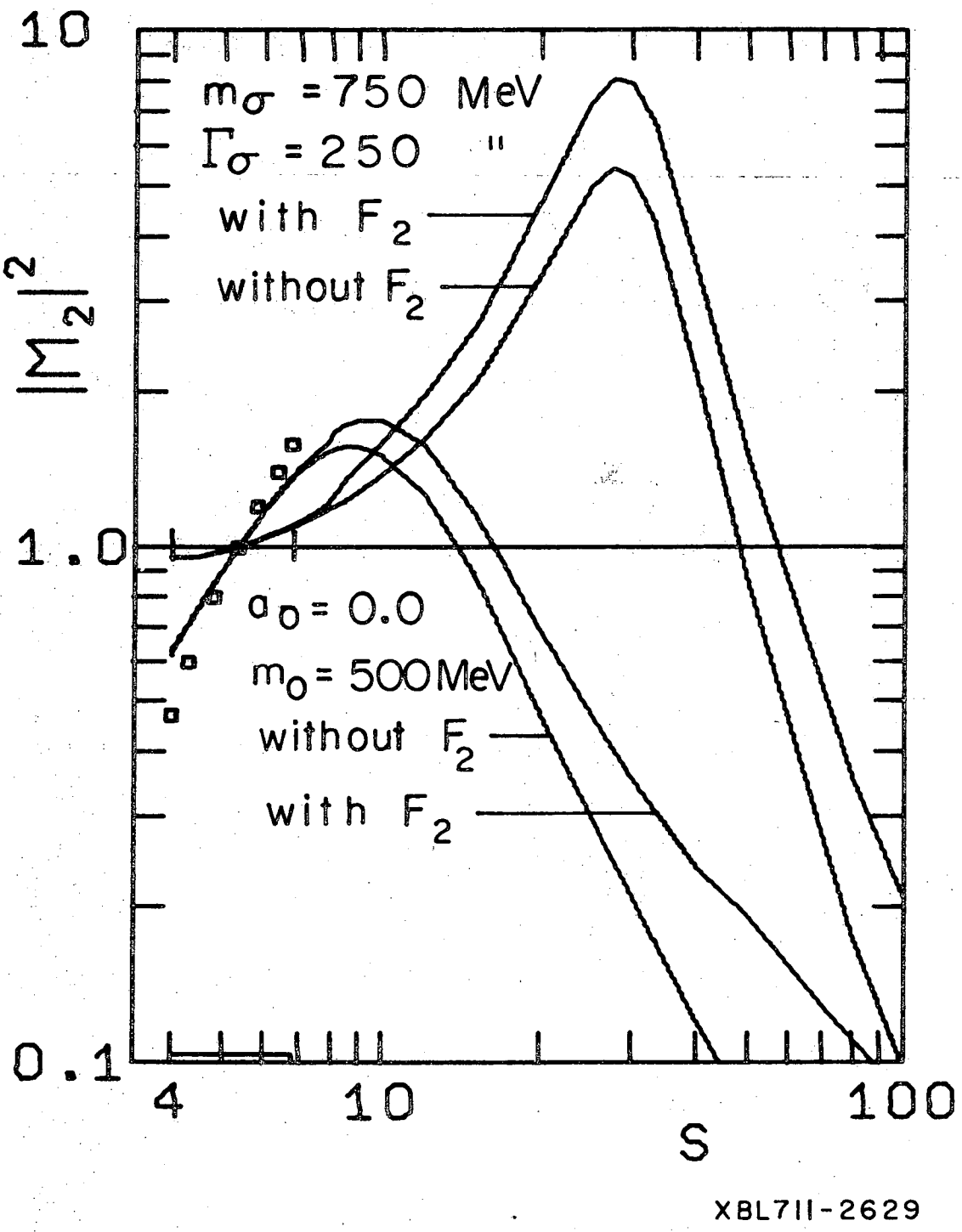
10
1.0
0.1
$|\Sigma_2|^2$
m_σ = 750 MeV
Γ_σ = 250 "
with F_2
without F_2
a_0 = 0.0
m_0 = 500 MeV
without F_2
with F_2
4
10
100
S
XBL711-2629

Fig. 13.

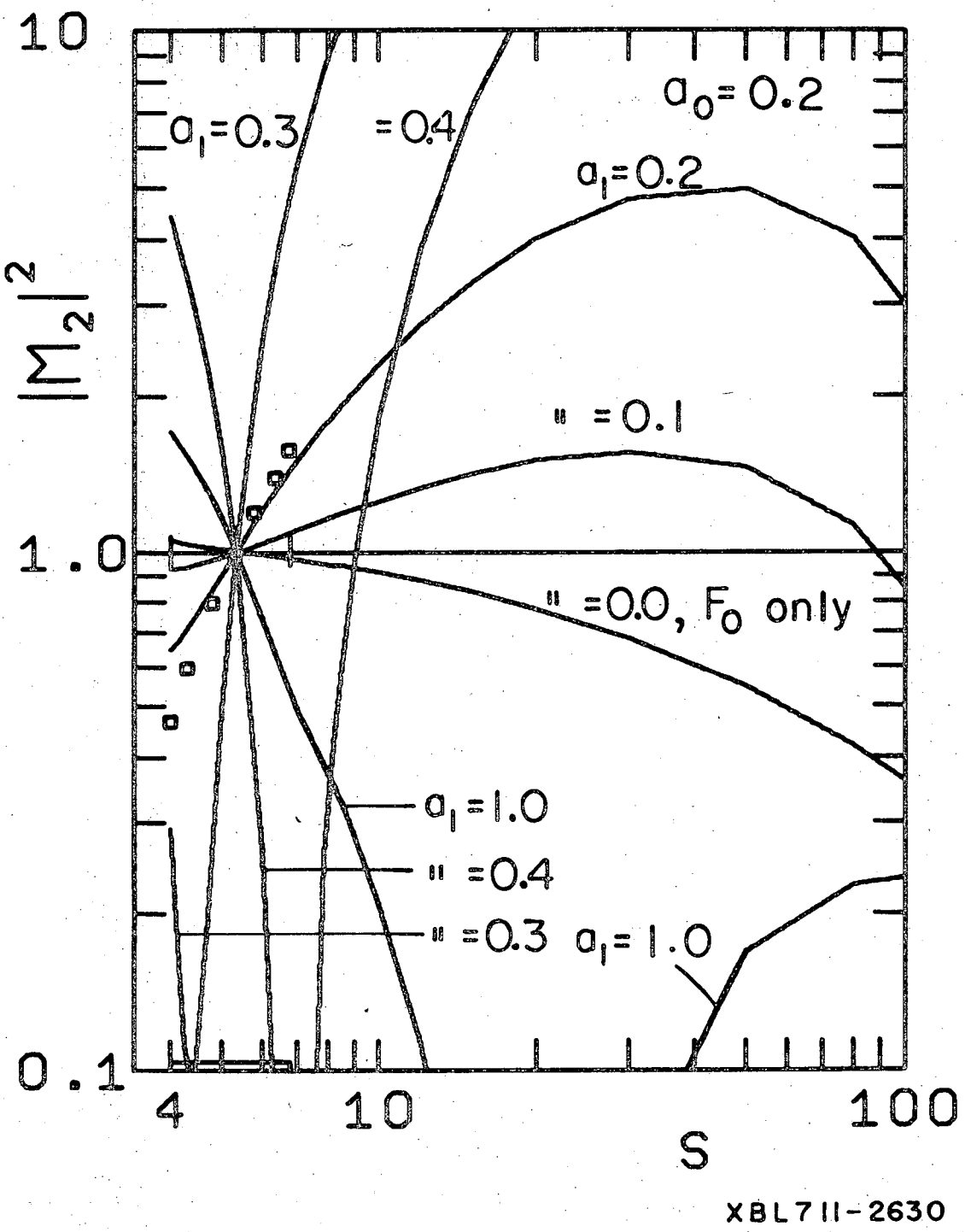
10
1.0
0.1
$|M_2|^2$
4
10
100
S
$a_0 = 0.2$
$a_1 = 0.3$
$= 0.4$
$a_1 = 0.2$
$= 0.1$
$= 0.0$, F_0 only
$a_1 = 1.0$
$= 0.4$
$= 0.3$
$a_1 = 1.0$
XBL711-2630

Fig. 14.

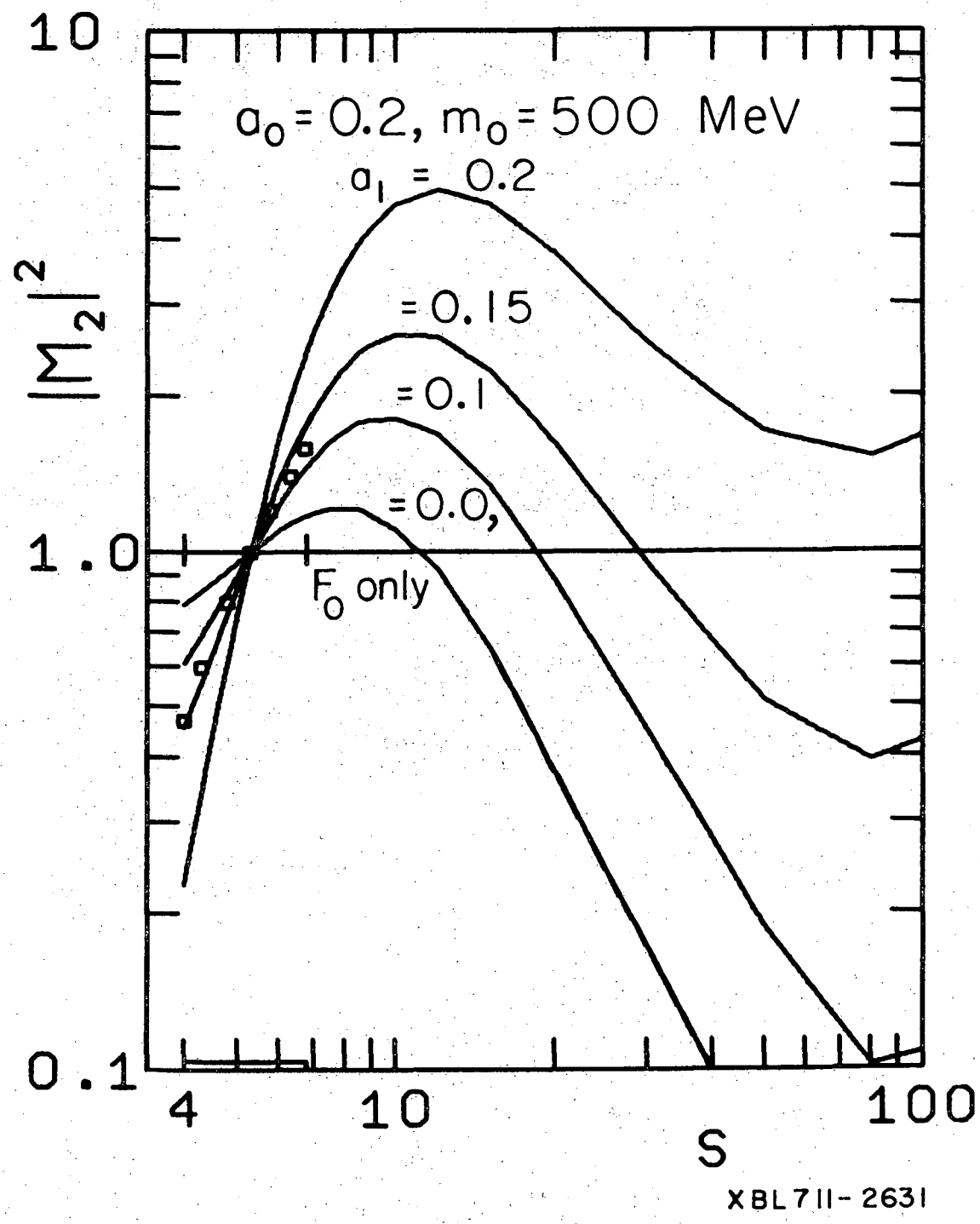
10
1.0
0.1
$a_0 = 0.2, m_0 = 500$ MeV
$a_1 = 0.2$
= 0.15
= 0.1
= 0.0,
F_0 only
$|M_2|^2$
4
10
100
S
XBL711-2631

Fig. 15.

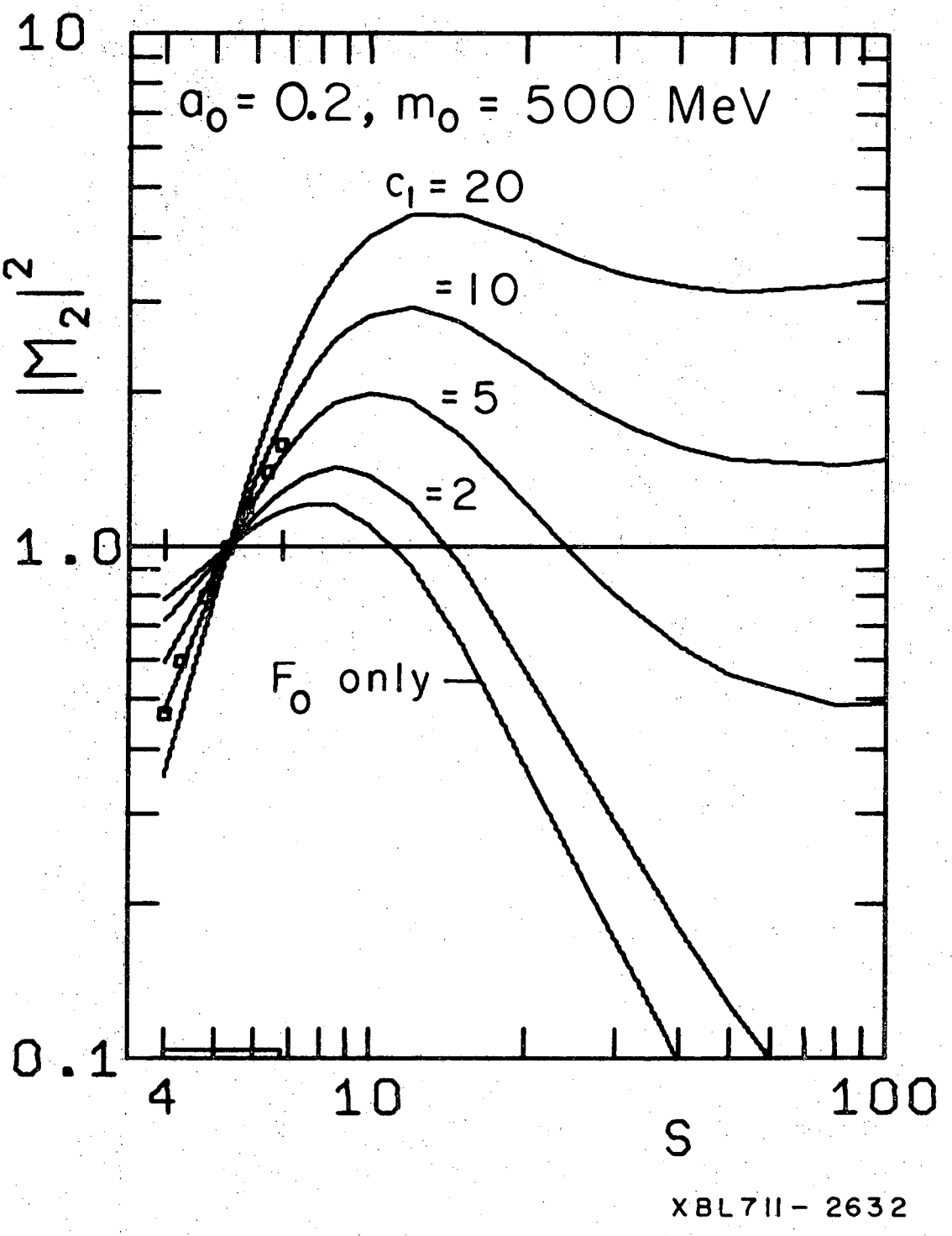
10
$a_0 = 0.2$, $m_0 = 500$ MeV
$c_1 = 20$
$= 10$
$= 5$
$= 2$
$|\Sigma_2|^2$
1.0
F_0 only
0.1
4
10
100
S
XBL711-2632

Fig. 16.

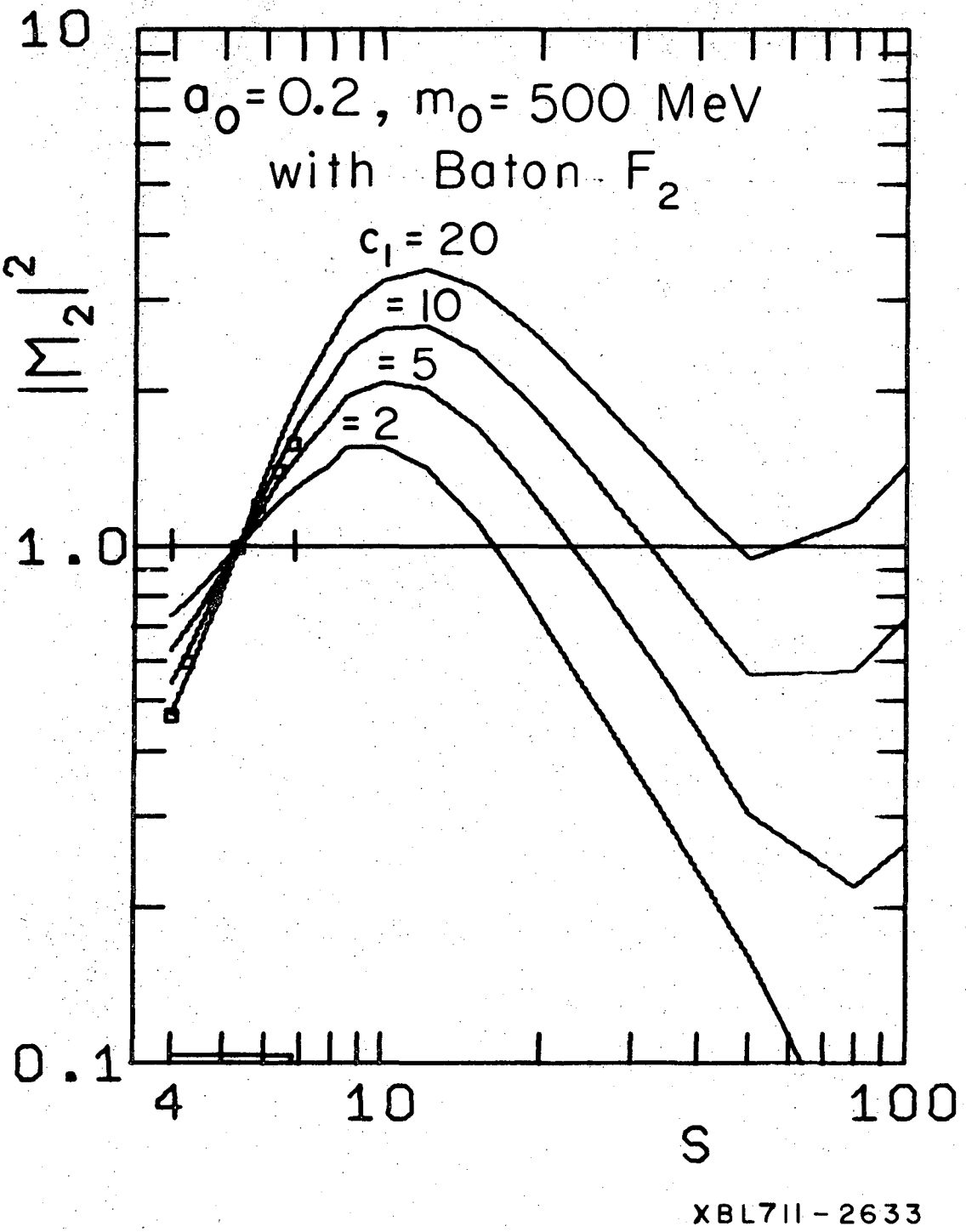
10
$a_0 = 0.2$, $m_0 = 500$ MeV
with Baton F_2
$c_1 = 20$
= 10
= 5
= 2
$|\Sigma_2|^2$
1.0
0.1
4
10
100
S
XBL711-2633

Fig. 17.

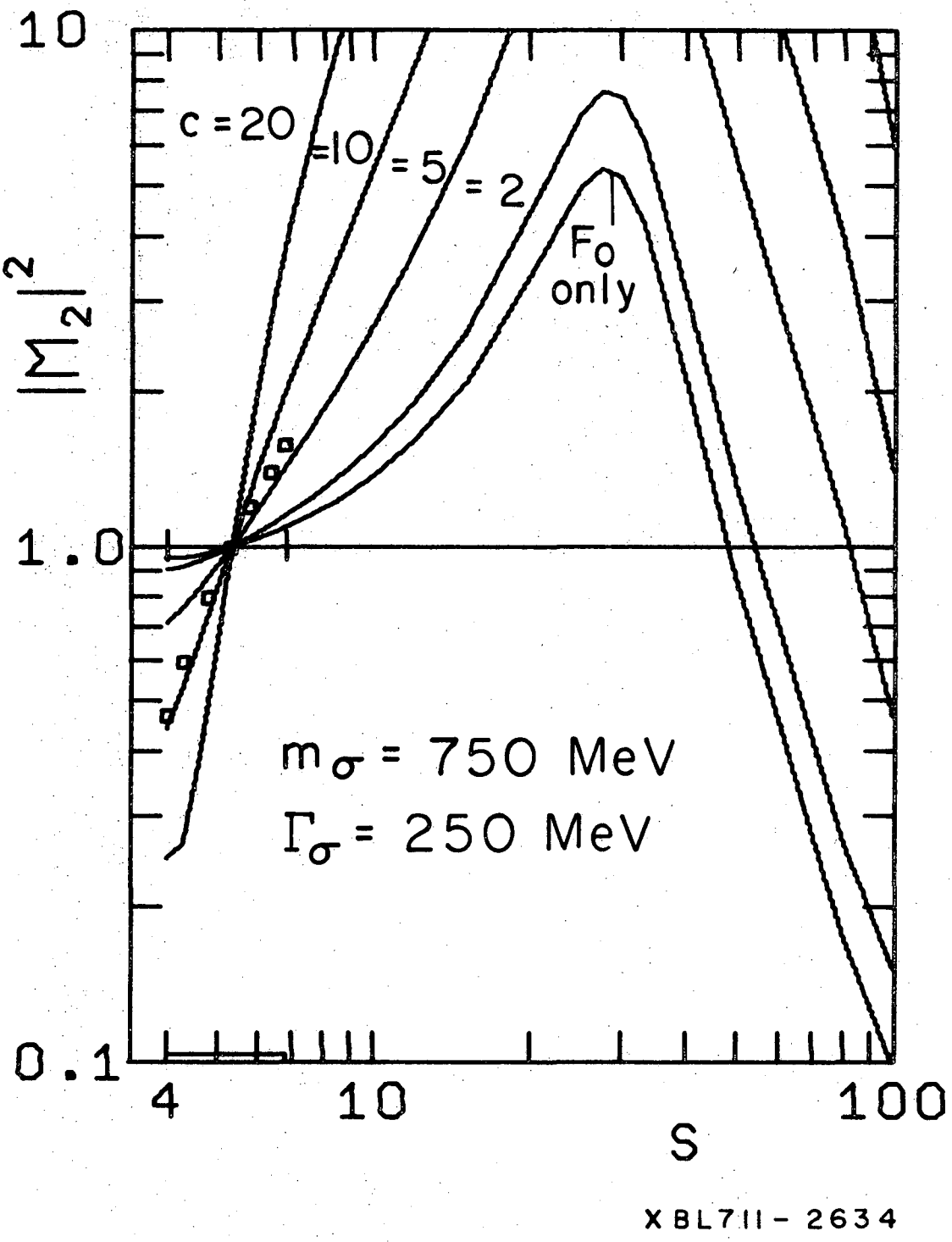
10
1.0
0.1
$|M_2|^2$
c = 20
=10
= 5
= 2
F_0 only
m_σ = 750 MeV
Γ_σ = 250 MeV
4
10
100
S
XBL711-2634

Fig. 18.

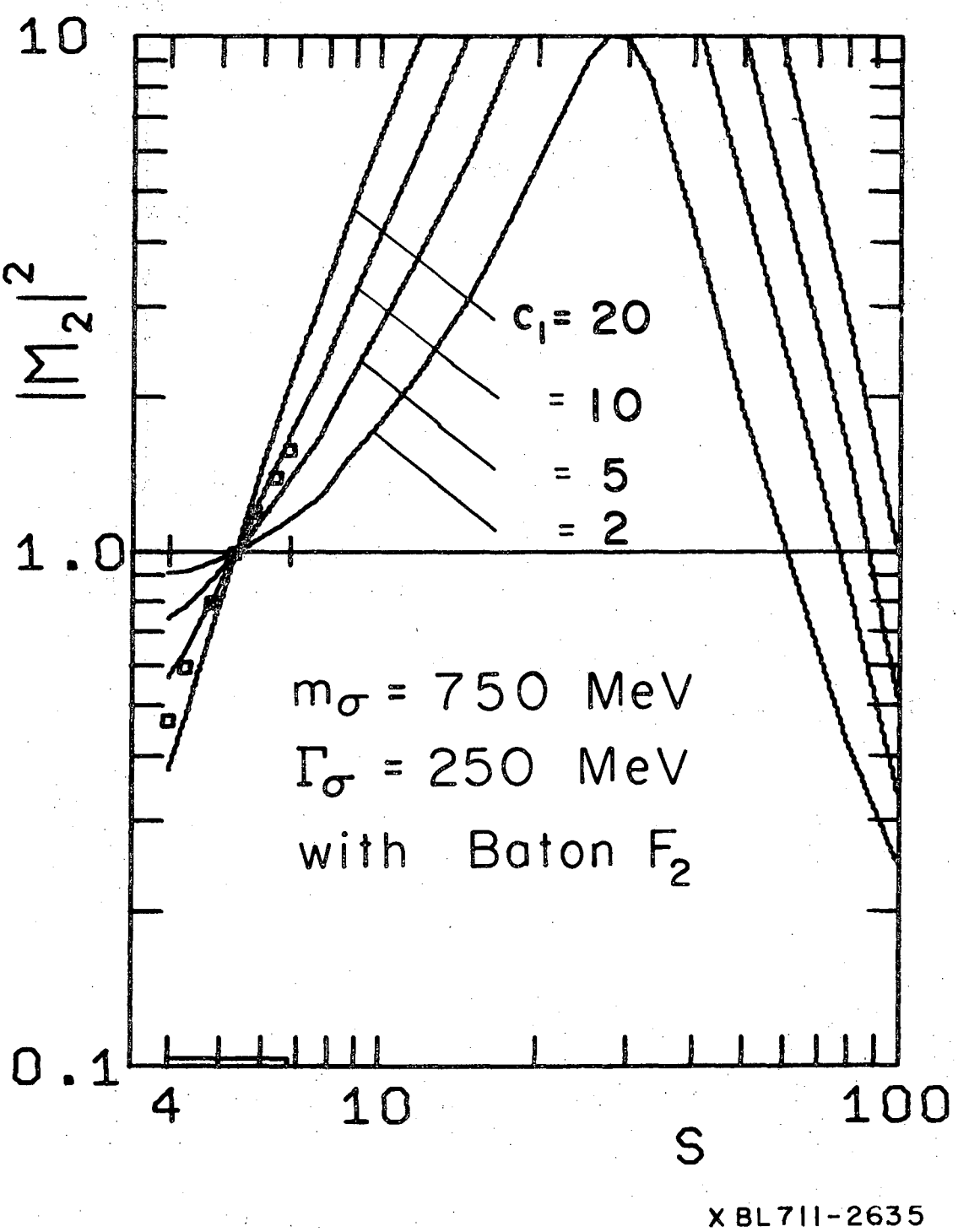
10
1.0
0.1
$|\Sigma_2|^2$
$c_1 = 20$
$= 10$
$= 5$
$= 2$
$m_\sigma = 750$ MeV
$\Gamma_\sigma = 250$ MeV
with Baton F_2
4
10
100
S
XBL711-2635

Fig. 19.

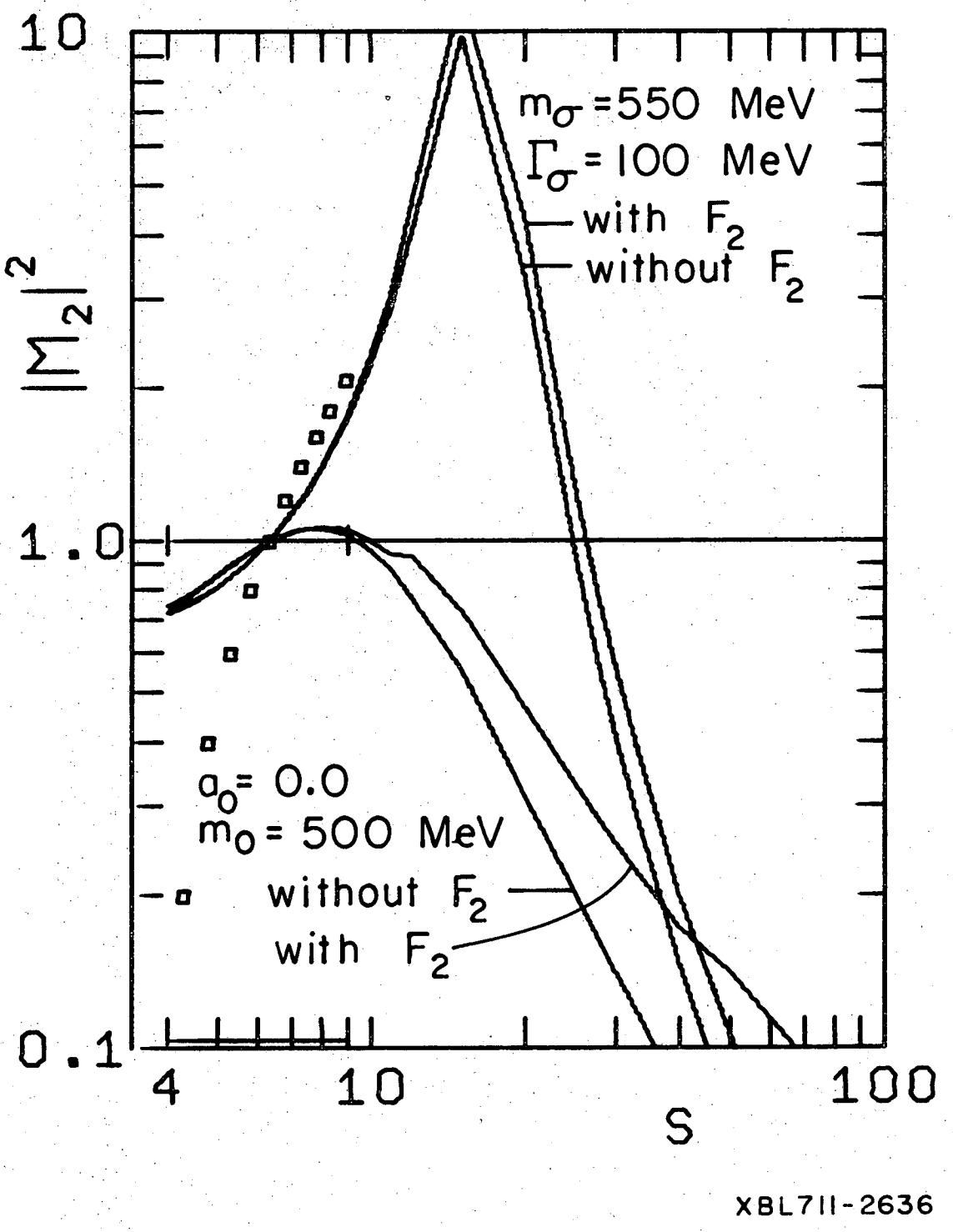
10
1.0
0.1
$|\Sigma_2|^2$
4
10
100
S
m_σ = 550 MeV
Γ_σ = 100 MeV
with F_2
without F_2
a_0 = 0.0
m_0 = 500 MeV
without F_2
with F_2
XBL711-2636

Fig. 20.

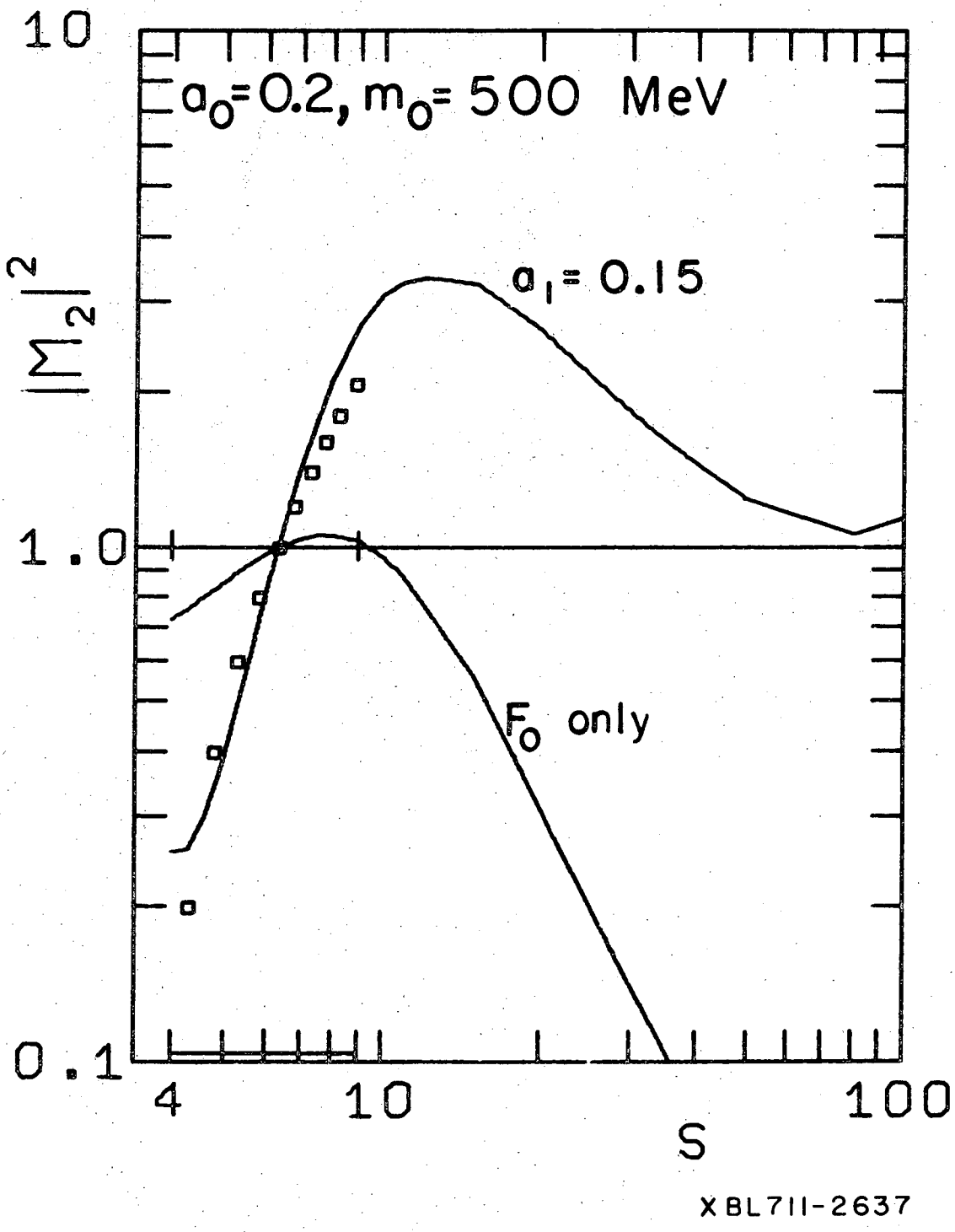
10
a_0=0.2, m_0= 500 MeV
$|\Sigma_2|^2$
a_1= 0.15
1.0
F_0 only
0.1
4
10
100
S
XBL711-2637

Fig. 21.

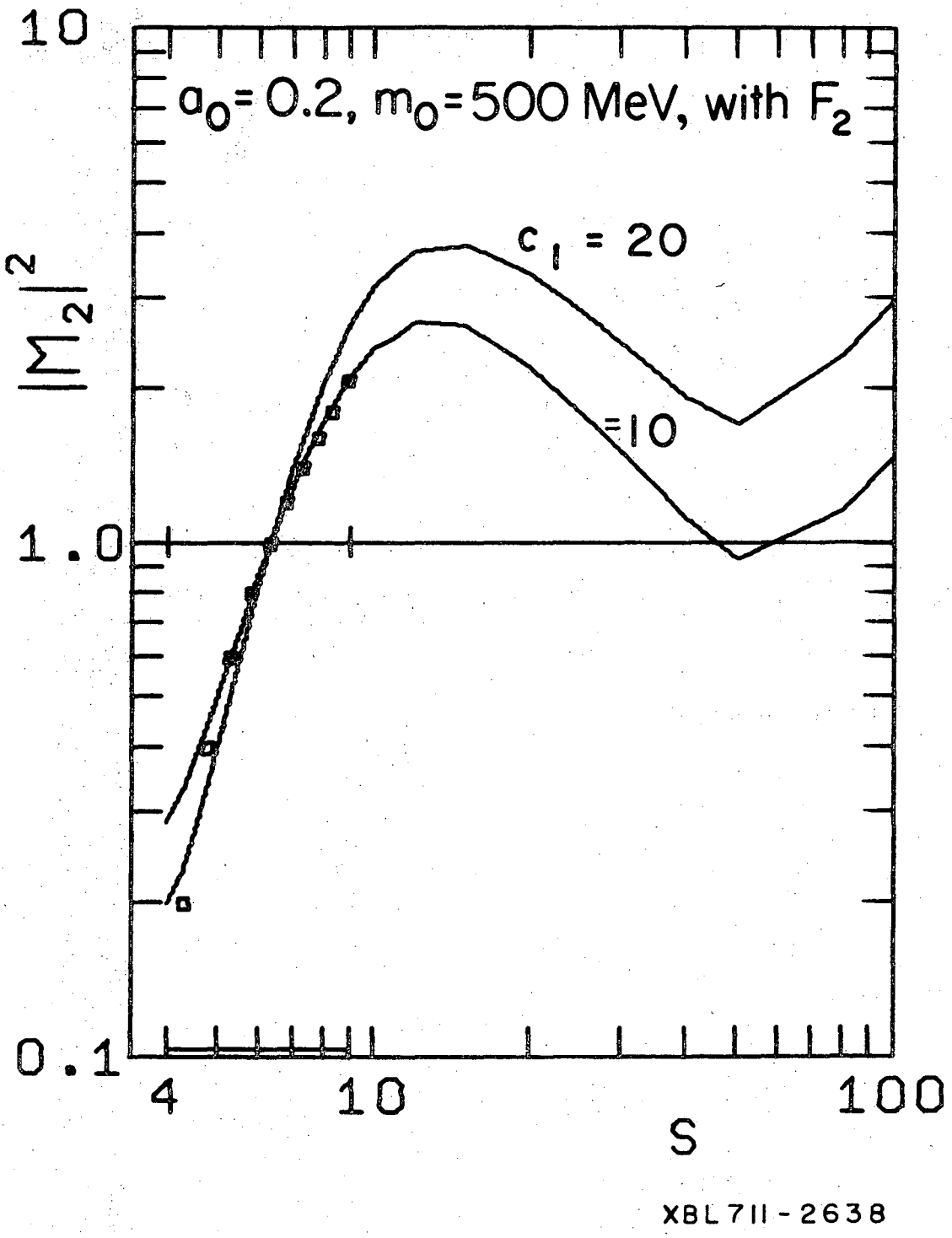
10
a_0= 0.2, m_0=500 MeV, with F_2
c_1 = 20
=10
$|M_2|^2$
1.0
0.1
4
10
100
S
XBL711-2638

Fig. 22.

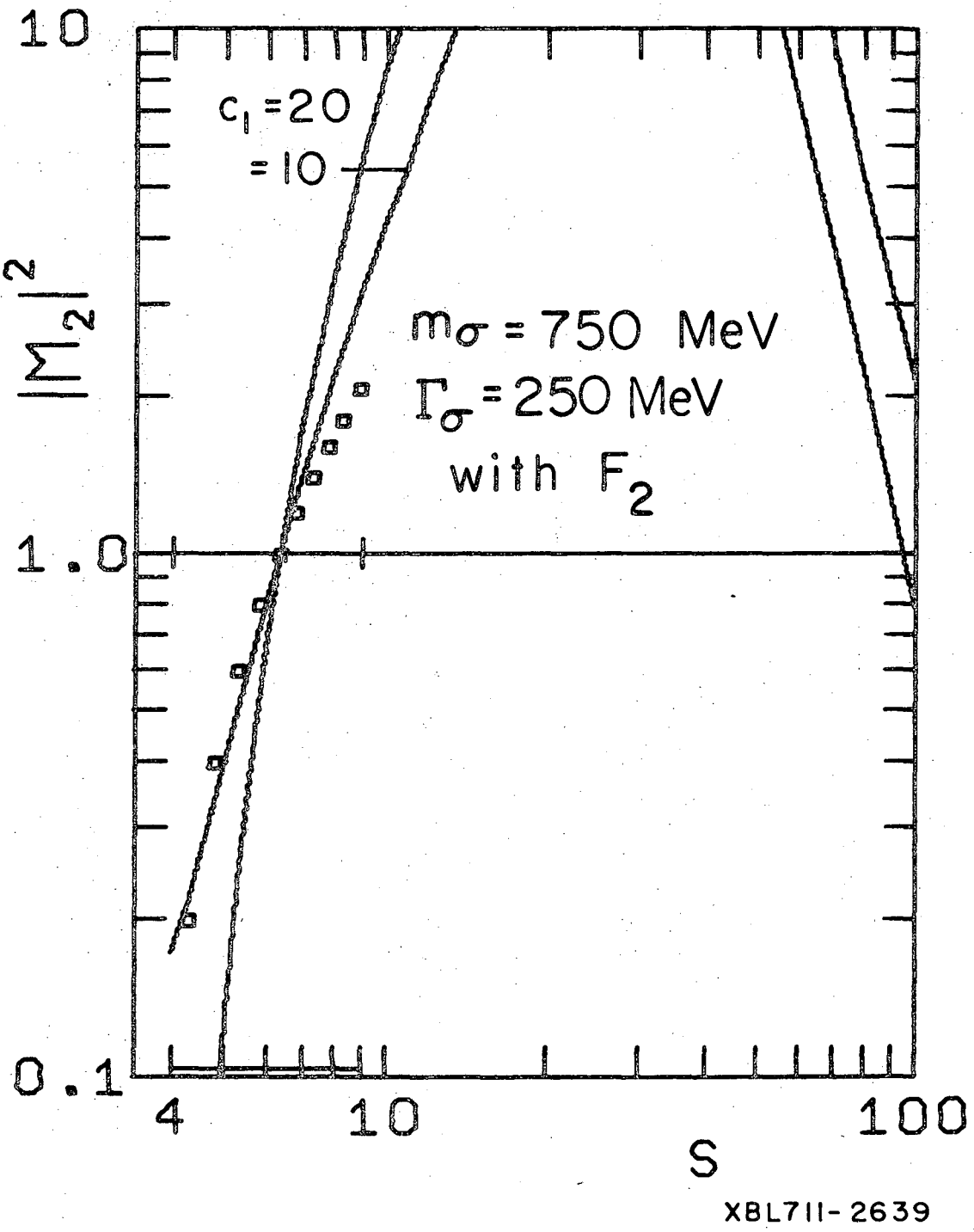
10
1.0
0.1
$|\Sigma_2|^2$
$c_1 = 20$
$= 10$
$m_\sigma = 750$ MeV
$\Gamma_\sigma = 250$ MeV
with F_2
4
10
100
S
XBL711-2639

Fig. 23.

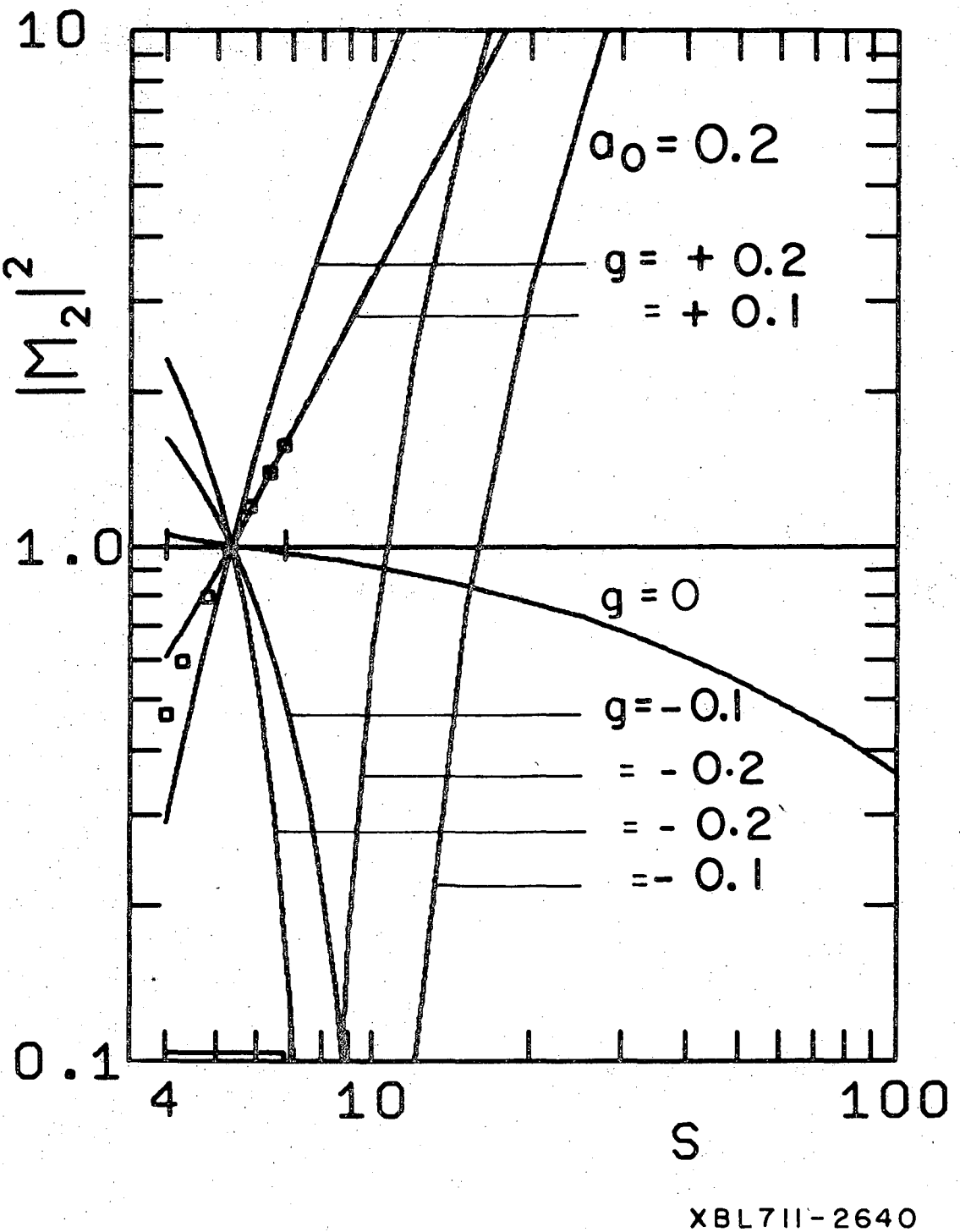

Fig. 24.

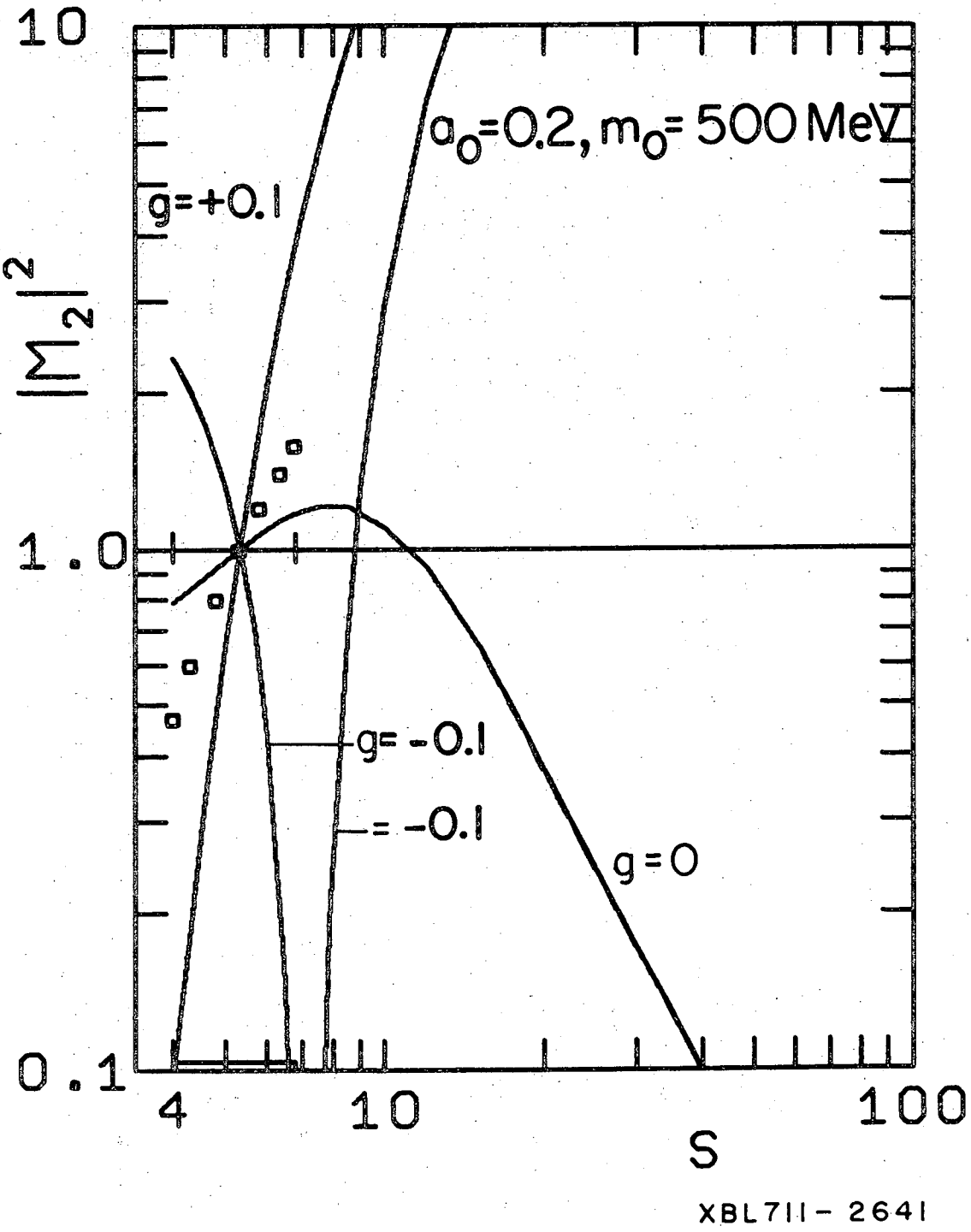
10
1.0
0.1
$|\Sigma_2|^2$
$a_0=0.2, m_0=500$ MeV
g=+0.1
g= -0.1
= -0.1
g=0
4
10
100
S
XBL711-2641

Fig. 25.

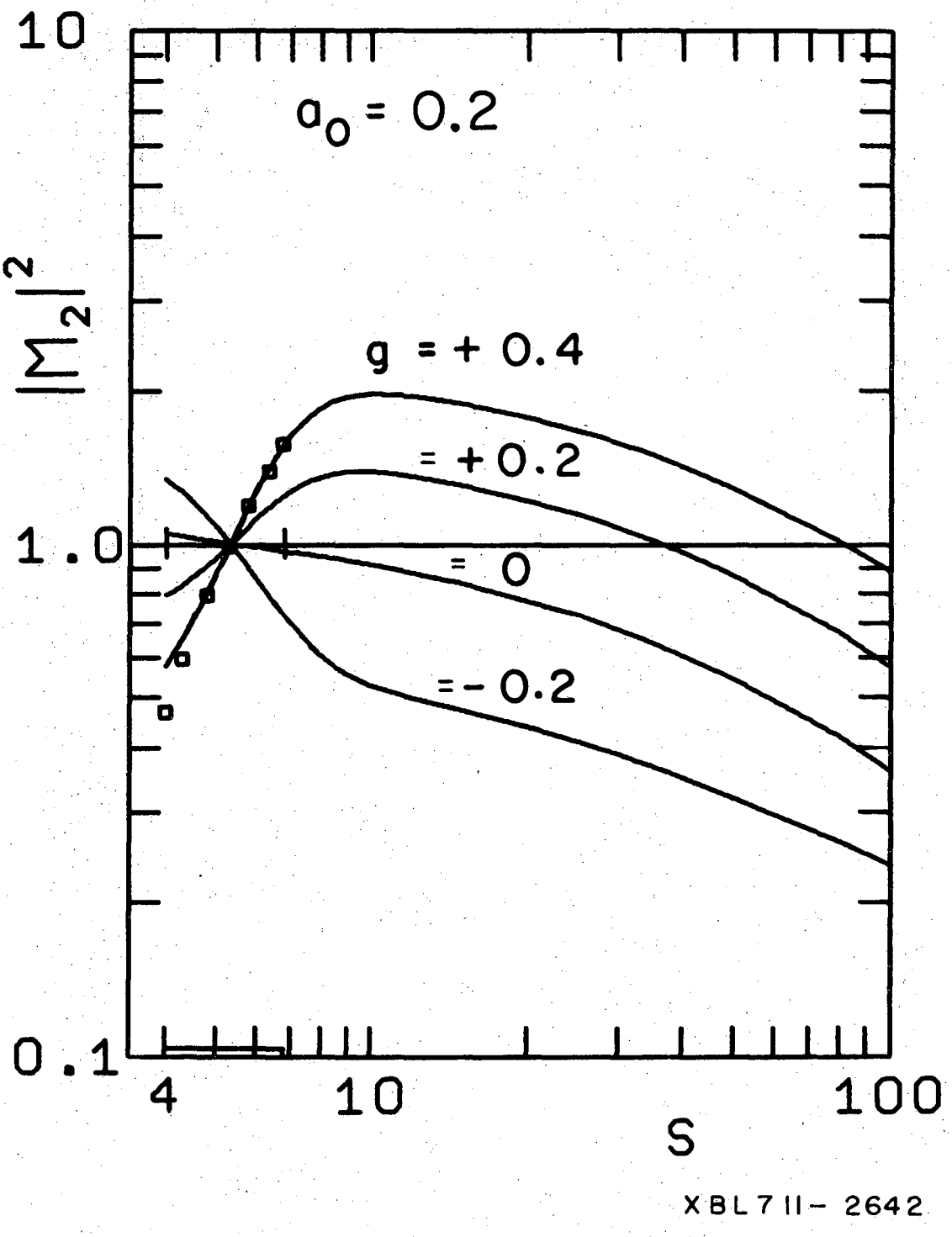

Fig. 26.

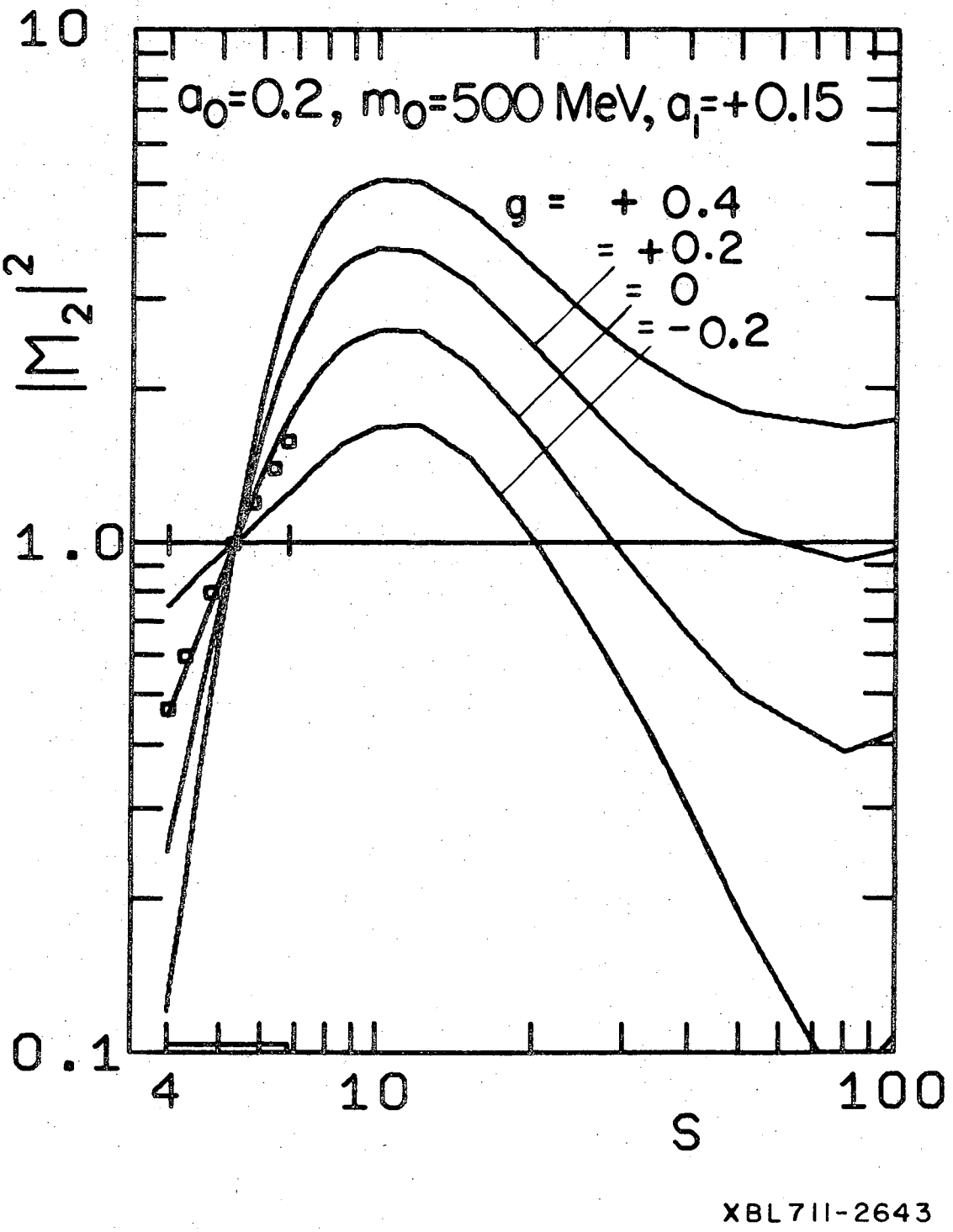
10
1.0
0.1
a_0=0.2, m_0=500 MeV, a_1=+0.15
g = + 0.4
= +0.2
= 0
= -0.2
$|M_2|^2$
4
10
100
S
XBL711-2643

Fig. 27.

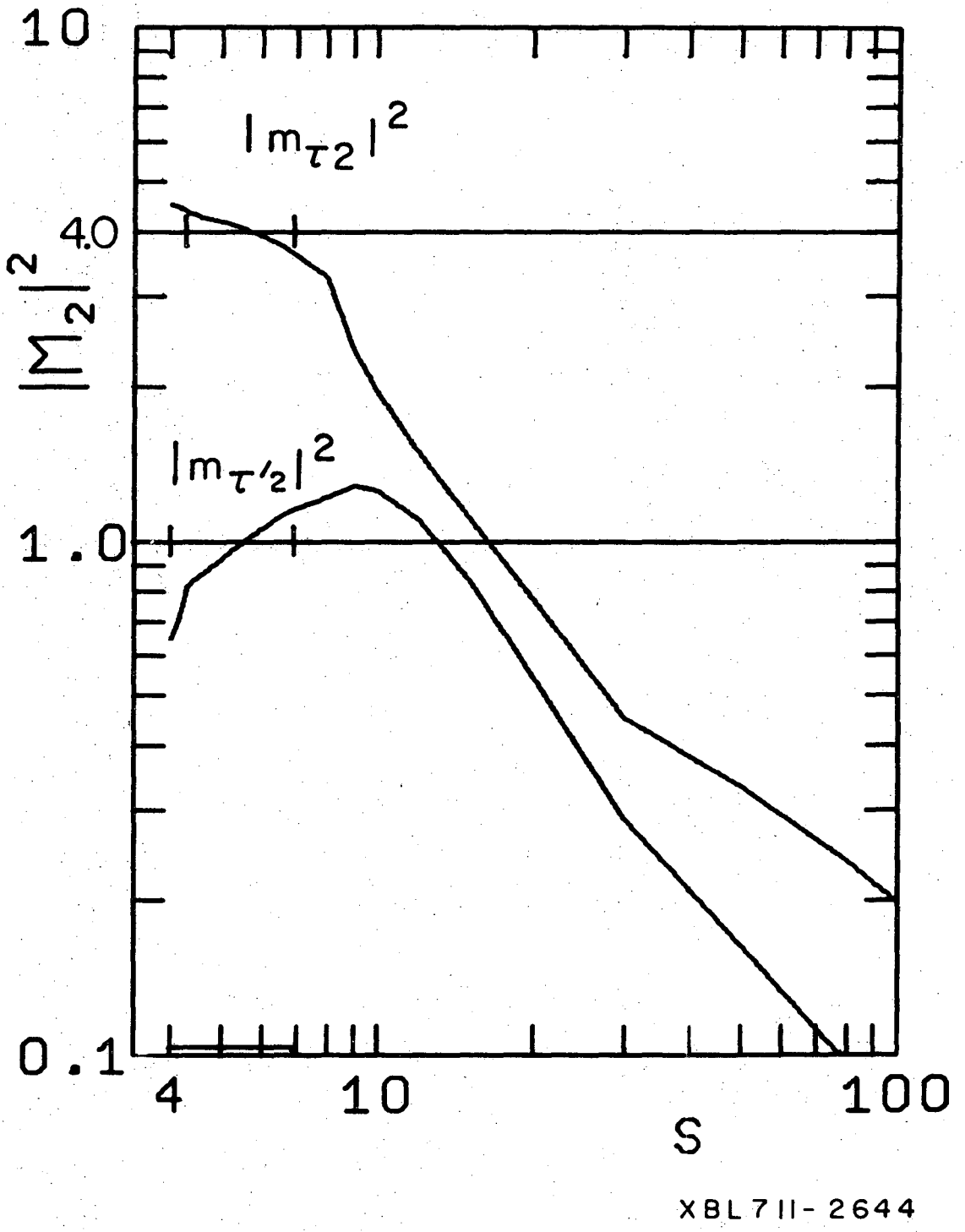

Fig. 28.

TECHNICAL INFORMATION DIVISION
LAWRENCE RADIATION LABORATORY
UNIVERSITY OF CALIFORNIA
BERKELEY, CALIFORNIA 94720